Influence of loading rate on pile capacity in unsaturated sand

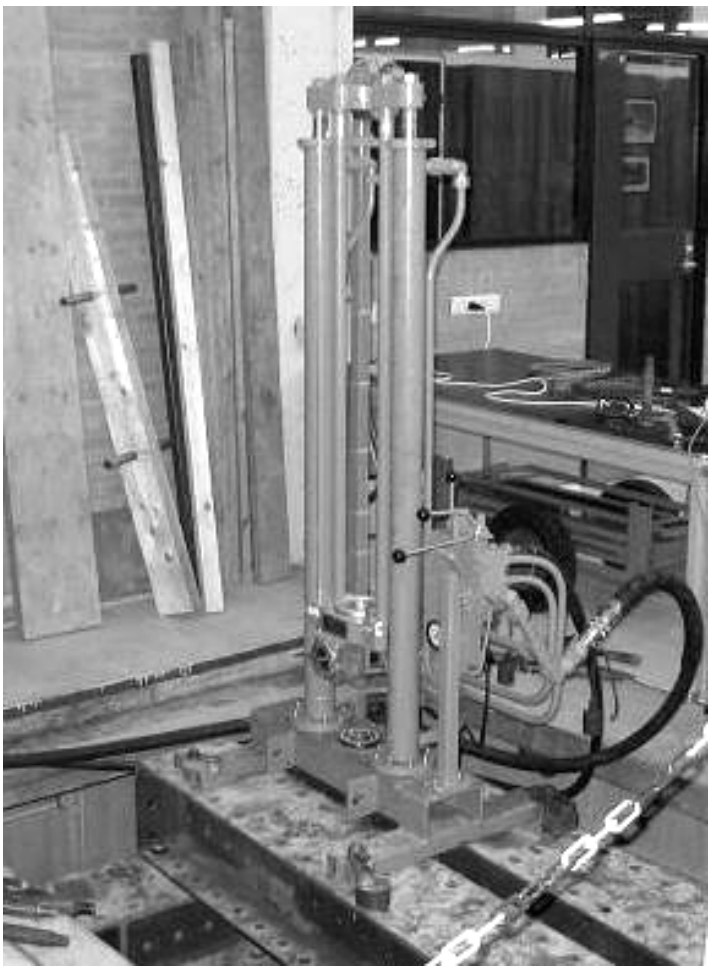

Jelke Dijkstra
Delft, November 2004

Influence of loading rate on pile capacity in unsaturated sand

Date: November 2004

Student: Jelke Dijkstra
S_{number}: 1004603
Address: Bosboom Toussaintplein 275
2624 DR Delft
E-mail: j.dijkstra-ct@student.tudelft.nl

Graduation: 30 November 2004, 16:00
Room V of CiTG section geotechniek TU Delft

Graduation committee:

Chairman:
Prof. ir. A.F. van Tol

Daily assistance TU Delft:
Ing. H.J. Everts

Daily assistance GeoDelft:
Dr. ir. P. Hölscher

External assistance TU Delft:
Ir. L. J. J. Speet

Coordinator:
Dr. ir. P. J.Visser

Key words: loading rate, unsaturated, sand, pile, foundation, bearing, capacity, statnamic, pseudostatic, dynamic

TU Delft GeoDelft 70 jaar

Abstract

When in-situ tests are performed to determine the ultimate capacity of a pile after the installation, quite a lot of types of tests are available. The following tests are generally used, in order from most used method to least used method: the static testing method, dynamic testing methods, pseudostatic and statnamic testing methods.

During a pseudostatic (or statnamic) test the pile is loaded with a ~ 70-150 ms loading pulse. In comparison with the dynamic test this loading regime is about 20 times as long, in comparison with the static test this is very short lasting. The difference in loading regime is influencing the bearing capacity of the pile.

In literature two main phenomena for the change in bearing capacity are recognized: the excess pore pressures and the loading rate. In the typical Dutch situation the end bearing piles are situated in the Pleistocene sand layer, so the influence of the loading rate in non-saturated and saturated sand are of interest. From literature is concluded that the effect of the loading rate on the strength and stiffness properties for dry sand are small, but for the rate effect on the shaft friction no conclusive answer could be found.
Therefore a series of model scale tests are performed to investigate the influence of the loading rate on the bearing capacity. Three different tests can be distinguished:

1. CPT-readings during installation with a constant rate of 20 mm/s.
   (large pile displacements of several D_{pile})
2. Very slow constant rate test at 1 mm/s (small deformations ~$2/3D_{pile}$ this test is considered as the static case)
3. The pseudostatic test where velocities up to 250 mm/s occur

The calibration chamber at the Geo-Engineering department of Delft University of Technology is utilized. This calibration chamber has a diameter of 1.9 m and is about 2 meters in height. The soil in the calibration chamber consists of non-saturated sand and is after each series of three tests fluidized, vibrated and drained.

A dynamic pile loading system with accompanying measuring system is designed to perform scaled (1:10) dynamic model pile tests in non-saturated sand. This system is capable of loading the pile with an in time extended blow and can measure in the millisecond range. The model pile is a CPT cone with a diameter of 36 mm which is ~1.3 m embedded into the soil. The upper rod is above soil level and equipped with strain gauges to measure the force on the pile head and with an acceleration transducer to monitor the acceleration of the pile.

From the tests the following is concluded:

1. Acceptable soil consistency is met when the results are differentiated to the several locations in the calibration chamber, however some improvements with regard to the soil preparation can be made.
2. The Static (1 mm/s) / CPT (20 mm/s) ratio or c_p is 0.82 for the tip resistance and 0.86 for the local shaft friction. Only for the tip resistance this result is significant and therefore can be concluded that a rate effect exist. The results of the shaft friction show a too large scatter.
3. In general can be said that with a velocity increase from 1 mm/s to ~250 mm/s the increase in bearing capacity found during the execution of pseudostatic model tests is a non-significant increase of ~ 4% for the tip resistance and also a non-significant increase of ~ 6% for the shaft friction.
4. When only the stiffness of the pile soil system is considered both the static and pseudostatic tests show good consistency in stiffness (2 tests within 10 %) and the rate effect is >>1, more research is needed to come to a better conclusion (chapter 10).
5. The initial steepness of the loading pulse which is applied on the model pile is important to classify the behaviour of the pile.

Preface

This is the final report of the master thesis: 'Influence of loading rate on pile capacity in sand'. The research is executed in cooperation with the Geotechnics section of the faculty of Civil Engineering and Geosciences at the Delft University of Technology. External assistance is performed by GeoDelft.

I would like to thank my supervisors: Prof. ir. A.F. van Tol, Dr. ir. P. Hölscher, ir. L.J.J. Speet and ing. H.J. Everts for their support during this project. I extend my thanks to Paul Hölscher who has always been very generous with his time and advice.

Also the vast technical knowledge, about almost every aspect of the realization of a measurement system and experimental setups, of Louis Speet, made it possible for me to build the system presented in this report.

Thirdly I want to thank Mr. Huy for his input during the committee meetings.

I also want to thank the staff and in particular Mr. J.J. De Visser at the geotechnical laboratory of the geotechnics section for their help with the realisation of the test set-up and the quick technical support.

Not to forget the people at GeoDelft who always helped me with my questions.

Finally I want to thank ir. P. Middendorp and Dr. A.J.G. Schellingerhout of IFCO B.V. who answered a lot of question regarding the statnamic and the PLST system.

Delft, November 2004,

Jelke Dijkstra

Table of contents

1. Introduction

In the case engineers want to know the ultimate bearing capacity of already installed piles, e.g. when an existing foundation is re-used or as part of the design process, quite a lot of types of tests are available. To discuss them all is beyond the scope of this report, also the interpretation methods accompanying those tests are not uniform, but the following tests, in order from most used method to least used method, are generally used:

1) The static testing method

In a static test the pile will be axially loaded 2-3 times of it's designed load or until failure. The failure point is standardized for the Dutch situation (NEN 6745) at a pile displacement of 10% of the pile diameter. These static tests can take days (depending on the soil conditions, in clay it takes longer then in sand due to consolidation effects, thus quite an expensive procedure. Also to load the pile under test, a massive construction has to be made to accommodate the load. When the reaction force of this construction is loaded on the neighboring piles also changes in the bearing capacity can be expected.

2) Dynamic testing methods

In the case of a dynamic test the loading consists of a short blow (O(4 ms)). The drop mass is about 2% of the ultimate capacity of the pile. During the test, acceleration and strain as function of time are monitored. The velocities and stresses in the pile during a dynamic test differ from the static situation. Some pile levels are moving up others down; with as result the possibility of tension cracks. The time needed to perform a dynamic test is in the order of magnitude of hours. To improve the reliability of the results of interpretation of the dynamic tests in practice most of the times the dynamic results are calibrated with a static test.

3) *Pseudo static and statnamic testing methods*

The statnamic test is designed to get a situation in-between the dynamic and static case; therefore the blow is lengthened to O(100 ms) and the mass is about 5%-10% of the ultimate capacity. The velocity and stress distribution is more like the static case, namely evenly distributed. All pile levels move in the same direction. The force and the displacement are measured; both quantities are described as a function of time. While pseudo static and statnamic tests behave more like the static case, these tests are still dynamic, and thus dynamic soil effects have to be incorporated. Pseudo static and statnamic tests are based on the same principle, but the loading system differs. While a pseudo static system lengthen the blow with a system of springs and dampers attached to the mass, the statnamic system uses a fast burning gas to detonate the reaction mass (the reaction mass combined with the combustion drives the pile). Pseudo static testing takes hours, while statnamic testing costs about a day.

The costs of the static and pseudostatic test are directly compared for the U.S. market as stated by Bermingham (during a workshop organized by Delft University of Technology 27-10-2004) the global figure for static testing is $ 100,-/ton and for statnamic testing $ 10,-/ton. Thus a tenfold price difference.

Of these tests only the static load tests are commonly used in the Netherlands, dynamic and statnamic testing is more commonly used in foreign countries, especially the U.S. and Japan or in offshore situations where static pile testing is not as easy executed as onshore.

Unfortunately these tests do not deliver the same results, in other words each method derives another type, depending on the used pile test, of pile capacity. The static testing method delivers the most accurate findings, related to the actual long term in-situ pile capacity. The interpretation of dynamic and statnamic tests is more diffcult because of the dynamic soil reactions during those tests.

The dynamic and statnamic tests give results which are harder to interpret, these interpretations can vary thus give less accurate findings, but are cheaper to execute.

It is therefore important to find a relation between the results of the dynamic and or statnamic tests and the static case. When static tests can be replaced by for example a statnamic test, more tests can be done in a more economical way.

Another aspect worth mentioning is if the load on a foundation has a dynamic character, for example wind or gales on a skyscraper, the foundation has to handle the extra load. If the dynamic part of the soil strength, the reaction of the soil on the dynamic loading, can be measured or calculated out of the dynamic or statnamic tests, then the design of a foundation which has to handle those forces can be better suited to the load.

For describing the relation between dynamic or statnamic and static tests conversion methods have been developed. For pseudo static and statnamic tests the conversion principle is the same and based on the unloading point method (UPM), the segmented UPM method (pile divided in several segments [Lin et al, 2004]) the 1D stress wave equation analysis, 2 or 3D FEM calculations. Last two methods are also used for the dynamic testing results.

The above mentioned calculation methods are not straightforward and phenomena which occur during dynamic and statnamic tests and the effect of these phenomena on the results are not clear. Of these phenomena the loading rate and excess pore pressures are the most important and influencing quantities. For soft soils, for example clay, research has been conducted by Brown (2002, 2004), but for granular material the effects of loading rate and excess pore pressures are not clearly documented.

To investigate the loading rate phenomenon a series of model pile tests (scale 1:10) in non-saturated sand are executed. For these tests a dynamic loading system and a measuring system capable of registering millisecond range are developed. In this report the loading and measuring system are presented together with the results of the effect of loading rate on the bearing capacity of piles in non-saturated sand.

2. Problem definition, important aspects, objectives and limitations

2.1 Problem definition

Statnamic and dynamic tests deliver an indication for the static pile capacity. The calculation methods used for deriving the results of these tests to the static case are not as precise as wanted, and depend heavily on the loading rate and the excess pore pressures present in the soil. For sandy soils the effects of loading rate and excess pore pressures are not clear. When model tests are executed the scaling of the applied load and the measurements are also problematic and need great care.

2.2 Important aspects

First some important aspects will be summarized.

1. Loading rate
When the rate of loading is increased the maximum bearing capacity can alter, therefore it's important to investigate the possible influence of loading rate on bearing capacity.

2. Excess pore pressures
It is still unknown, and for each type of soil different, how to implement the effects of excess pore pressures in the scaling of the dynamic/statnamic measurements into the static case. The pore pressures can affect the penetration resistance and thus the bearing capacity.

3. Type of soil
As mentioned under 'excess pore pressures', the type of soil has some effect on the pore pressures. The pile capacity is also determined by the strength and stiffness parameters of the soil. In case these parameters are controlled[1] quantities, thus of lesser importance. The chosen quantities however have to be representative for the modeled reality.

4. Model conditions
The tests have to be performed under equal conditions, so the different outcomes can be compared. The used test-chamber must have reproducible and known soil conditions.
Of course the soil conditions cannot be controlled as tightly as wanted. To acquire a homogeneous soil with the wanted soil conditions is quite a labour-intensive process. The following difficulties arise when preparing the test-chamber at Geotechniek:

1) The vibration and fluidisation method used gives different densities and soil structures even when all boundary conditions are held constant (i.e., vibration time, soil type and fluidisation parameters)
2) Vertical deviations in stratification after each tank preparation.

Of course these difficulties have to be incorporated in the setup and interpretation phase.
Also the physical limits have to be considered, for example, the radius and height of the tank, these conditions limit the size of the used model pile.
Because the tests are performed in a 1g environment the stress-conditions aren't directly comparable with the real in-situ situation and therefore need to be scaled to make a comparison possible.

[1] The 'Model conditions' paragraph will make some comments on this statement

5. Loading system
When scale tests are executed, then the loading system has to be setup such that the actual in-situ loads can be reproduced, because pile length and the loading system as a whole are different. The imposed impulse has to be scaled as well.

6. Measurement system
Dynamic and statnamic systems are generating very short lasting quantities, in the case of dynamic tests even sub millisecond. The measurement system has to be up to the task, not only for recording the wanted phenomena, but it has also to be interpretable.

The first and second are very important quantities for the results of statnamic and dynamic tests. The effects of these aspects aren't precisely documented for sand. The last three (aspect 4,5,6) are more a practical side effect, but quite important to succeed.

2.3 Objectives

Main objective
-Qualify and quantify the effect of the loading rate on the bearing capacity of a pile, by means of the execution of 1g model tests. With as result a force-loading rate relationship and/or graph for sand[2]

Sub objectives
-Research into the feasibility of model testing in 1g conditions and the specific boundary conditions of the used calibration-chamber.
-Extensive research into loading mechanisms has to be done, to model exactly the pseudostatic behaviour of the load. With this goal in mind the loading- and measurement-setup will be determined which results in the possibility of executing tests at different loading rates.
-For executing 1g-modeltests, we examine the dependency of the loading rate on, the pile capacity, dynamic tests and pseudstatic tests

2.4 Limitations

During this research, certain limitations will be made to restrict the boundaries, and make the research more attainable.

Pile geometry
The test pile can have different cone-shapes and a certain skin roughness. The effects of these conditions aren't taken in consideration and held constant during al tests.

Soil condition
The soil condition is limited to unsaturated sand. Also the tank in which the tests are performed limits the soil conditions, because the preparation method used, first fluidization and subsequently vibration, does not handle all types of granular material. The effects of the vibration methods to increase the density are not consistent enough to be able to directly compare the results between two tank preparations. Therefore the number of tests must have statistical value to be able to compare the results.

Loading
The loading consists only of pressure forces. A tension force will not be applied.

[2] See appendix A for considerations about the choice of model tests.

3. Literature study

3.1 Introduction

In literature roughly three types of loading rate tests can be identified, firstly in the soil tests the load rate dependent soil strength is investigated, secondly in the loading rate dependent interface tests the influence on the interface strength is studied and thirdly the pile soil interaction as a whole system. In this chapter the soil tests are dealt with first, the interface tests are dealt with next, and the pile-soil system is a whole is studied.

The loading rate is a rather poorly defined quantity. Mathematically it's the force differentiated with respect to time, but practically the force increment induced by a velocity increment is also called a rate effect. When last criterion is used also tests which are applied at different constant velocities are incorporated.

3.2 Soil tests

Casagrande and Shannon (1948) performed triaxial compression tests on dry Manchester sand. The sand samples were 7.1 cm in diameter and 18 cm in height. The void ratio varied from 0.61 (dense) to 0.88 (loose). The confining pressures were varied from 30 to 90 kPa. The loading velocity applied on the sample ranged up to 0.2 m/s. From the ten minutes static tests they concluded that the strength of dry sand increases about 10 to 15 % when tested at a higher loading velocity.
Seed and Lundgren (1954) performed drained and undrained triaxial tests on saturated sands at a confining pressure of 200 kPa and a loading velocity up to 1 m/s. During transient drained testing it was observed that the pore pressure had insufficient time to drain so the tests approached undrained conditions. They concluded that the increase in strength of saturated dense sand was about 10-15 % due to loading rate effects. This effect decreases as the void ratio increases. In loose saturated fine sand the increase of loading velocity possibly decreases the strength.
Whitman and Healy (1962) presented the results of drained and undrained triaxial tests on dense and loose sands with confining pressure of 70 kPa and loading velocities up to 0.5 m/s. The results indicated 10 % increase in drained strength and up to 100 % increase in undrained strength when compared to static values (a failure time of 5 min).
Schimming and Haas (1966) have performed several shear tests on cohesionless and cohesive soil. The time until failure is for dynamic tests about 1 – 5 ms and for the rapid static case 30 s – 50s. For the cohesionless soils the ratio of the angle of internal friction is used to compare the strength properties in both tests with saturated sand and dry sand no rate effect was present. Also some silt and air dried powdered clay is tested and resulted in no rate effect. The cohesive soils (different clays and clay with different moisture content) did result in an increase of 100%.
Gibson and Coyle (1968) performed also some triaxial tests on three types of sand with different loading velocitues ranging from 0 to 12 feet/second (3.6 m/s). An increase of 50 % was measured for Victoria and Arkansas sands, but for Ottawa sand the increase was >100 % compared to the static load. See Figure 3.1.

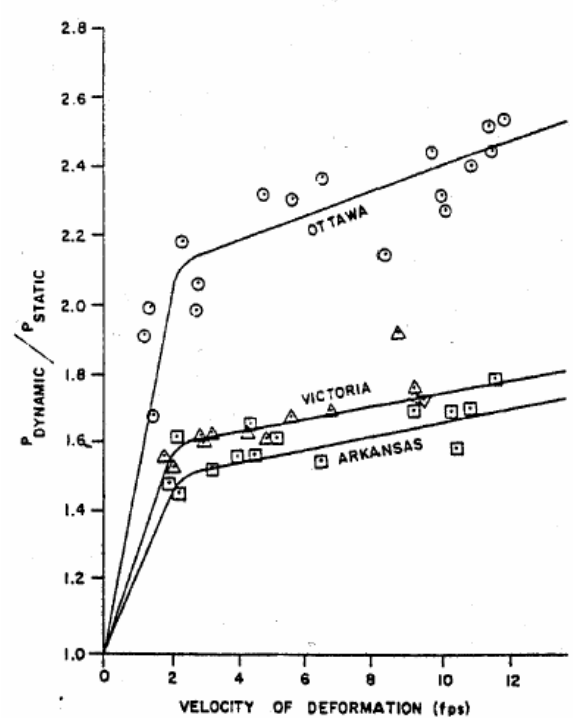

Figure 3.1 Pdynamic/Pstatic vs. velocity of deformation

Lee, Seed and Dunlop (1969) performed triaxial compression tests on dense and loose sand with various confining pressures ranging from 100 to 1475 kPa with loading velocities up to 0.22 m/s. The results indicate a 7 % increase in strength of loose sand with increasing loading velocity in all confining pressure and up to 20 % increase for dense sand in high confining pressure.
Farr (1990) studied the one dimensional loading rate effects on enewetak beach sand with a special designed loading device which is able to range the time to failure from 0.0004 s up to 155 s. The soil sample cavity is only 1.27 cm high and 9.65 cm in diameter. For the maximum dynamic young's modulus twice the static young's modulus is found. See Figure 3.2.

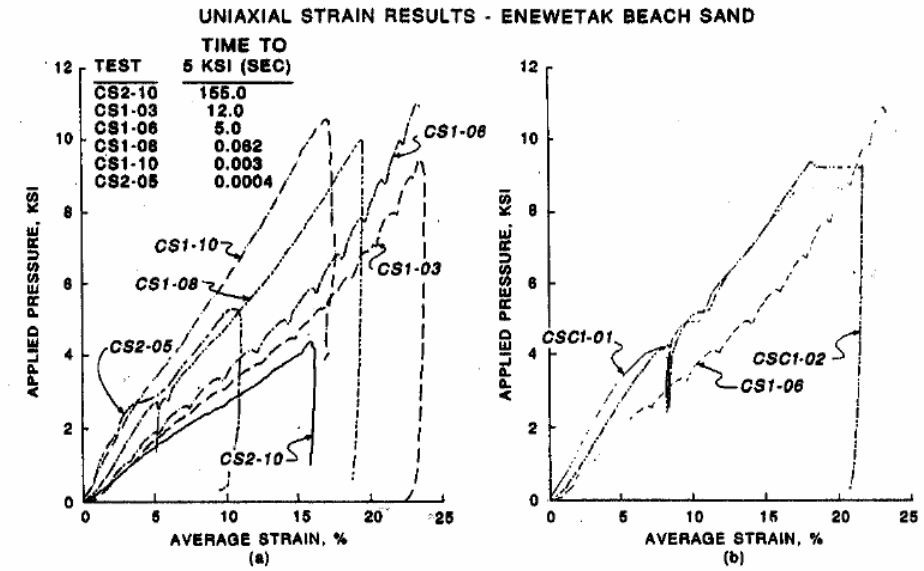

Figure 3.2 Uniaxial strain results enewetak beach sand: (a) loading rate effects (b) dynamic creep behaviour

3.3 Interface strength

In the following tests special test set-ups are designed to test solely the interface shear strength between two types of materials.

Brumund et al (1973) used a shear box test to measure the static and dynamic friction between sand and a typical construction material. The normal stress ranged from 1.25 – 12.5 psi.
The loading time was 1-2 ms for the dynamic case and 5 minutes for the static case. The friction coefficient is defined as

$m_{static} = \frac{F_{static}}{N_{static}}$ for the static case

and

$m_{dynamic} = \frac{F_{dynamic}}{N_{dynamic}} = \frac{F - ma}{N_{static} + \Delta N_{static}}$ for the dynamic case.

During the tests the measured ΔN_{static} is unmeasurable small; therefore the following relation between the ratio of friction and the force ratio can be made:

$\frac{m_{dynamic}}{m_{static}} \approx \frac{F_{dynamic}}{F_{static}}$

Their results show that the dynamic wall friction was about 26 % greater compared to the static wall friction, in the case for sand-steel.

Heerema (1979) performed a simple laboratory test which simulates the interaction of a steel pile wall in the soil during driving to determine the relationships between wall friction, horizontal stress and pile wall velocity. His results on sand showed that the friction force was linearly dependent on normal stress and independent of velocity (see Figure 3.4).

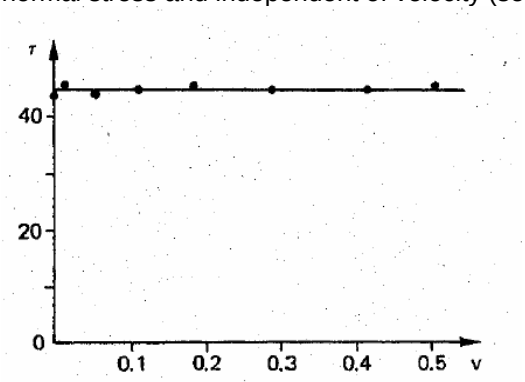

Figure 3.3 Velocity variation test on a sand sample σ_h = 85kN/m^2, v in m/s

As seen in Figure 3.3 the ratio Fdynamic/Fstatic is 1.

3.4 Loading rate effects on pile resistance

In this type of test the actual pile-soil system is investigated.

Jezequel (1969) pushed an electric cone penetrometer in medium dense sand at different rates of penetration, namely 0.2 cm/s to 2 cm/s. His results showed an 8 % increase of resistance above the water table and a decrease of 21 % below the water table.
Dayal and Allen (1975) used an instrumented (cone load cell, friction sleeve and velocity) impact cone penetrometer with a diamter of 35.6 mm and area of 10 cm^2 for the base and 150 cm^2 for the sleeve. The loading is applied with a hydraulic actuator. The set-up consists of a cylindrical steel mold of 46 cm diameter and 61 cm height filled with cohesionless soil, namely dense sand (built in compacted layers of 6 inch) and loose sand (poured through a sieve). Four different

velocities are utilized (0.13, 1.28, 13.9 and 81.14 cm/s). They concluded that the effects of penetration velocity on cone and sleeve resistances are insignificant for cohesionless soils. These results are listed in Figure 3.4a-b.

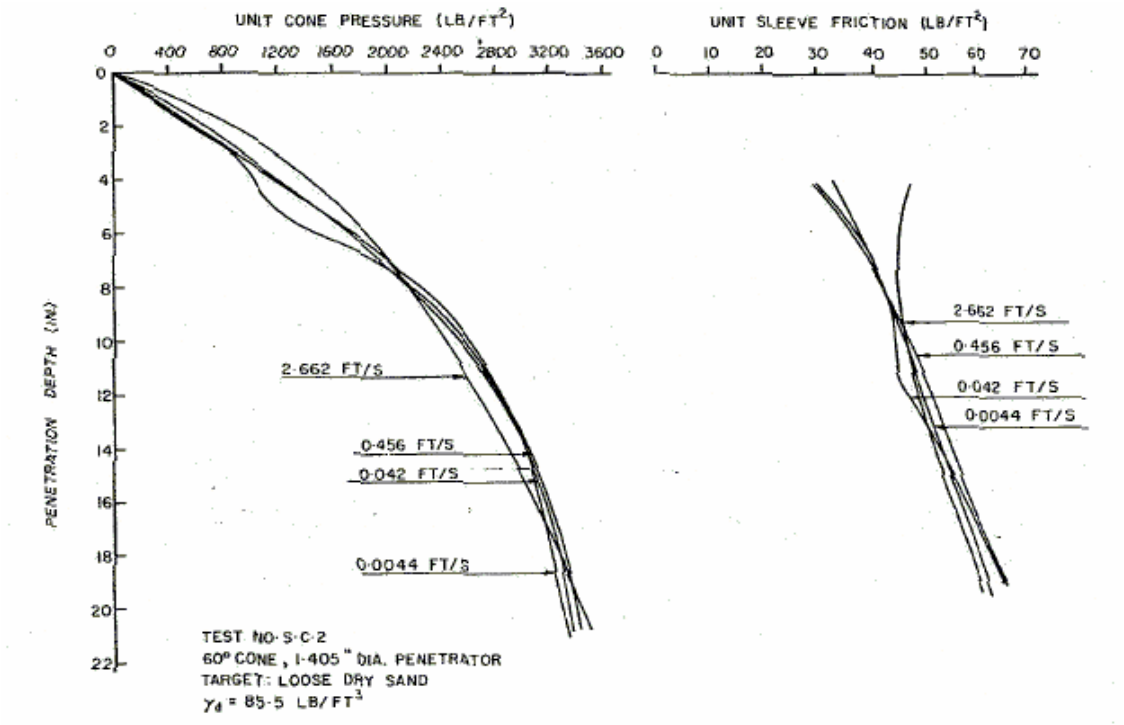

a) loose sand

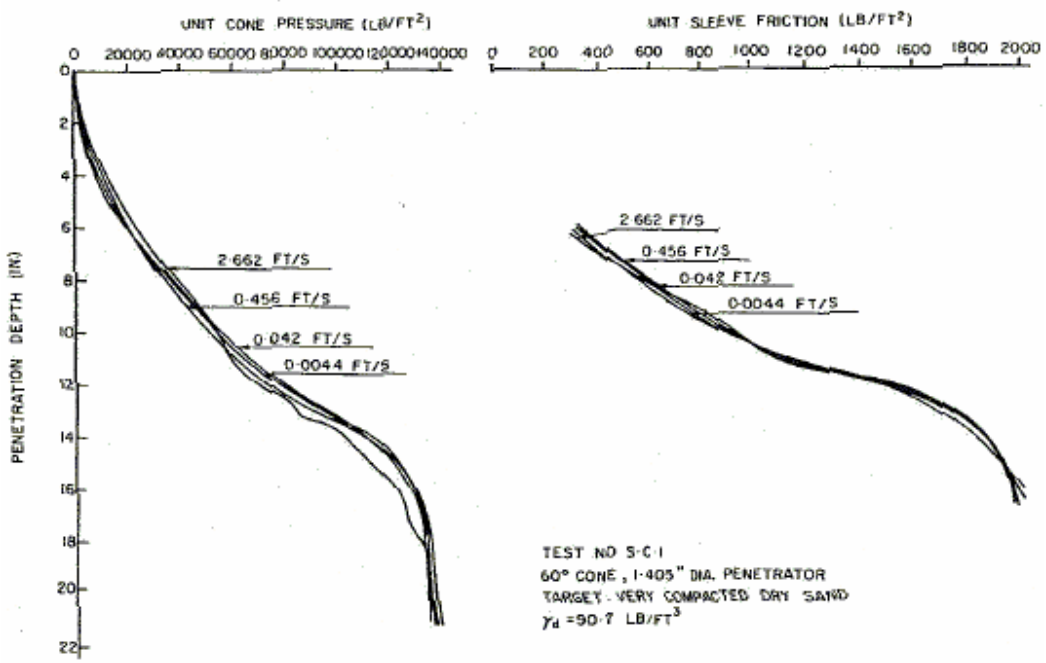

b) dense sand

Figure 3.4a-b Results of Dayal and Allen

Horvath (1991) performed a total of 160 statnamic tests on 18 dry soil sample setups on a model pile with a diameter of 12.7 mm and a length of 508 mm (embedment = 350 mm). Two types of sand were used, namely Ottawa sand and concrete sand. The influence of test duration, soil density, type of sand and repetitive testing was studied. Also one series of tests were executed in wet sand. A rate effect in dry Ottawa sand of 10 % was found up to a test duration of 2 s, however when the test duration is decreased a sharp transition of the rate behaviour is found. Above 2 s the loading capacity increases, below a loading duration of
1 s the loading capacity decreases. The shortest loading duration which is used is 50 ms. The place of this transition depends on the grading of the sand. See Figure 3.5 for the rate effect.
The transition in soil behaviour is accounted to the change from 'static' to 'dynamic' pile soil behaviour. A decrease in void ratio (more dense) resulted in increasing loading capacity for all load durations. The influence of repetitive testing was found to be negligible (1 %).

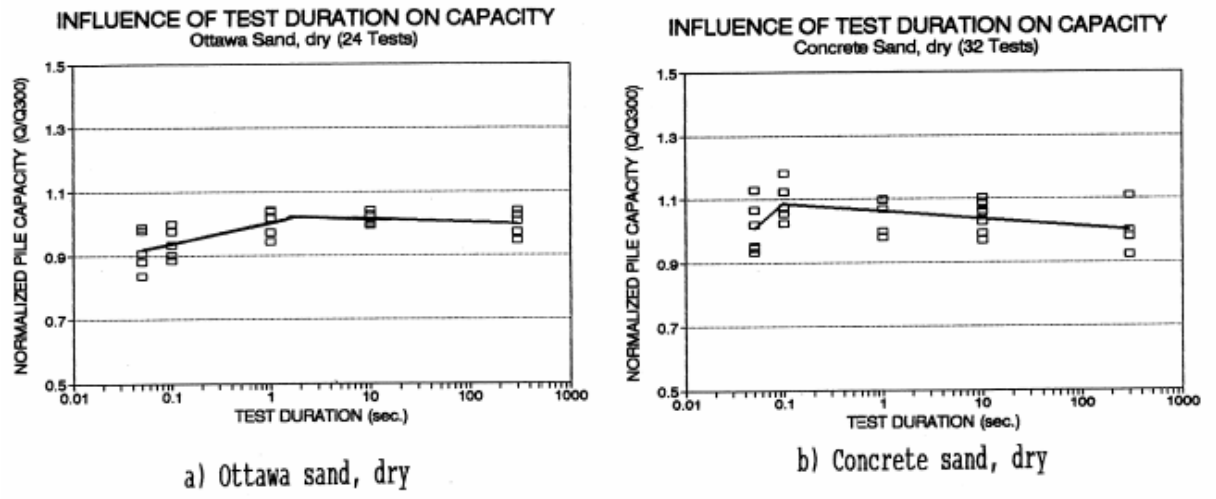

Figure 3.5 Influence of test duration on capacity

Eiksund and Nordal (1996) performed dynamic load tests on a model pile in a calibration chamber. The model pile had a length of 1.07 m. and a cross sectional area of 406 mm^2. The tests were performed in F-75 Ottawa sand and Lebanon Silt. Tests with different actuator loading velocities showed an increase of less than 10 % with velocities up to 1100 mm/s see Figure 3.6.

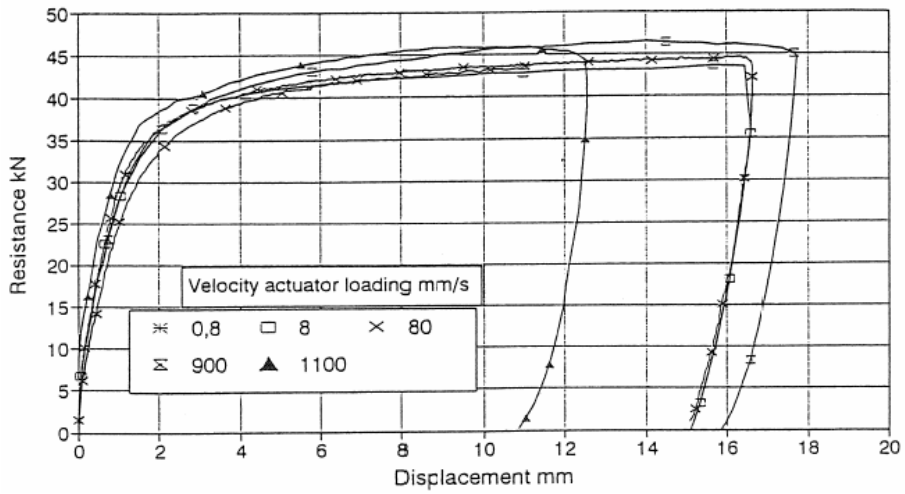

Figure 3.6 Penetration resistance at several velocities

Eiksund performed also tests in saturated sand and measured the pore pressures. According to the author the pore pressures are a function of the stress distribution and the soil dilatancy. In dense sand negative pore pressures will occur, which increases the dynamic resistance.
Al – Mhaidib (1999) performed 45 compressive capacity tests. A model steel pile in sand with D = 30 mm is loaded with a constant rate of 1 mm/min, 0.5 mm/min, 0.1 mm/min, 0.05 mm/min and 0.01 mm/min. The embedded length is also varied (l/d=7, 10 and 15). The preparation of the soil is quite consistent (sand raining device). Three types of density are investigated, loose (Dr = 30%) medium (Dr = 55%) and dense (Dr = 80%) sand. The pile was brought in during the preparation of the tank, so no disturbance from driving. The influence of boundary conditions can have influenced the results (tank diameter = 15 times pile diameter, so the pile is about 7-8 pile diameters from the boundary). Figure 3.7 shows the result of one of the performed tests.

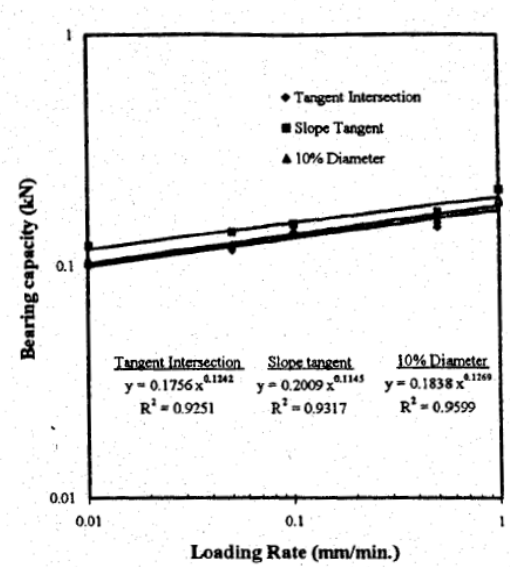

Figure 3.7 bearing capacity vs. loading rate in loose sand (l/d=15) (log,log)

Gennaro et al. (2001) studied the effects of loading rate on pile resistance by performing a series of model pile tests in a calibrated sand chamber. Two loading velocities were applied, namely 60 mm/min and 1 mm/min. Also two length/diameter ratios were tested, namely D/B=17.25 (D=345mm) and D/B=25 (D=500mm) (D= embedded length [mm], B=diameter [mm]) D/B=17.25 gives lower values compared to the D/B=25 ratio. The test results show that with increasing loading velocity a higher tip resistance is measured (~18 %), while the shaft friction decreases with increasing loading velocity. See Figure 3.8.

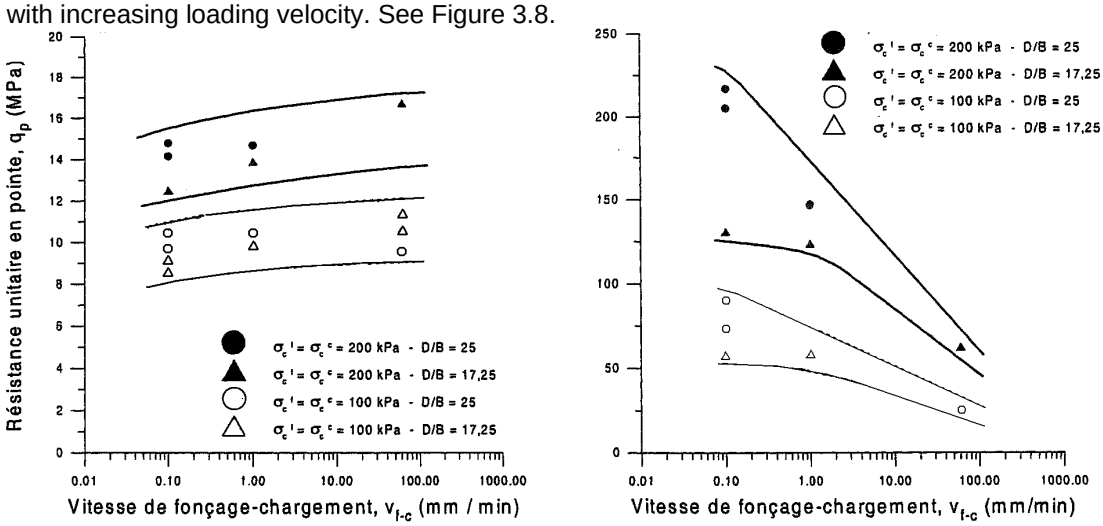

Figure 3.8 Loading rate dependence of the tip resistance and the shaft friction

Kimura and Boonyatee (2002) did several statnamic model tests on friction piles and end bearing piles in sand. The test setup consists of a statnamic loading device with pre-compressed air. Two types of tests were conducted on the two different pile types, namely small loads and large loads. The small loads were used to determine the initial stiffness and the large loads for obtaining the ultimate capacity. The soil consists of sand with D_{60} of 310 μm and a D_{10} of 120 μm with a relative density of 59.6 %. They concluded that due to dynamic resistance a time lag exist between the maximum displacement and the loading peak and this also accounts for the difference between statnamic and static loading. The damping coefficient in the UPM method for end bearing piles out of the model tests is constant while for friction piles only a constant damping coefficient is found when the magnitude of the loading force is not close to the ultimate resistance (thus forcing of plastic deformations).

3.5 Comparison

When all results are summarized in a table for the soil tests (Table 3.1) and a table for the interface + model pile tests (Table 3.2) a couple of remarks can be made.

Authors	Test type	Sand samples	Results	V_{min}	V_{max} (mm/s)
Casagrande & Shannon (1948)	Vacuum triaxial compression	Dry Manchester sand	10% increase in strength	?	200
Seed & Lundgren (1954)	Drained and undrained triaxial tests	Dense saturated Loose saturated	15-20% increase may be decreased	0.016	1000
Whitman & Healy (1962)	Drained and undrained triaxial tests	Dense saturated Loose saturated	10% increase in drained strength 100% increase in undrained strength	- (Tmax = 5 min)	500
Schimming, Haas & Saxe (1966)	Direct shear test	Dry sand and Saturated sand	Almost no loading rate effect	- (Tmax = 50 s)	- (Tmin = 1-5 ms)
Gibson & Coyle (1968)	Undrained triaxial test	Fine saturated Coarse saturated	50% >100%	0	3600
Lee, Seed & Dunlop (1969)	Triaxial compression	Loose dry Dense dry	7% increase up to 20% increase	0	220
Farr (1990)	Uniaxial strain	Partially saturated	up to 100%	- (Tmax = 155 s)	- (Tmin = 0.4 ms)

Table 3.1: Overview of soil tests

Two types of rates can be recognized a variation of the loading time or time to failure and a variation in the applied loading velocity.

The values presented in table 3.1 cannot be plotted, because only the dry tests are of interest, and for a proper presentation both the minimum and the maximum velocity are needed (in that case the velocity range wherein the authors have done their research is more detailed) only one test is left.

A wide range of velocities can be distinguished, ranging from more or less static till dynamic loading. When the results of Al – Mhaidib and De Gennaro are studied closer even the 'fast' tests are more or less static. For a better comparison the velocities are normalized with the diameter of the pile.

When this comparison is made the influence of void ratio, confining pressures, sand type, dilatancy behaviour, scale effects and preparation problems aren't considered, or believed to be negligible for the time being.

Authors	Test type	Sand samples	Results when loading rate is increased	D_{pile} (mm)	v_{min} (D_{pile}/s)	v_{max} (D_{pile}/s)
Jetzequel (1969)	Penetrometer test	Medium dense	8% increase above water table 17% increase below water table	36	$5.56 \cdot 10^{-2}$	$5.56 \cdot 10^{-1}$
Brumund et al (1973)	Shear between two types of materials	Interface testing	20% increase of wall friction	n/a	- (Tmax = 5 min)	- (Tmin = 1 ms)
Dayal and Allen (1975)	Penetrometer test	Loose Dense	No increase No increase	36	$3.61 \cdot 10^{-2}$	$2.25 \cdot 10^{1}$
Heerema (1979)	Soil – steel interaction	Interface testing	No increase	Eq. D of ~50 mm	n/a	n/a
Horvath (1991)	model pile	Medium Dense	Increase of 10%, sharp transition in soil behaviour when loading duration <2s.	12.7	- (Tmax = 300 s)	- (Tmin = 50 ms)
Eiksund and Nordal (1996)	model pile	Dense	No increase (actually <5%)	63.5	$1.26 \cdot 10^{-2}$	$1.73 \cdot 10^{1}$
Al – Mhaidib (1999)	model pile	Loose Medium Dense	up to 50%	30	$2.77 \cdot 10^{-5}$	$5.57 \cdot 10^{-4}$
De Gennaro (2001)	model pile	Medium	Increase of tip resistance Significant decrease of shaft resistance	20	$8.35 \cdot 10^{-5}$	$5.00 \cdot 10^{-2}$
Kimura (2002)	model pile	Dense	No Increase	24	$1.04 \cdot 10^{-3}$	5.21

Table 3.2 Overview of the loading rate dependent results of the interface and pile tests

Two types of graphs are presented:

1) Figure 3.9a Influence of increase of loading velocity on tip resistance during the pile system tests. Or total force, when tip resistance isn't specified. From each individual test a line containing of v_{min} and v_{max} is plotted. Also a cumulative curve is plotted this curve consists of all superimposed results and is depicted in 3.9b.
2) Figure 3.9c Influence of increase of loading velocity on shaft friction during the pile system tests, unfortunate in those tests the interface tests couldn't incorporated properly.

The T/T_0 values are also not plotted.

Out of the first two graphs it becomes apparent that a rate effect exists even in cohesionless soil. The strength ratio F/F_0 is >1 for several authors and decreases when it is shifted in a higher velocity range.

When the hypothesis is made that all results are comparable, implying that material type (sand) is the major contributor for the soil behaviour, a cumulative curve of all results can be compiled. A very interesting global overview over a wide velocity range is obtained. For velocities of v > ~0.0008 D_{pile}/s more or less a continuous curve is found this curve can be approximated by a straight line (trend) at logarithmic scale. Per decade an increase of ~10 % is found. The interception of this line is uncertain, because the 50 % increase in strength which is found by Al – Mhaidib is questionable because of the large deviation from the other authors.

For the shaft friction no clear tendency is found, partly due to the absence of results from literature and partly by the variance in the results of the different authors. Also the results of Heerema are incorporated by introducing an estimated equivalent D_{pile} just to extent the comparison, but the legitimacy can be questioned. This results in the need for further research in the rate effect of the shaft friction.

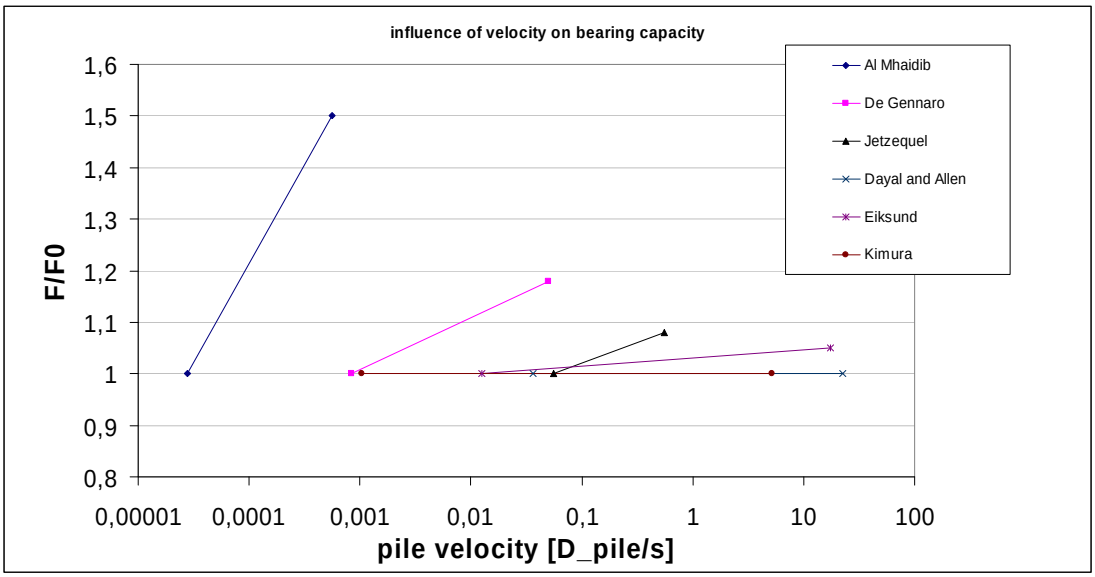

a) pile-soil interaction tip resistance individual results (table 3.2) velocity in D_{pile} /s

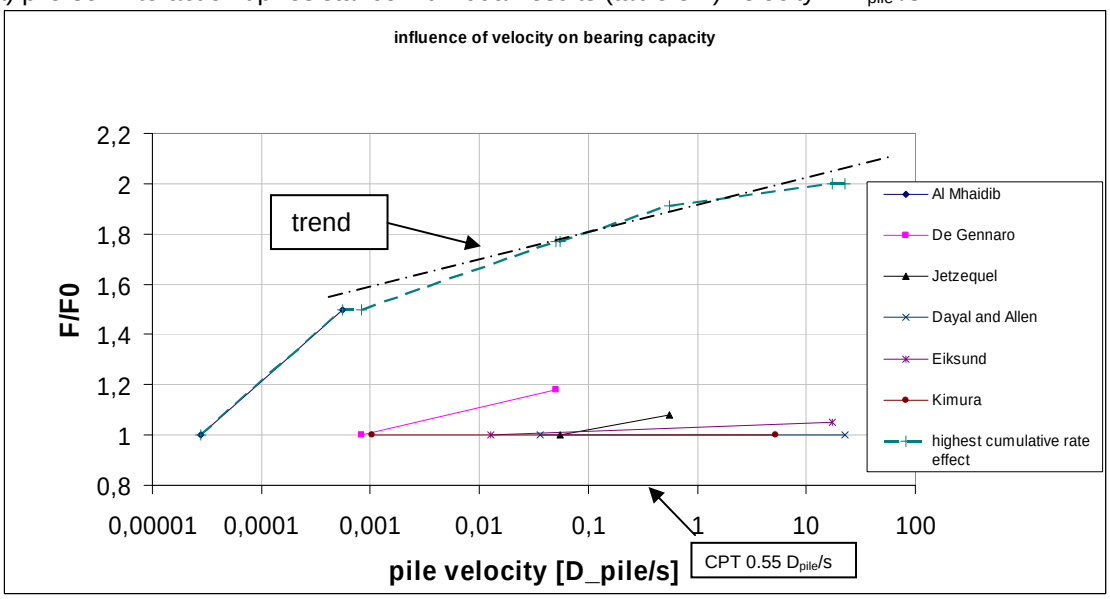

b) pile- soil interaction tip resistance v in D_{pile} /s including cumulative curve

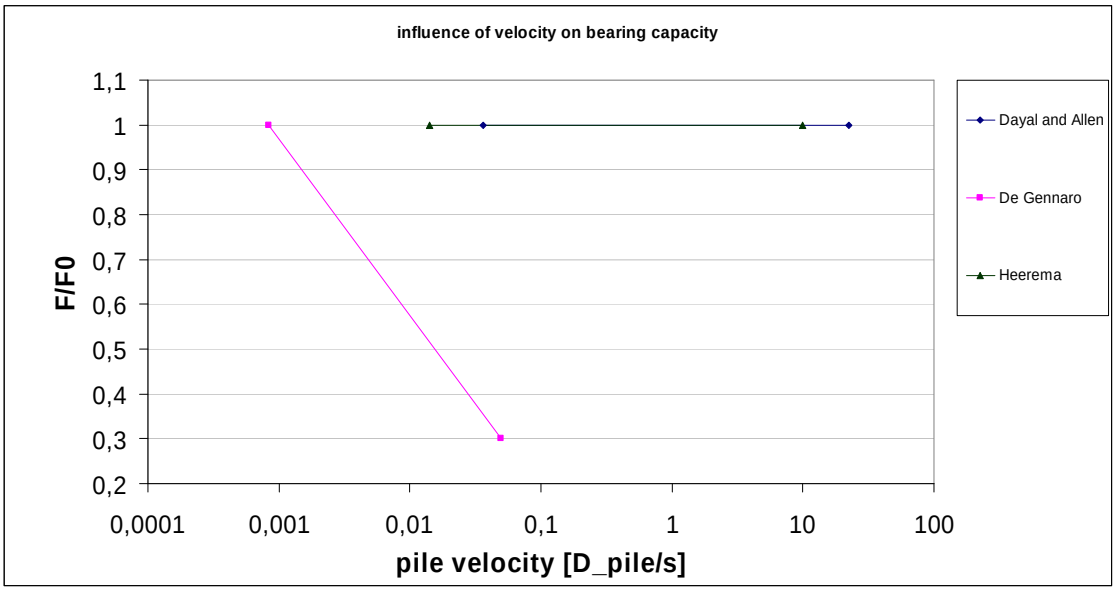

c) pile-soil interaction shaft friction individual results (table 3.2) velocity in D_{pile} /s
Figure 3.9a-c Comparison outcome of literature

3.6 Conclusions

- For the soil tests on cohesionless soil a structural increase of about 10-15 % in strength is found when the velocity is increased or the time to failure is decreased. Not enough data from literature is found to form a general trend for dry sand.
- For the tip resistance or the total resistance during model pile tests (when no differentation into tip or shaft is given) a tenfold increase of $v_{pile} > 0.0008*D_{pile}/s$, possibly gives a smaller increase in bearing capacity then a tenfold increase of $v < 0.0008*D_{pile}/s$. For $v_{pile} > 0.0008*D_{pile}/s$ the trend gives about 10 % /decade.
- The differences in the influence of the rate on the shaft friction during model pile tests are huge (factor 3) and needs further investigation. The lack of proper tests only enlarges this effect.

4. Scaling of the in-situ dynamic and statnamic load

4.1 Introduction

In this chapter some background theory is used to investigate the scaling of the in-situ dynamic and statnamic load. First some additional information about the shape of the in-situ dynamic and statnamic load is given. Subsequently a model of the loading mechanism is given and the scaling of the model's parameters is discussed. Finally, the implementation of the model problem is elaborated and thus the range of the sensors can be determined.

4.2 In-Situ load

A typical force-time diagram of the loading during a statnamic test is shown in Figure 4.1 [Middendorp, 1992]. The typical dynamic load is depicted in Figure 4.2 [Middendorp, 1992]. The magnitude of the force depends on the weight of the reaction mass, the volume and shape of the cylinder and the amount and type of fuel (see fig. 4.3) [Brown, 2002]. As rule of thumb in in-situ situations this mass is chosen at about 5-10% of the design strength of the pile under test.
The distribution of the force over time, as seen in Figure 1, determines the loading rate. When a model pile is loaded and the time distribution is the same, the loading rate will alter, because the force differentiated with respect to time is the loading rate. The time has to be scaled the same way the dimensions are scaled, to obtain a similar force-dt ratio, the loading rate.

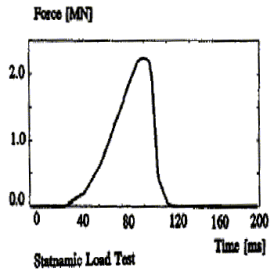

Figure 4.1: Typical force-time diagram for statnamic loading

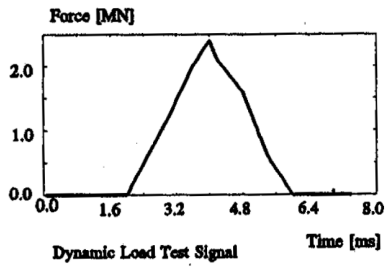

Figure 4.2: Typical force-time diagram for dynamic. load

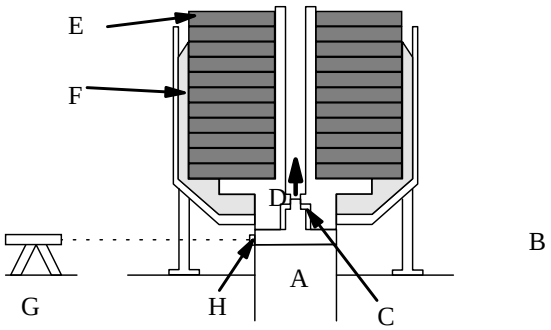

A, Pile
B, Load cell/fuel chamber
C, Pressure chamber
D, Load hanger/silencer
E, Reaction Mass
F, Gravel catch mechanism
G, Laser source
H, Laser sensor

Figure 4.3: Schematic of the statnamic device

The easiest way to get the order of magnitude of the force is out of old CPT-data of the geotechniek test tank [Broere, 2001]; his work indicates for the pile capacity an order of magnitude of ~5 kN tip resistance and ~2 kN shaft resistance. The distribution over time has to be derived out of Figure 4.1 and 4.2.

4.3 The model

4.3.1 Theoretical model

Of course it isn't trivial to copy the in-situ loading scheme, but for a simplified situation a model is derived [Hölscher, 1996] to estimate the initial velocity-time and initial force-time relationship.
In Figure 4.4 the model is schematized. The following equations are found for the pile head velocity (v). The force F is obtained after multiplying the velocity with the pile impedance Z_p.

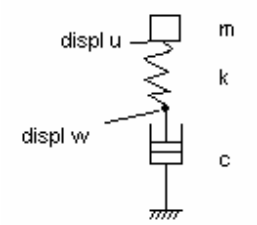

Figure 4.4: Schematic representation

$$w(t) = \frac{2av_0}{a^2+h^2}\left\{1-\left(\cos ht + \frac{a}{h}\sin ht\right)e^{-at}\right\}$$

$$\frac{dw(t)}{dt} = v(t) = \frac{2av_0 e^{-at}\left(h^2+a^2\right)\sin(ht)}{\left(a^2+h^2\right)h}$$

with

$$a = \frac{k}{2c}; h = \frac{k}{2c}\sqrt{\frac{4c^2}{mk}-1}$$

The force will be: $F(t) = Z \cdot v(t)$, where the pile impedance Z_p is calculated with the following expression: $Z_p = \frac{E_s A_p}{c_w}$. In this expression c_w is the wave velocity in the pile, this velocity can be calculated with the following expression: $c_w = \sqrt{\frac{E_s}{r_s}}$.

The following quantities have to be known:

-mass of the ram	m	[kg]
-initial velocity of the mass	v_0	[m/s]
-the spring stiffness	k	[N/m]
-damper coefficient	c	[Ns/m]
-young's modulus of steel	E_s	[N/m^2]
-section surface	A_p	[m^2]
-wave velocity in the pile	c_w	[m/s]
-the volumetric mass of steel	ρ_s	[kg/m^3]

The following properties of the model pile have to be converted in this problem:
Steel tubular pile with a section surface A_p of 7.63 cm^2 and length L_p of 2.5 m.[1]
Because it is a steel pile, the Young's modulus of steel and the volumetric mass of steel are needed: E_s= 210 GPa
ρ_s= 7850 kg/m^3

[1] The length is determined by the dimensions of the geotechniek test tank

4.3.2 The mass of the ram m

In the in-situ case for the dynamic load the mass is estimated at ~1-2% of the bearing capacity and for the statnamic load the mass is estimated at ~5-10% of the bearing capacity.
The bearing capacity in the geotechniek calibration chamber is, as mentioned earlier, about 7 kN.
The resulting estimated mass is:

m=10 kg for the dynamic case
m=70 kg for the statnamic case

4.3.3 Initial velocity of the mass v_0

The initial velocity is derived for the situation without air resistance. In this case all potential energy is converted in kinetic energy. The following equation can be formulated:

$$mgh = \frac{1}{2} m v_0^2$$

$$v_0 = \sqrt{2gh}$$

with:
h = drop height [m]
g = acceleration of gravity [m/s^2]

The drop is varied during the calculation process within reasonable and practical executable, range, to acquire an initial velocity which alters the magnitude of the maximum force.

4.3.4 The spring stiffness k

The spring stiffness is varied during the calculation process to obtain a scaled force-time plot of the dynamic loading and the statnamic loading.

4.3.5 Damper coefficient c

The damper coefficient can be calculated with the following formula:

$c = A_p \sqrt{E_s r_s}$ with:

A_p= surface of pile section	7.63	cm^2
E_s= young's modulus of steel	210	GPa
ρ_s= volumetric mass of steel	7850	kg/m^3

This results in a damper coefficient c of $3.1 \cdot 10^4$ Ns/m. This value is the same as the pile impedance Z_p.

4.3.6 Wave velocity in the pile c_w

The expression to calculate the wave velocity is already given:

$$c_w = \sqrt{\frac{E_s}{r_s}}$$ with:

E_s = 210 GPa
ρ_s = 7850 kg/m^3

the wave velocity c_w becomes 5172 m/s.

4.4 The scaled model problem

4.4.1 Results of the scaling

For linear scaling the in-situ case to the model conditions, the base scaling parameter is chosen as the dimension. All other quantities which are related to the dimensions are scaled as well. The influence of the dimension on the way the other quantities have to be scaled is derived in Appendix B. The in-situ situation is called the prototype (subscript p) and the model is indicated by subscript m. The results are listed below. Problems occur, as can beseen in Appendix B not all scale rules are consistent.

$$h_p = n \cdot h_m$$
$$A_{p;p} = n^2 A_{p;m}$$
$$m_p = n^3 \cdot m_m$$
$$v_{o;p} = \sqrt{n} \cdot v_{0;m}$$
$$t_p = \sqrt{n} \cdot t_m$$
$$s_p = n \cdot s_m$$
$$F_{\max;point;p} = n^3 \cdot F_{\max;point;m}$$
$$F_{\max;shaft;p} = n^3 \cdot F_{\max;shaft;m}$$
$$k_p = n^2 \cdot k_m$$
$$c_p = n^2 \cdot c_m$$

The major scaling problem is the fact that sand is a non-linear material of which the strength and stiffness properties are dependent on the stress conditions. When only the dimensions are scaled the stress alters, so the strength and stiffness are also altered, this results in different material behaviour. Therefore the mobilized friction and tip resistance are not scaled properly. If the stress conditions are similar, by scaling the acceleration of gravity and the dimensions in a geo-centrifuge, all scale rules for the other quantities are consistent. This can be seen in Appendix C.

The chosen model boundaries in 1g conditions are not ideal and render the interpretation of the results more difficult.

4.4.2 Choosing the scaling parameter n

To obtain the scaling parameter n, the base quantity (the dimension) has to be scaled out of the in-situ case. A typical pile has dimensions of 320 mm x 320 mm. Or a point surface of $1.024 \cdot 10^5$ mm^2. The surface of the CPT-cone is $1 \cdot 10^3$ mm^2, thus the ratio of the surfaces is

$A_p : n^2 A_m \rightarrow 102.4 : n^2 \rightarrow n = 10$.

The resulting time scale is therefore $t_m = \frac{1}{\sqrt{10}} \cdot t_p$ .The t_p can be derived out of Figure 1 and Figure 4.2. Figure 1 is a quite optimistic curve for the statnamic load. A typical duration of a statnamic load is about 70 ms this pulse-width is measured on the x-axis. A typical pulse-width of the dynamic load is ~4 ms. therefore the pulse duration for the statnamic and dynamic case becomes:

$t_{m;statnamic}$ = 22 ms.
$t_{m;dynamic}$ = 1.3 ms.

The statnamic pulse can be considered statnamic if the wavelength of the pulse is larger then the pile length, or the duration of the pulse much longer then the wave is travelling in the pile:

$$t >> \frac{2l}{c_w}$$

In practice >> can be translated in >12 times. In the case of a 2.5 m long model pile which consists of steel this is the case:

$$\left.\begin{array}{l} 0.022ms >> \dfrac{2 \cdot 2.5m}{5172m/s} \\ 0.022 >> 0.001 \end{array}\right\} \frac{2l}{c_w} =\sim 22 \cdot t$$ The pile is behaving pseudostatic.

4.4.3 Scaling of the target force

To copy the loading pulse of the in-situ problem in the model problem, the peak value of the force has to be known. This value can be derived out of the expression for impulse, the intermediate behaviour is not described by this expression:

$$\mathbf{r}\ \vec{p} = \int \vec{F} dt = mv_{pre} - mv_{post}$$

with

$$\mathbf{r}\ \vec{F} = Z_p \vec{v}$$

becomes

$$\mathbf{r}\ \vec{p} = \int Z_p \vec{v} dt = Z_p \int \vec{v} dt$$

$$\mathbf{r}\ \vec{p} = Z_p (w(t_{post}) - w(t_{pre}))$$

$$\mathbf{r}\ \vec{p} = Z_p \Delta w$$

In which m = the mass used for the test, v_{pre} and v_{post} the velocities of the mass before and after the interaction with the pile, Z_p = pile impedance, w = the displacement of the pile.

As seen in the above equation the pulse is determined by the pile impedance and the total displacement. So the target force is chosen such the scaled displacement is reached, because the pile impedance is unchanged. In-situ the displacement during pile driving (dynamic case) and statnamic testing is O(cm), so the scaled displacement is in the order of mm for both cases. But to get failure of the soil, at least a displacement as large as 10-20% of the pile diameter needs to displace, this results in a displacement of about 3-6 mm. This condition is easily reached in the statnamic case, for the dynamic case however this condition in combination with the used model gives unobtainable situation (negative square root of eta with high spring stiffness). So another solution of the model has to be adopted, but even with the stiff spring model (see paragraph 4.5.2) the maximum displacement is limited to 1 mm. When an empiric expression for pile driving is used (appendix D) the results seem conservative, because with the empiric relationship larger deformations are expected.

4.5 The calculation

4.5.1 Target curve:

To obtain the force-time relationship the above mentioned formulae are implemented in a spreadsheet for several time steps. All things considered the force-time diagrams can be calculated by varying the k and h. The h is only influencing the magnitude of the force, while k influences the magnitude of the force and the time dependence. All other parameters are held constant. For the dynamic case the target time-scale is 1.3 ms and the target displacement is

6 mm while for the statnamic case the target time-scale is 22 ms and a displacement of also 6 mm. In Figure 4.5 the force-time diagram is depicted, while in Figure 4.6 the displacement-time diagram is shown. The used parameters are summarized in Table 4.1.

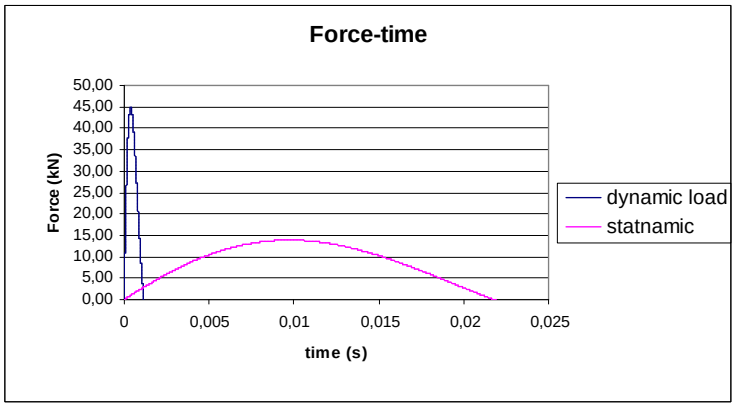

Figure 4.5: force-time diagram for dynamic and statnamic loading

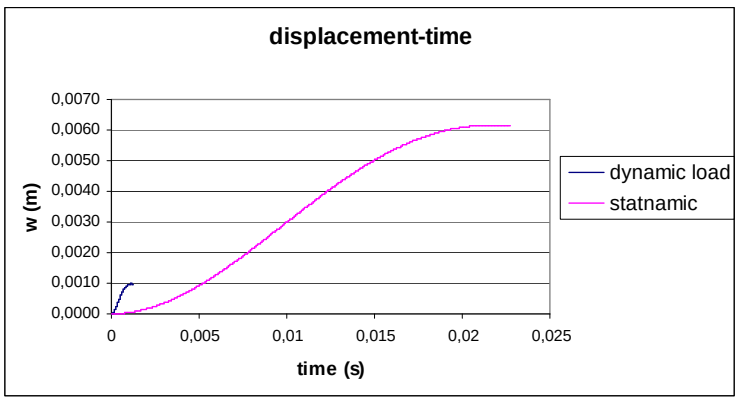

Figure 4.6: displacement-time diagram for dynamic loading and statnamic loading

	quantity	dynamic	statnamic
drop height	h [m]	0.35	0.15
accel. of gravity	g [m/s2]	9.81	9.81
mass	m [kg]	10	70
damper	c [Ns/m]	3.10E+04	3.10E+04
spring stiffness	k [N/m]	1.00E+08	1.50E+06
initial velocity	v0 [m/s]	2.62	1.71
vol. weight steel	ρs [kg/m3]	7850	7850
elast steel	Es[kN/m2]	2.10E+08	2.10E+08
pile surface	Ap[m2]	7.63E-04	7.63E-04
wave velocity	cw [m/s]	5172	5172
pile impedance	Zp [kNs/m]	30.98	30.98

Table 4.1: Overview used parameters.

4.5.2 Variance in the k

The influence of the k on the total duration T and the maximum force is given in Table 4.2, these values are calculated in the same way as in 4.5.1 only no target curve is set. The results are depicted in Figure 4.7. During the calculation all other variables are held constant.

type model	k (N/m)	Fmax (kN)	T (ms)
soft spring	2,50E+05	6	53
	5,00E+05	9	38
	7,50E+05	10	31
	1,00E+06	12	27
	1,25E+06	13	24
	1,50E+06	14	22
	1,75E+06	15	20
	2,00E+06	16	19
	2,50E+06	17	17
	5,00E+06	22	13
	7,50E+06	24	11
	1,00E+07	27	9
	1,25E+07	28	8.7
	1,50E+07	30	8
	5,00E+07	39	7
stiff spring	1,00E+08	42	7
	2,50E+08	47	6.7
	5,00E+08	49	6.5
	1,00E+09	50	6.5
	1,00E+10	52.7	6.5
Infinite stiff spring	∞	53.2	-

Table 4.2 Variance in k

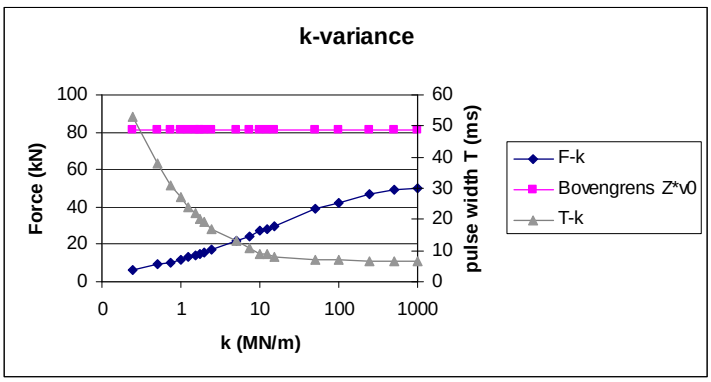

Figure 4.7 F-k and F-T (k plotted on logarithmic

As seen in the Figure above, with increasing spring stiffness the force increases, while the total duration of the pulse decreases. When the stiffness of the spring passes the value of ~$5 \cdot 10^7$ N/m the solution of the model is going from a solution in which the spring is dominating to a solution in which the damper is dominating.

Because in the expression for ω the square root is becoming negative if the spring stiffness k is

$$k > \frac{4 \cdot c^2}{m}$$

$$k > 5.4 \cdot 10^7 \, N/m$$

where:

the spring stiffness	k	[N/m]
mass of the ram	m = 70	[kg]
damper coefficient	c = $3.1 \cdot 10^4$	[Ns/m]

Therefore a model for stiff springs is needed Hölscher derived for this special case:

$$w(t) = \frac{2av_0}{a^2 + b^2}\left\{1 - \left(\frac{a + w}{2w}\right)e^{(-a+w)t} + \left(\frac{a - w}{2w}\right)e^{(-a-w)t}\right\}$$

$$\frac{dw(t)}{dt} = v(t) = \frac{2av_0}{a^2 + b^2}\left\{\left(\frac{a^2 - w^2}{2w}\right)e^{(-a+w)t} + \left(\frac{a^2 - w^2}{2w}\right)e^{(-a-w)t}\right\}$$

with

$$a = \frac{k}{2c}; w = \frac{k}{2c}\sqrt{1 - \frac{4c^2}{mk}}$$

When the spring stiffness is taken very high, the solution is converging to the solution of pile driving. Namely the initial velocity of the mass multiplied with the pile impedance (the expression $Z_p \cdot v_0$).

5. Loading mechanism and measuring set-up pseudostatic

5.1 Introduction

In this chapter the design considerations of the loading mechanism and measuring setup for the pseudostatic case will be discussed. It is important to combine those two functions of the test setup, interaction between the loading mechanisms and measuring setup needs to be tuned. First the loading setup will be discussed subsequently the measuring setup will be treated. Larger versions of the drawings can be found in appendix M.

5.2 Loading mechanism

Out of the preliminary calculations the following conditions for the loading mechanism are distilled:

$k = 1.5 \cdot 10^6$ N/m
m = 70 kg
h = 15 cm

First the realization of the spring will be discussed, next the mass and finally the drop height.

5.2.1 The spring

The resulting k is implemented in the set-up, to obtain the type of material and thickness for the implementation of the spring. The following expression can be used to calculate the thickness (d) of the spring:

$$k = \frac{EA}{d}; d = \frac{EA}{k}$$

When is chosen for a wooden block, with a typical young's modulus (E) of 10 GPa the needed thickness for the dynamic case becomes 0.08 m and for the statnamic case 6.7 m those dimensions are not practical. Thus another type of material or cross-section has to be found. In this case the cross-section cannot be changed, thus another type of material is needed. When is chosen for PVC (E=800 MPa[1]) the thickness (d) is 7 mm for the dynamic case, but still 0.53 m for the statnamic case, thus PVC will be sufficient for the spring in the dynamic case. While another material for the spring is needed in the statnamic case. When a nature rubber is used (E=~10 MPa[2]) the thickness of the material (d) becomes 7 mm for the statnamic load. By using a rubber the strength parameters cannot cope with the massive force, the mass will pierce the material. Therefore a mechanical spring is chosen, those springs can handle large forces more easily.

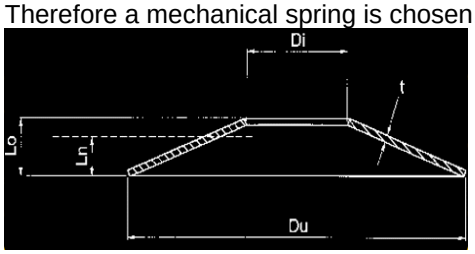

Figure 5.1 Disc spring

[1] Source: polytechnisch zakboekje
[2] A mean value for the young's modulus of rubber is very hard to determine therefore this value is imprecise

Of the mechanical springs, the disc spring (see Figure 5.1) is the most robust and compact spring money can buy. These springs can resist high loads in combination with a relative small displacement. Another advantage is the compact size of these springs. Several of these springs can be combined into one new spring, which results in the fact that almost any spring stiffness can be chosen.

When linear spring stiffness is required the disc springs can be stacked in two ways. This can be seen in Figure 5.2. On the left the springs are stacked to increase the maximum force, while the displacement is not changing, or the spring stiffness k is scaled up:

$$k = \frac{nF}{L_0 - L_n}$$

with:

k	= spring stiffness	[N/mm]
F	= maximum force	[N]
L_o	= initial height	[mm]
L_n	= height when loaded	[mm]
n	= amount of springs	[-]

When the spring stiffness needs to be decreased the stacking as depicted in Figure 5.2 on the right is used. In this case the displacement is increased while the force is kept constant.

$$k = \frac{F}{n(L_0 - L_n)}$$

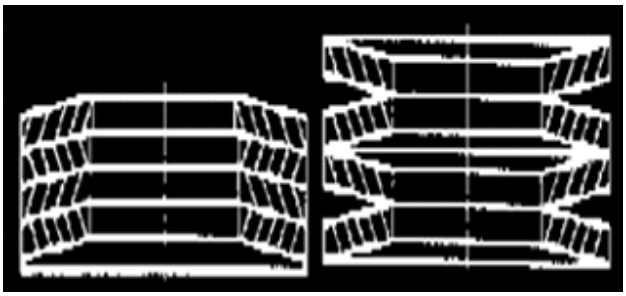

Figure 5.2 Stacking of the disc spring

The firm Tevema has several of these springs in stock. When the condition is met two types of springs are selected:

5 pieces of S84370 (D_o = 112 mm; D_i = 57 mm; L_o = 7.2 mm; L_n= 4.8 mm; F = 18 kN) special stacked to increase the maximum displacement and lower the stock stiffness. See stacking on the right in Figure 1. Price is € 5.40/each

4 pieces of S84390 (D_o = 125 mm; D_i = 51 mm; L_o = 8.2 mm; L_n = 5.1 mm; F = 20 kN) also special stacked. € 8.08/each

The best way disc springs can be stacked is to guide them on a rod or in a tube. When a spring is loaded the diameter of the spring is increasing, thus some clearance is needed. DIN 2093 is recommending the values stated in table 5.1. If a stack of springs is utilized these springs need a pretension force so the springs mobilize their stiffness at once.

D_i or D_o [mm]	Clearance [mm]
0 - 16	0.2
16 - 20	0.3
20 - 26	0.4
26 - 31.5	0.5
31.5 - 50	0.6
50 - 80	0.8
80 - 140	1.0
140 - 250	1.6

Table 5.1 Clearance of disc springs

To be flexible in choosing the spring stiffness and considering the price of the disc springs the use of 5 pieces of S84370 is chosen in the design.

5.2.2 The mass

The mass has to have a total mass of 70 kg, when is chosen for steel, and a diameter of 115 mm (> D_o of the spring) the height becomes 859 mm. The aspect ratio is chosen such that the drop mass is not suspicious to trembling. Also in this case flexibility is paramount, thus the mass is composed of separate parts. To move the lump of steel around the crane at geotechniek can be used.

At geotechniek a mass is already available; it is rated at ~64 kg. Together with the spring assembly the total mass it 69 kg.The dimensions are: height 275 mm diameter 197 mm. Although it is not up to optimal specs with regards to the aspect ratio, it is usable for these tests.

5.2.3 The drop height

To obtain the needed drop height 0.15 meters will suffice, but to be able to vary the height 0.5 m will be chosen. So some flexibility is guaranteed. The guidance is realized with a tube of metal wherein the mass is falling. The pile has to be hit on axis; else bending waves occur, which hamper the interpretation. By drilling holes in the wall of the tube several drop heights can be executed.

5.2.4 The release mechanism

Some sort of mechanism has to be chosen to release the mass. At first a simple rod through the side of the tube into the mass seems sufficient. On one side of the tube only, to release simultaneous two rods is difficult, in practice there is always one rod released a moment later.

If a rod has to be removed the friction force between the rod and the mass is about 10% of the normal force (in this case the normal force is about 700 N) or 70 N. The same friction is mobilized in the wall of the tube, also 70 N. Thus it requires a total force of about 140 N to release the rod. To consistent reproduce this force is quite difficult if done manually.
If the wall friction is demobilized the total friction force will be halved. A special release mechanism is designed to achieve this. See the Figure 5.3 below. The rod has only contact with the mass. The vertical lever rolls and rotates around a point this generates less friction than the wall of the tube. The angle of the rod into the mass, gives a shorter lever, so the horizontal force component is smaller. The total length of the lever is larger than the height of the mass, so no drilling in the mass is needed. The mass is therefore situated between the two points of the release mechanism.

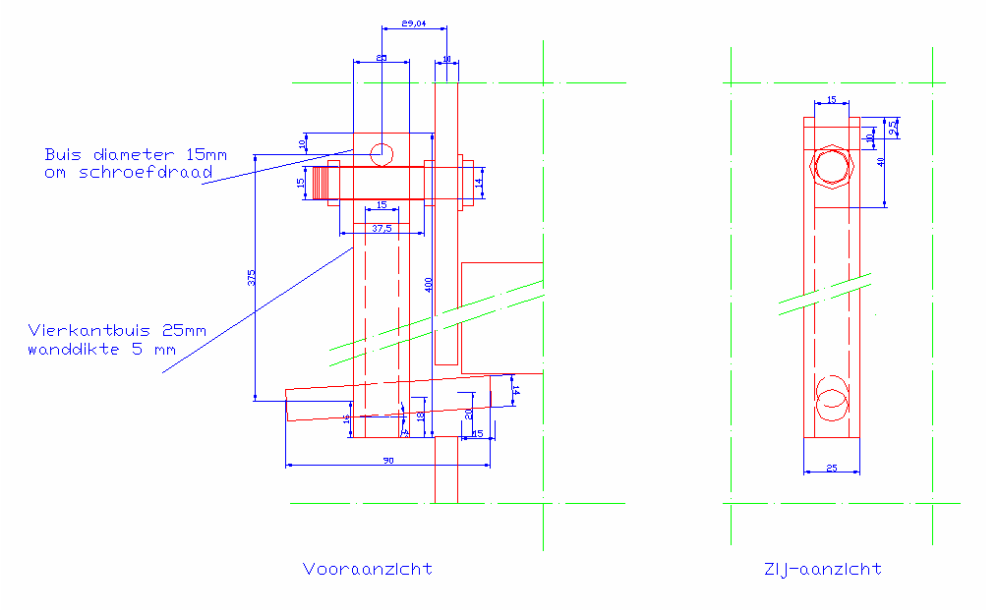

Figure 5.3 Release mechanism

5.2.5 Final design and costs

In Figure 5.4 the design for the spring drop mass mounting is drawn. This design facilitates the geotechniek drop mass with outer diameter of 195 mm and the S84370 disc springs. The springs are attached to the mass in such a way that the springs bear the force during impact. Actually a piece of square tubing will suffice. The total travel of the disc springs is about 12 mm, so the internal height of the square tube with the height of the bolt subtracted has to be >12 mm. All the holes in the metal are tapped, so the mass spring assembly can be dismantled.

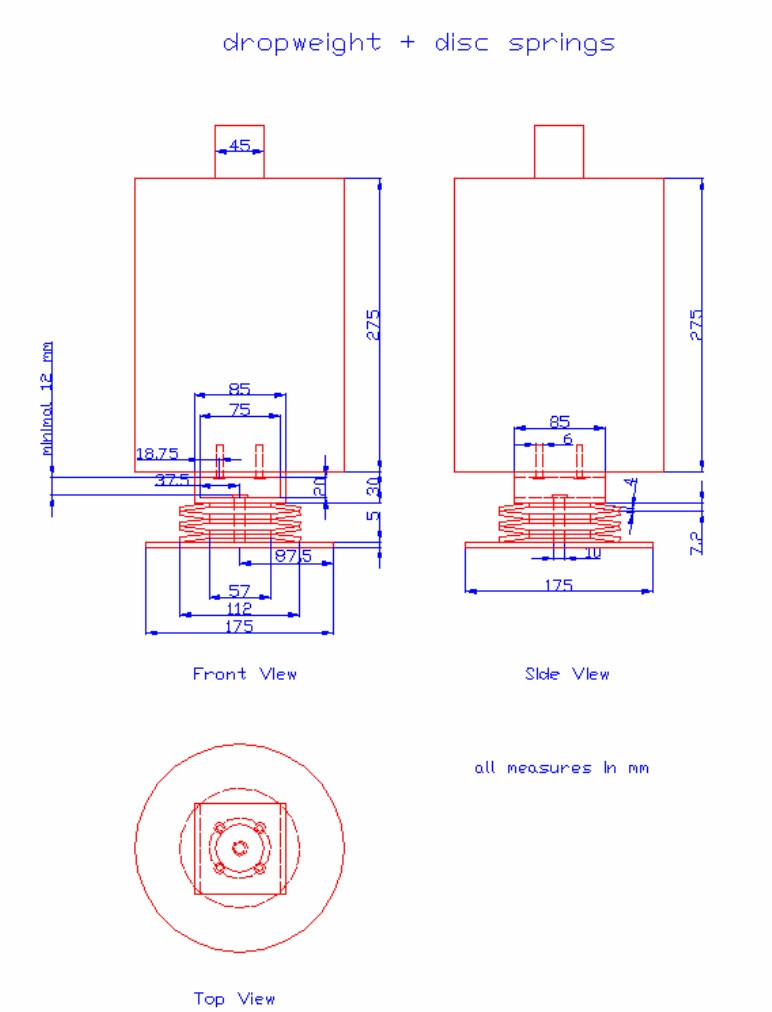

Figure 5.4: drop weight + disc springs

As earlier mentioned the drop mass needs guidance of some sort. A tube on the outside of the mass spring assembly is selected. The release mechanism is bolted against the tube.

The loading device needs to be mobile in all directions, because in all cases axial loading is of great importance. Two alternatives are given.

1) Bolt the guide tube directly to the beams across the calibration tank. The guide tube can be moved on the major beams which are bolted on the geotechniek test tank. To be able to bolt the guide tube on the beams a piece of L-bar can be used on 4 sides of the tube see Figure 5.6. The tube is also supported by the beams on which the tube is bolted down. A major drawback of this alternative is that the speed of the execution of the tests is hampered. To outline and bold the sub frame with great precision is difficult and sometimes even impossible to use all mounting holes.

2) Use the already available crane at geotechniek. The top side of the guide system can be hooked to the crane with chains or cables, the bottom of the guide tube can be mounted to the beams across the geotechniek test tank also with a cable. The cables have to be pretensioned, otherwise lateral movement is still possible, because the cables extend.

At first is chosen for the first solution, because it is quite easy to implement and the tube is supported by the beams, so compared to solution two a more secure solution is guaranteed. In Figure 5.5 a cross section is given in Figure 5.6 the top view is given, including the assembly on the beams.

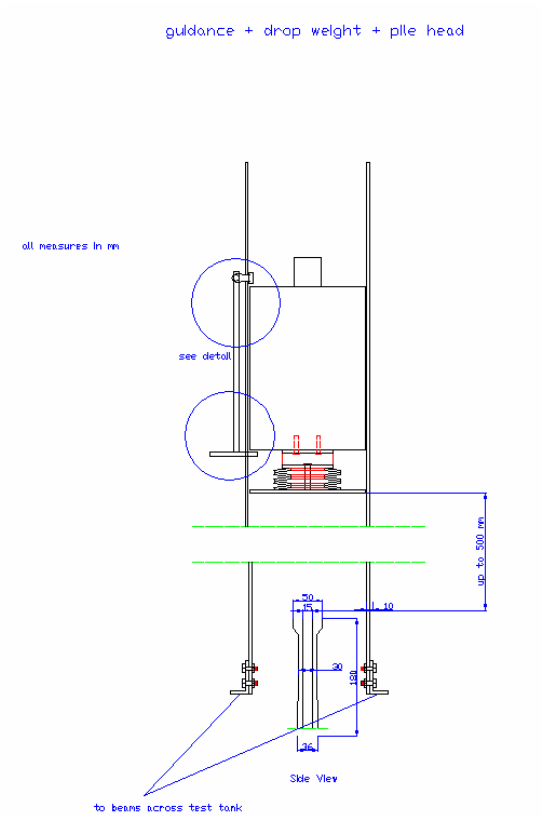

Figure 5.5: cross section of the guide system detail in Figure 5.3

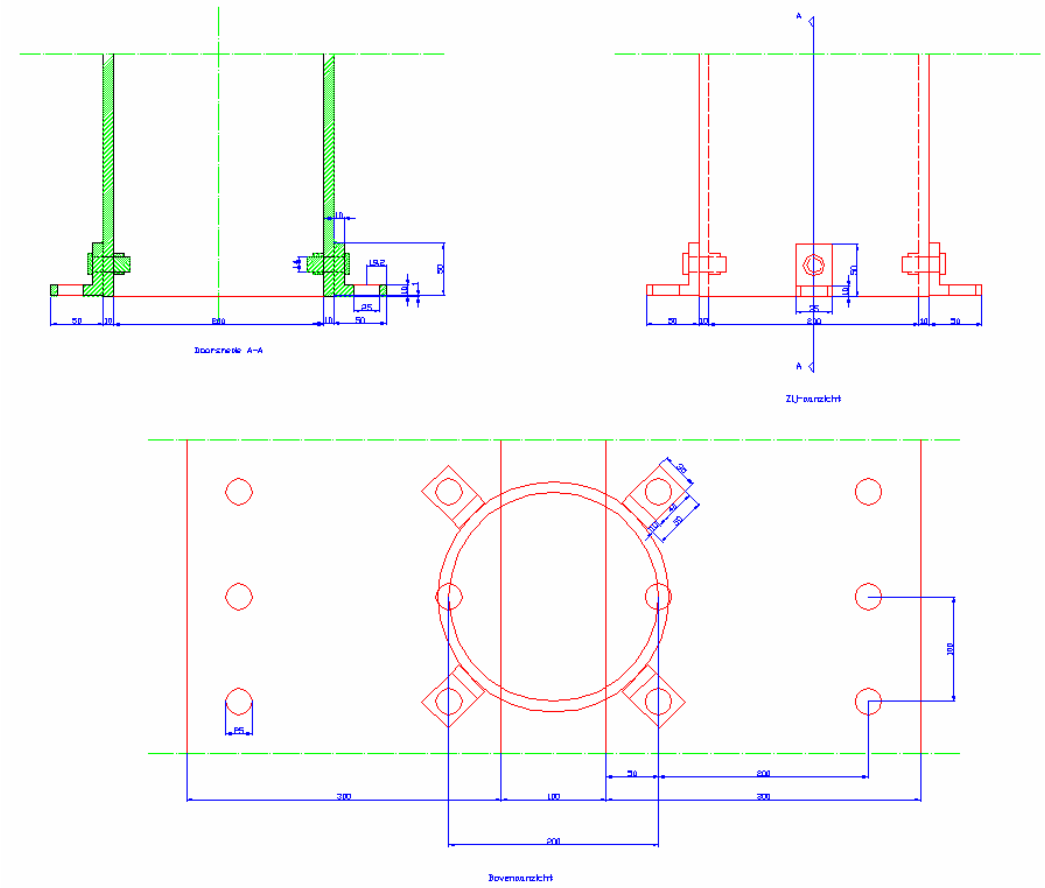

Figure 5.6 Top view of guiding tube

piece	mechanical work	comments	cost (€)
aluminium tube		Salomons Groningen	400
	drill holes	centrale werkplaats, because it has to be precise	100
L-bar	drill/mill holes/slots	Han/CW	150
release mechanism	drill/saw	home made from scrap pieces	0
disc springs		Tevema A'dam	50
	mount to mass	enough clearance for spring travel	50
mass		Geotechniek	0

Table 5.2 Overview of the mechanical costs

5.2.6 Rebound

The loading mechanism is loading the pile with a drop mass this mass is bouncing back after the pile is hit. A rebound can occur when the mass is not caught. The effects of the rebound on the interpretation of the results are discussed in this chapter.

First a definition of a pseudo static (or statnamic) load is given. The statnamic pulse can be considered statnamic if the wavelength of the pulse is larger then the pile length, or the duration of the pulse is much longer then the duration of the reflected stress wave in the pile:

$$t_{statnampulse} >> \frac{2l}{c_w}$$

In practice '>>' can be translated in 12 times. In the case of a 2.5 m long model pile which consists of steel this is the case:

$$\left.\begin{array}{l} 0.022ms >> \dfrac{2 \cdot 2.5m}{5172m/s} \\ 0.022 >> 0.001 \end{array}\right\} \frac{2l}{c_w} =\sim 22 \cdot t_{statnampulse}$$

The pile is behaving pseudo-static in other words as a rigid body. This does not mean that the soil is behaving static! Only the dynamic phenomena in the pile are negligible.

The pseudo static loading consists of the following procedure:

1) Load the pile statically with the weight of the intended drop mass
2) Load the pile with the drop mass from a prescribed drop height
3) repeat (2) several times until enough cycles are recorded

Record the displacement and force.

In the UPM method [Middendorp ,1992] 5 consecutive phases are recognized. See Figure 5.7:

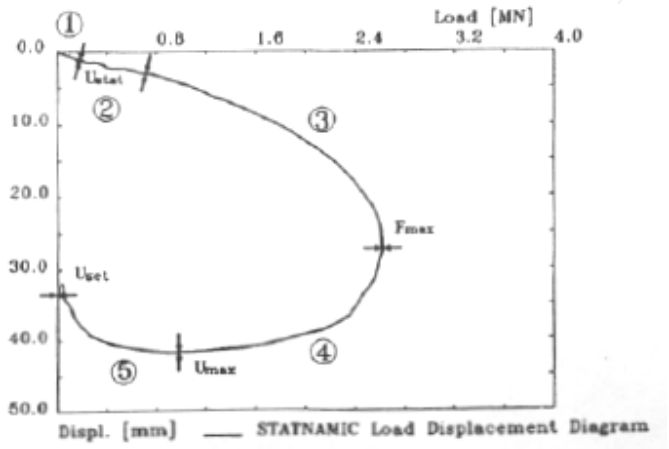

Figure 5.7 Statnamic load-displacement

1) Static behaviour because of the static loading of the pile with the drop mass.
2) The start of the statnamic loading (pile is hit) the soil reacts elastic, inertia and damping forces are acting on the pile.
3) The development of the static soil resistance until yielding of the soil the velocity and inertia effects are increasing. The maximum statnamic load is reached.

4) The decrease of the statnamic load, but the inertia of the pile still delivers displacement of the pile. The velocity decreases to 0, at the end of this period (t_{max}) the maximum displacement is reached. Because of zero velocity the damping is also zero. (the mass bounces back of the pile)
5) The static soil resistance overcomes all other forces and pushes the pile upwards. At the end of this area the final settlement is reached.

The rebound is of importance for phase 5, if the mass compared to the loading force is significant (>10%) the upward movement of the pile is limited or even non-existent. As a result the final obtained force - settlement curve is not a complete loading-unloading cycle.

Thus the rebound has to occur after the end of phase 5 or is very limited in magnitude, else the measurements are disrupted. A conservative estimate out of old data would be a time difference of at least 50% of the total pulse duration. In this case the duration is ~22 ms. so the rebound has to occur after 11 ms. Or the magnitude of the rebound force has to be insignificant compared to the maximum value of the primary loading pulse. 10% of the $F_{pulse;max}$ is about 1.5 kN.

The mentioned condition can be checked in the calculations, but the limitation of the analytical model is reached. The analytical model describes an infinite long pile while in reality it is not. If another analytical model is adopted, better rebound behavior can be estimated. In appendix E a derivation is been made for the 2-masses-spring-system, out of the calculations the drop mass pile behaviour can be estimated. The accuracy of the calculation is mainly dependent on the value for the soil stiffness. By the lack of an appropriate value for the soil stiffness the effect of a range of spring stiffnesses on the behaviour of the displacement of the drop mass is checked.

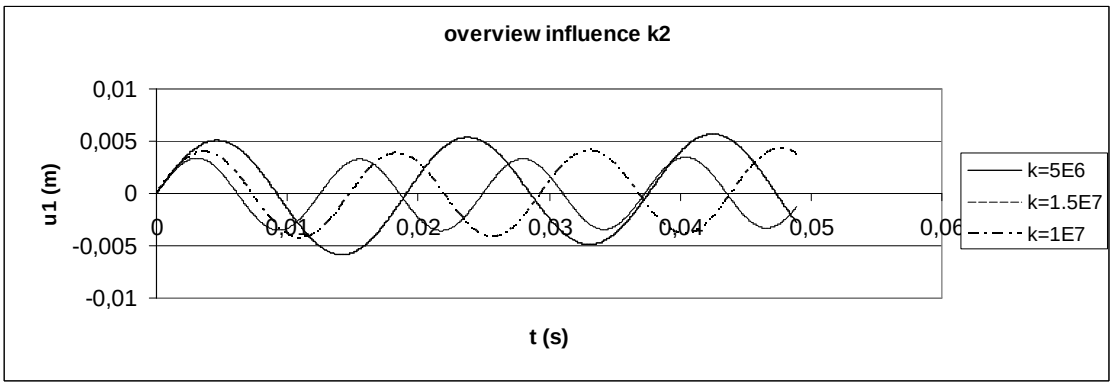

Figure 5.8 influence of k2 on the displacement of the drop mass

Also a limiting case where the value for k2 = infinite large, a 1-mass-spring-system, is evaluated. The resulting displacement of the drop mass is depicted in Figure 5.6.

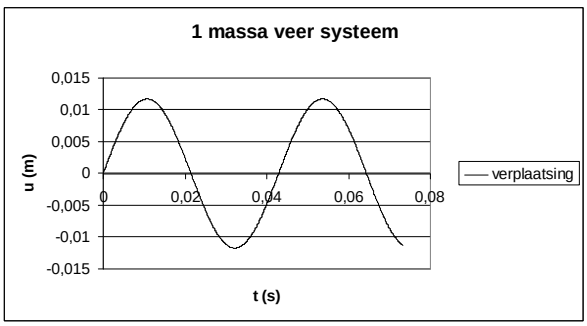

Figure 5.9 1 mass spring system displacement-time

Both calculations indicate a small rebound height. But in reality the spring is not coupled to the pile when the mass is moving upwards. Therefore the spring does not give a reaction force during the upward movement. The rebound occurs too early in this model.

Even in this conservative situation of the incomplete model the rebound is not an issue, thus when in practice the soil stiffness is high (one mass spring system) and the mass can bounce from the pile without constraints the rebound will be far enough in time.

Intermezzo

After the initial tests this is also the case!

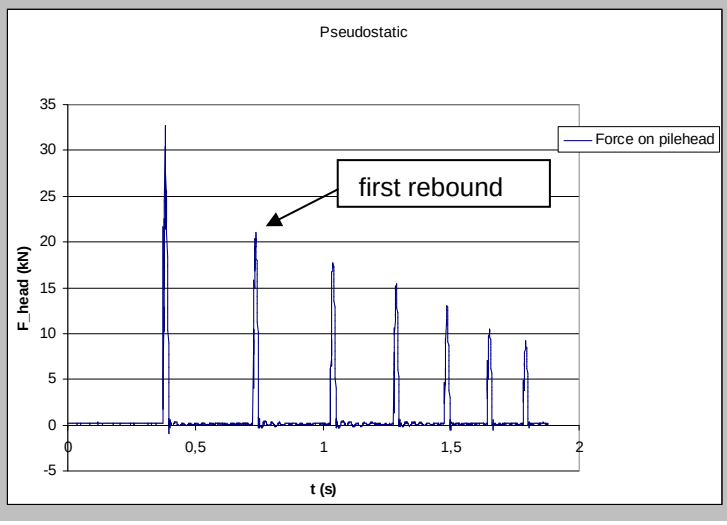

5.3 The measuring set-up

5.3.1 What to measure

The following quantities have to be measured.

Quantity	range
-Pile displacement	0-15 mm
-Pile velocity via acceleration	0-0.7 m/s
-Loading force via strain	0-20 kN compression force
-Shaft friction (in CPT cone)	0-4 kN compression force
-Tip resistance (in CPT cone)	0-10 kN compression force

(-water pressures)

The range is estimated out of the calculations of chapter 4. See paragraph 5.3.2 for a detailed explanation.

5.3.2 Range

In this paragraph the justification of the specs is elaborated. Not only is the physical range of importance, also the registration frequency and the sampling frequency are important topics to get the measuring set-up right. The sensors have to be 'fast' enough to keep up with the phenomena which are been measured. Not only the sensors, but also the amplifiers (which amplify the tiny signals of the strain gauges) and the AD-converter (which converts the analog signal of the sensors into the digital domain) have to keep up.

Sampling frequency

Strain gauges and amps

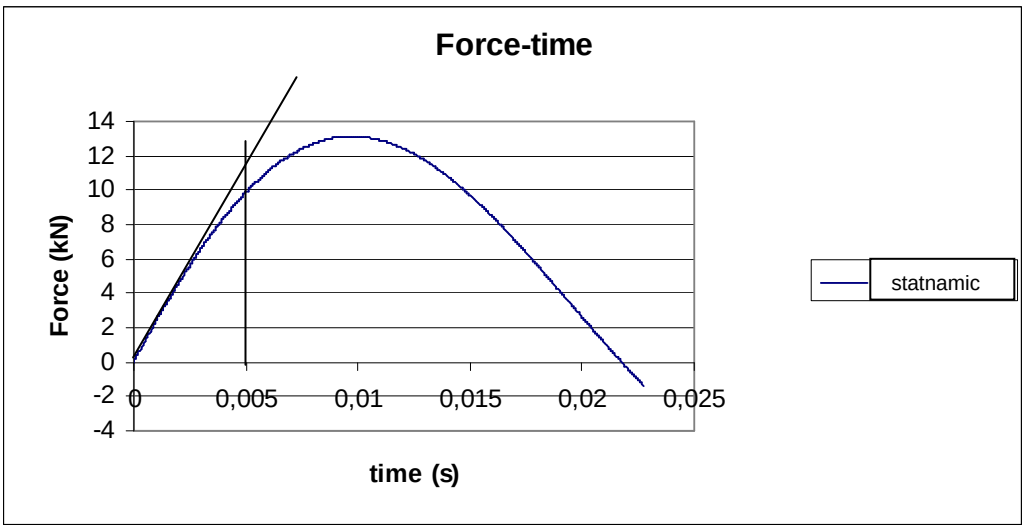

Figure 5.10 Force time diagram

The steepest line in Figure 5.10 has to be measured in at least 5 samples, thus:

$$dt = \frac{T}{n} = \frac{5ms}{5} = 1ms$$

$$f = \frac{1}{dt} = \frac{1}{1ms} = 1kHz$$

So the strain gauges and the accompanying amplifiers need at least a bandwidth of 1 kHz.

Acceleration device + amp:

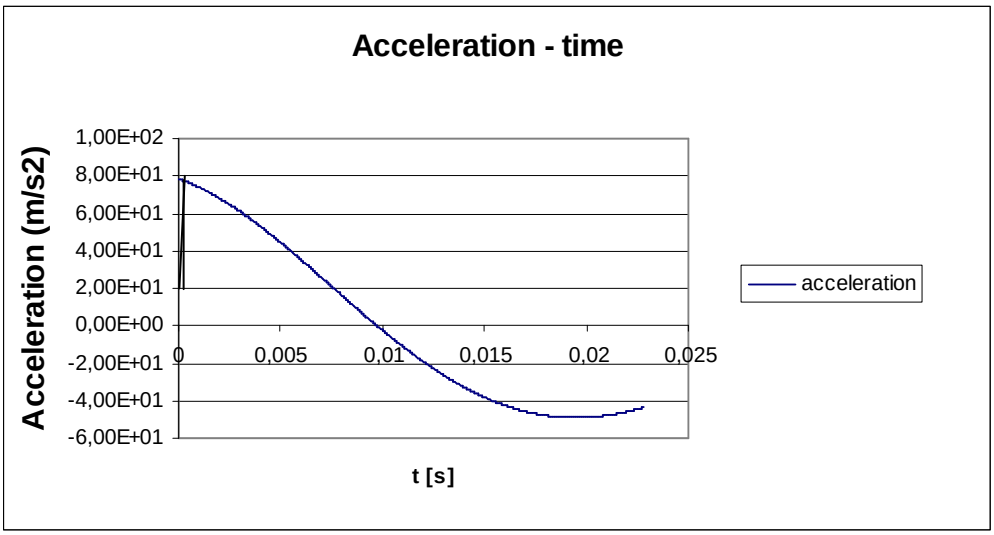

Figure 5.11 Acceleration-time diagram

The initial step up in Figure 5.11 is estimated to have duration of about 0.5 ms (The nature of the model implies that the step-up is not modeled correctly). This time is divided in 10 samples, thus the frequency becomes:

$$dT = \frac{T}{n} = \frac{0.5ms}{10} = 0.05ms$$
$$f = \frac{1}{dt} = \frac{1}{0.05ms} = 20kHz$$

So the acceleration transducer and the accompanying amp need at least a bandwidth of 20 kHz.

Physical range of the sensors

The strain gauges on the pile head have to measure a maximum force of 20 kN (1.5 times maximum F out of the calculations), thus the strain becomes:

$$F = eE_sA_p \rightarrow e = \frac{F}{E_sA_p} = \frac{20kN}{210GPa \cdot 7.63^{-4}m^2} = 125mstrain$$

This value is close to the threshold value of the straingauges (~100μstrain), if smaller forces have to be measured accurately the cross section of the tube has to be decreased. An outer diameter of the rod of 25 mm is chosen. For the acceleration see the velocity-time diagram below (Figure 5.12):

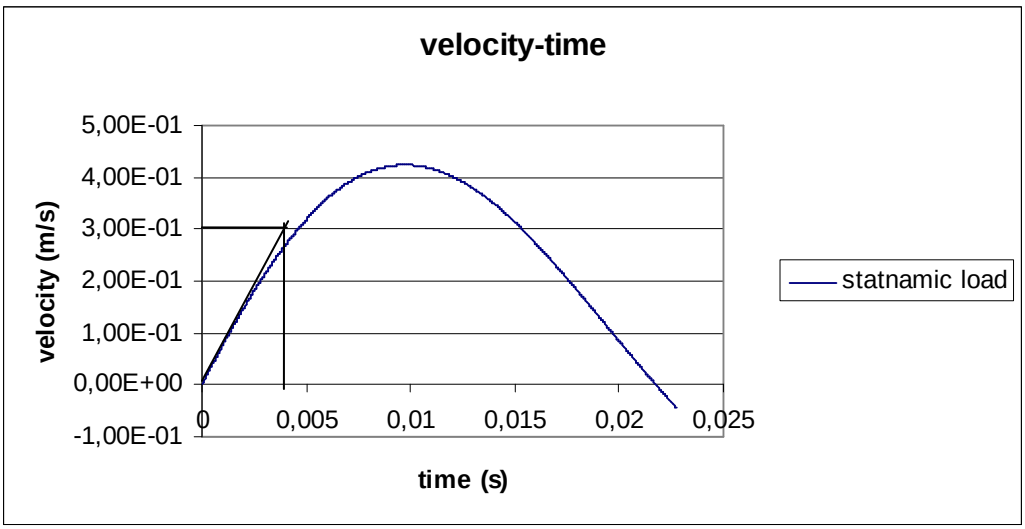

Figure 5.12 Velocity-time diagram

The maximum acceleration therefore is:

$$a = \frac{dv}{dt} = \frac{0.30m/s}{0.004s} = \sim 75m/s^2 = 7.5g$$

5.3.3 Equipment chain

In Figure 5.13 below and the accompanying table 5.3 all the needed equipment of the measuring chain is listed.

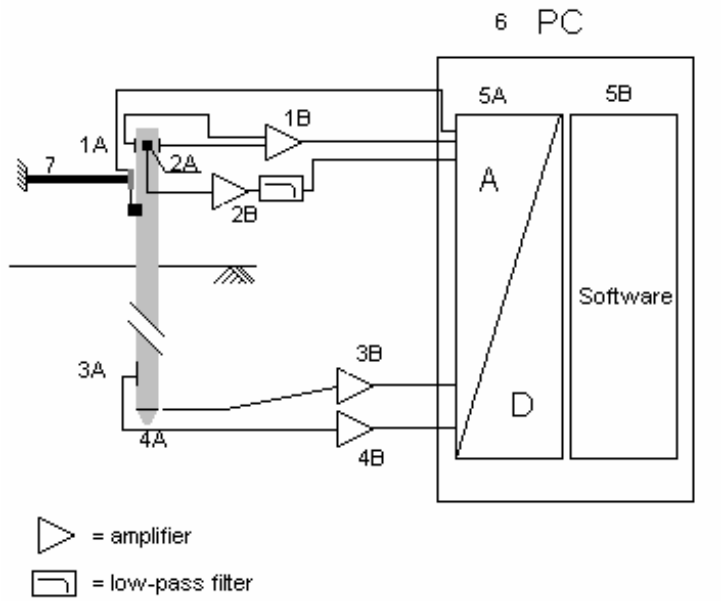

Figure 5.13 Schematized view of needed equipment

#	description	specs
1A	4 strain gauges to monitor the force	> 1 kHz; 95μstrain
1B**	Strain gauges Amplifier + low-pass filter (eliminates high freq)	> 1 kHz
2A	Acceleration transducer	> 20 kHz; 75 m/s^2
2B	Acceleration amp + filter	> 20 kHz
3A	CPT shaft friction	> 1 kHz; 10 kPa
3B	Amp+filter for the shaft	> 1 kHz
4A	CPT tip resistance	> 1 kHz; 10 kPa
4B	Amp+filter for the tip	> 1 kHz
5A	AD converter card (to be placed in a PC)	5 channels at least 100 kHz
5B	Software accompanies the AD	-
6	Personal Computer	Desktop PC with a free isa/pci slot
7	Displacement transducer or potmeter	Maximum stroke > 15 mm
8	Optical Displacement device	Optional

*Table 5.3: list of equipment ** both strain gauges are connected to one amplifier (only the mean values are measured)*

The specifications are only suitable for the statnamic case. If the dynamic case is considered new specifications have to be defined.

As seen in Figure 5.13 and table 5.3 the displacement is measured with a linear stroke potentiometer. The velocity is measured with analog integration of the acceleration transducer. The integration of the acceleration is done in the load amplifier of the acceleration transducer, but with the limited bandwidth of the PC artifacts can occur. The velocity can also be differentiated out of the displacement, but the signal contains less high frequency information. Both measurements are combined to obtain the velocity information.

Costs

quantity to measure	method	associated equipment/assembly work to be done	cost (€)
force on pile head	strain gauges	assembly and calibration of the strain gauges strain gauge amplifier	150 320*
shaft friction	CPT cone	strain gauge amplifier	GD
tip resistance	CPT cone	strain gauge amplifier	GD
velocity	accel transducer	assembly of the transducer amplifier with analog integration	50 section
displacement	pot (variable resistor)	assembly to the tube power supply	50 section
data acquisition	PC + AD	testing of the bandwidth of measuring system	240**

*16 channels 2months for €40/week
**€30/week the chain of amplifiers and data acquisition is tested to work >2 kHz

The measuring group has done 16 hours of work at €44/hour	704
total	1514

Table 5.4 Costs of the measuring setup

5.3.4 Mounting of the acceleration transducer

Unfortunate the acceleration transducer can not be placed in the center of the sounding rod because the cable which transports the signals of the instruments in the cone is in the way. Therefore the transducer is mounted on the side. A sleeve where against the transducer can be mounted is needed. The design is depicted in Figure 5.12. The sleeve is symmetrical to get at least a symmetrical cross section. For the same reason the position on the model pile of this clamp is on the first sounding rod after the pile head.

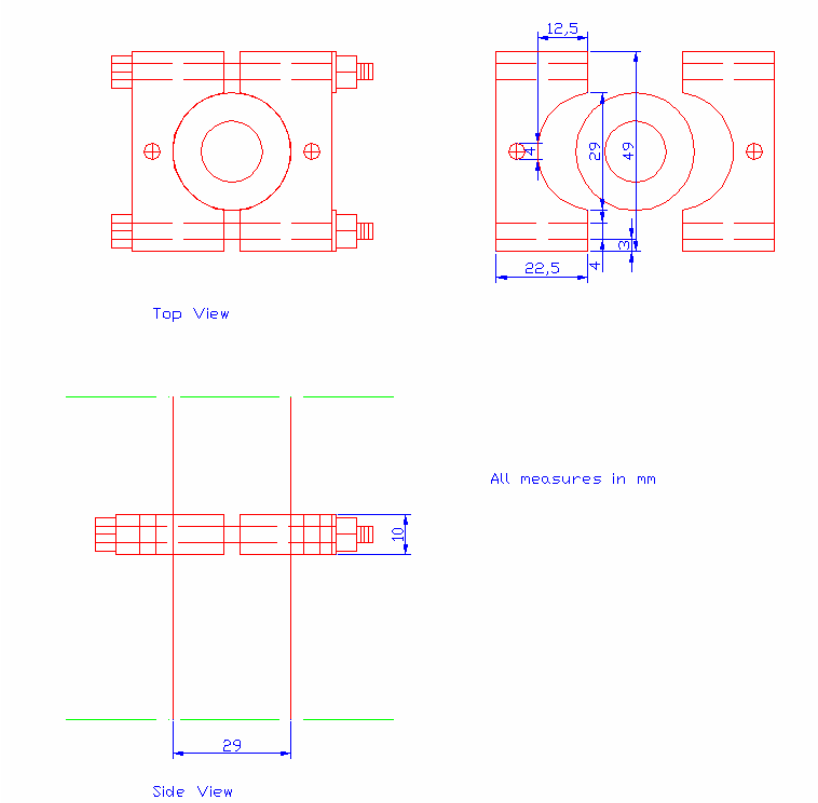

Figure 5.14 mounting of the acceleration transducer

5.3.5 Mounting of the displacement pot

Displacements are measured with a linear stroke potentiometer. This potentiometer is mounted on a fixed boundary. The catch is pressed with a spring against the notch of the pile. This notch is represented by the before mentioned acceleration transducer. For an illustration see Figure 5.15
In this way the velocity and displacement are measured on the same location, therefore time differences due to distance between two sensors are minimized.

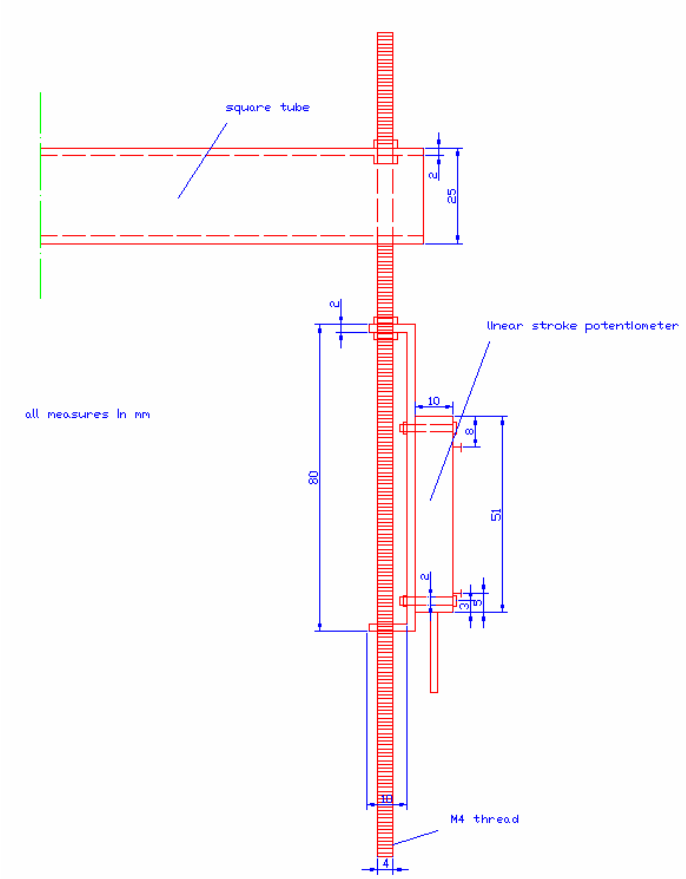

Figure 5.15 fixation of the displacement pot

5.3.6 Final remarks on realisation of measuring set-up

A complete list of the used equipment is given in appendix H, in this appendix also the calibration constants are elaborated. With these constants the measuring system is returning for all channels (with exception of the velocity/acceleration data) the engineering quantities.

The data acquisition system has a minimum sample time of 470 μs or a f_s of 2.1 kHz. The Nyquist frequency is half of that thus ~1kHz. This is the range which gives reasonable data.

After the first tests it became apparent that the utilized acceleration amplifier is not able to properly convert the acceleration signal to velocities. Therefore the raw acceleration data is fed to the A/D card. Because this A/D card barely could cope with the high frequency of the velocity data, the acceleration data is not measured as well as wanted. The peak velocity can be derived from the signal, the inertia effects also, but the amount of data points and therefore the resolution is limited.

The measuring system is able to make a gated measurement after it is triggered. This post triggering system is further elaborated in appendix I.

6. Realisation of the loading mechanism and measuring setup pseudostatic

6.1 Introduction

In this chapter the actual realisation of the test set-up and the encountered practical problems are elaborated. First some photographs of the test set-up are given. Then some practical problems and their solution are given.

6.2 Some photographs of the test set-up

6.2.1 Calibration tank

In Figure 6.1 the calibration tank is shown, in the front the water reservoir of the fluidization system can be distinguished. A close up of the vibration engine is given in Figure 6.2

Figure 6.1 Calibration tank

Figure 6.2 Vibration motor

The top view of the tank is given in Figure 6.3. The two beams are supporting the loading apparatus.

Figure 6.3 Top vie of the calibration tank

In Figure 6.4 the preparation cycle is shown. First (a & b) the tank is fluidized, secondly the tank is vibrated for several minutes during drainage (c), drainage is completed (d).

a) First water at the top of the tank

b) Some moments later

c) Vibration (interference in water surface)

d) Drained situation

Figure 6.4 Preparation of tank

6.2.2 Loading system

The loading system consists of the constant rate apparatus (Figure 6.5). The guidance tube with drop mass (Figure 6.6) and a detail of the release mechanism (Figure 6.7) and disc spring (Figure 6.8)

Figure 6.5 Constant rate loading apparatus

Figure 6.6 Guidance tube and drop mass with spring assembly

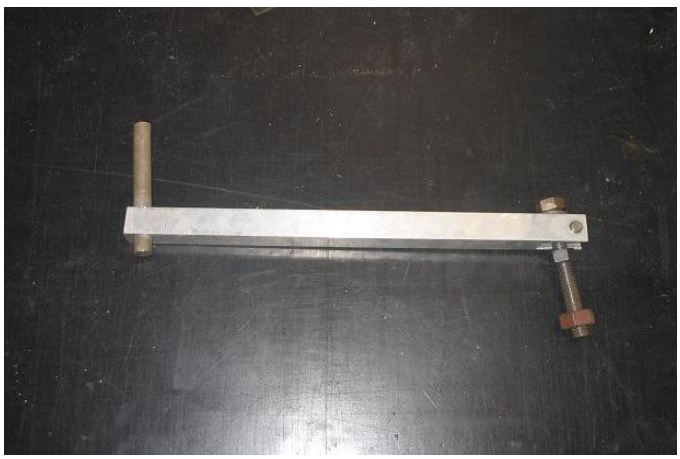

Figure 6.7 Release mechanism

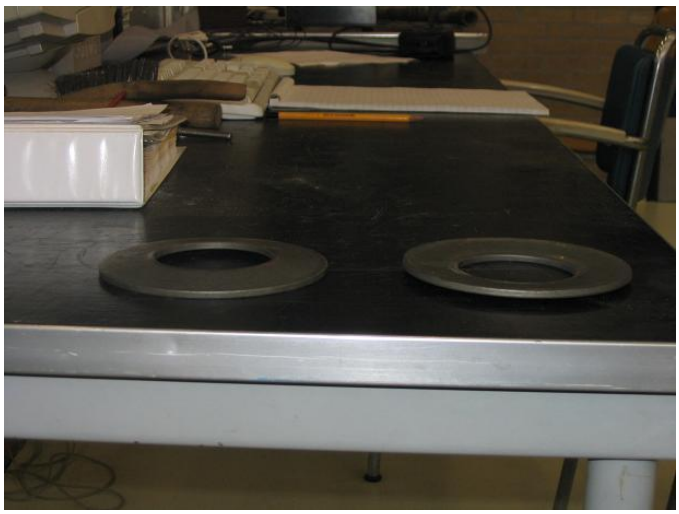

Figure 6.8 Disc spring

6.2.3 Measuring system

The CPT cone is depicted in Figure 6.9 the strain gauges at the upper rod in Figure 6.10 with a close up of the acceleration transducer in Figure 6.11.

Figure 6.9 CPT cone and rods

Figure 6.10 Strain gauges at upper rod

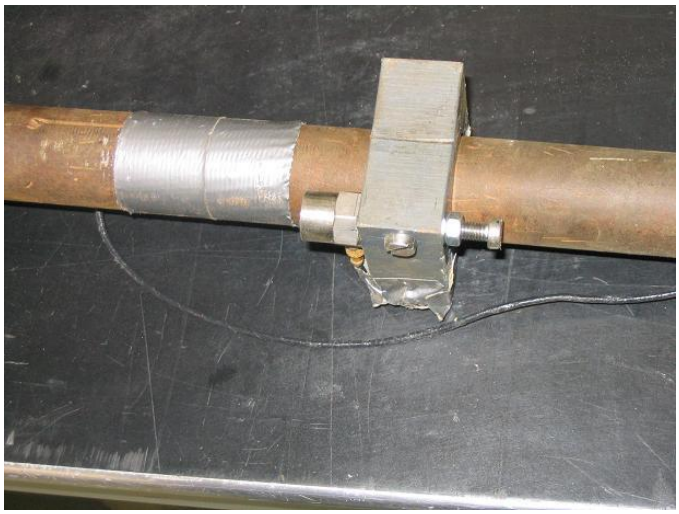

Figure 6.11 Acceleration transducer and it's mounting

The displacements are measured with a linear potentio meter as depicted in Figure 6.12.

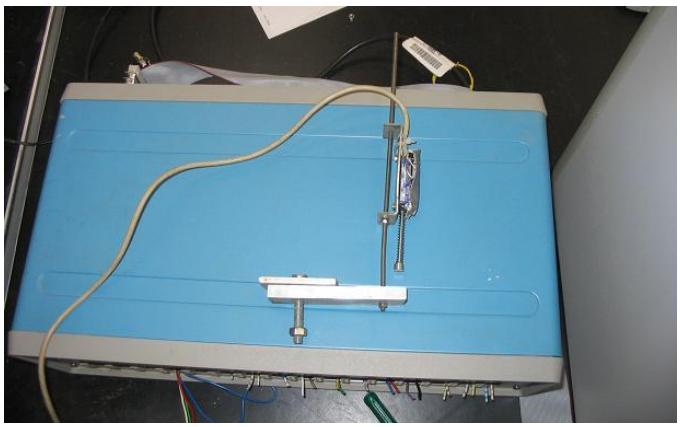

Figure 6.12 Displacement pot and mounting system (the box under it is the strain gauge amplifier)

6.3 Problems during realisation of the set-up

After the first few tests it proved useful to incorporate a tension relieve system for the cable to the CPT-cone. In this way the cable is not pulled out of the socket of the CPT-cone. The same is realized for the displacement pot (a simple tie wrap did the trick).

The disc springs are moving a lot during the pseudostatic test, therefore a center piece was added as core of the springs. This centerpiece is only guiding the lower three disc springs (else the springs do not function anymore). But the amount of shift of the springs during the pseudostatic test has reduced a lot.

The fixation of the guidance tube to the beams across the tank becomes difficult if the pile is not truly centered between the beams. Therefore only 2 of the 4 holes could be utilized most of the time. The same holds for the CR-apparatus for the fixation of this device a piece of steel is bridged over the cross beam of the device (see sketch in Figure 6.13)

To let the cable from the cone undisturbed out of the pile head a special cable side guide was used this piece is shown in Figure 6.14

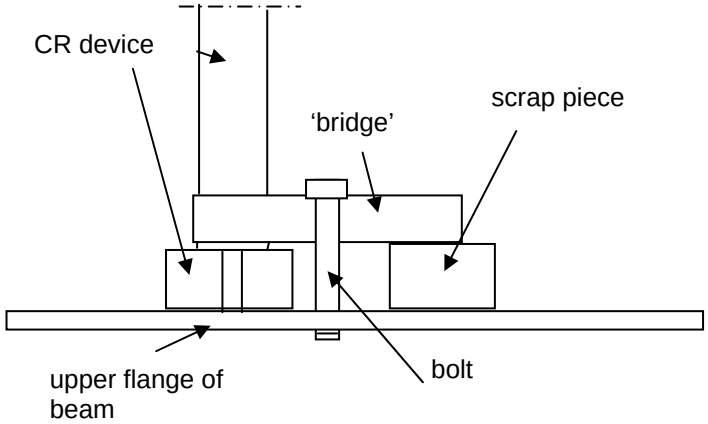

Figure 6.13 Sketch of fixation of the loading device

Figure 6.14 Side guide of cable at the pile head

7. Presentation and verification of the test results and equipment

7.1 Introduction

In this chapter the final test results of the test setup phase are presented. In this phase the last unforeseen problems are tweaked out of the test setup. The final results are then compared with model data and checked on consistency of physical laws.

7.2 Presentation of the test results

7.2.1 Background of the test

After the preliminary tests to check the geotechniek test chamber conditions (see appendix G) and the design of the test setup, mechanical as well electrical, a series of tests were performed to adjust and tune the setup. The last series of tests of this phase are presented in this paragraph. These tests consist of loading of the test pile with the loading mechanism as described in chapter five, to obtain a loading characteristic as predicted in chapter four. A total of six tests are presented. Three tests per location on two different locations, location I and III to be precise. Unfortunate the tests on location II couldn't be performed properly (pile placed too far in the soil).

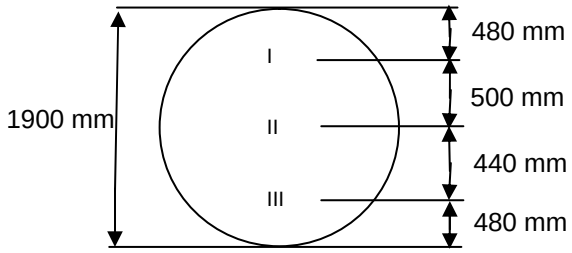

Figure 7.1 Test locations

A total of 5 quantities are recorded, namely:
1) Tip resistance
2) Shaft friction
3) Pile velocity
4) Pile displacement
5) Force on the pile head

7.2.2 Test results

For both locations the recordings of the five different quantities are given on the following two pages. This gives a total of 10 graphs.

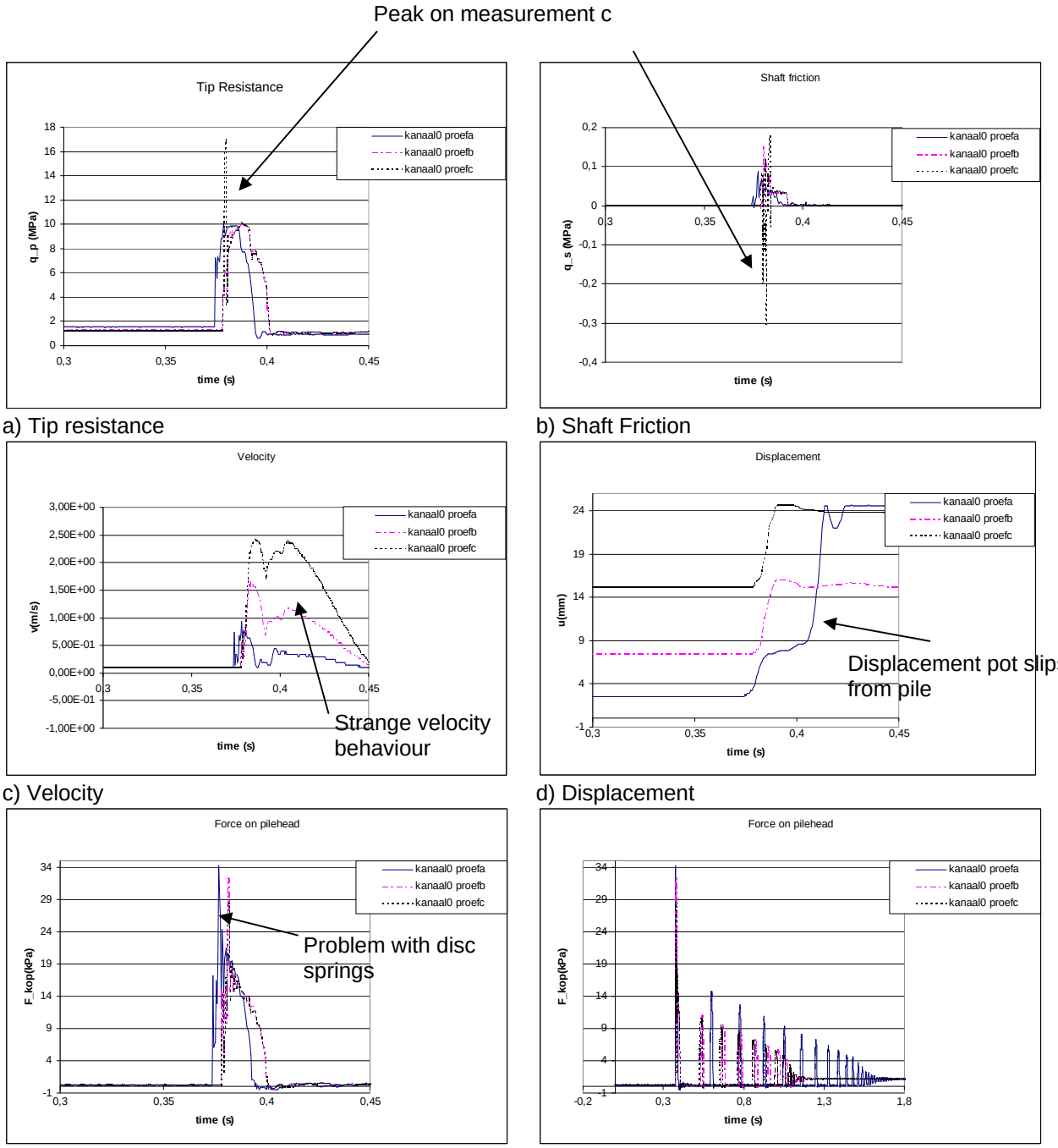

a) Tip resistance

b) Shaft Friction

c) Velocity

d) Displacement

e) Force on the pile head

f) Rebound behaviour of force on pile head

Figure 7.2 a-f Results of three consecutive tests on location I

As seen in the Figure several comments are made on location I some problems occurred with the acceleration transducer, the origin of the problems is unclear. The irregularities on the pile head force-time diagram in 7.2e are created by the fact that the spring travel was too much limited, causing an unlimited stiff spring for a short moment on the end of the spring travel. The strange reaction of the tip resistance and the shaft friction (fig. 7.2a and b) in the third consecutive test does come back in the second series of tests in Figure (7.3a-b)

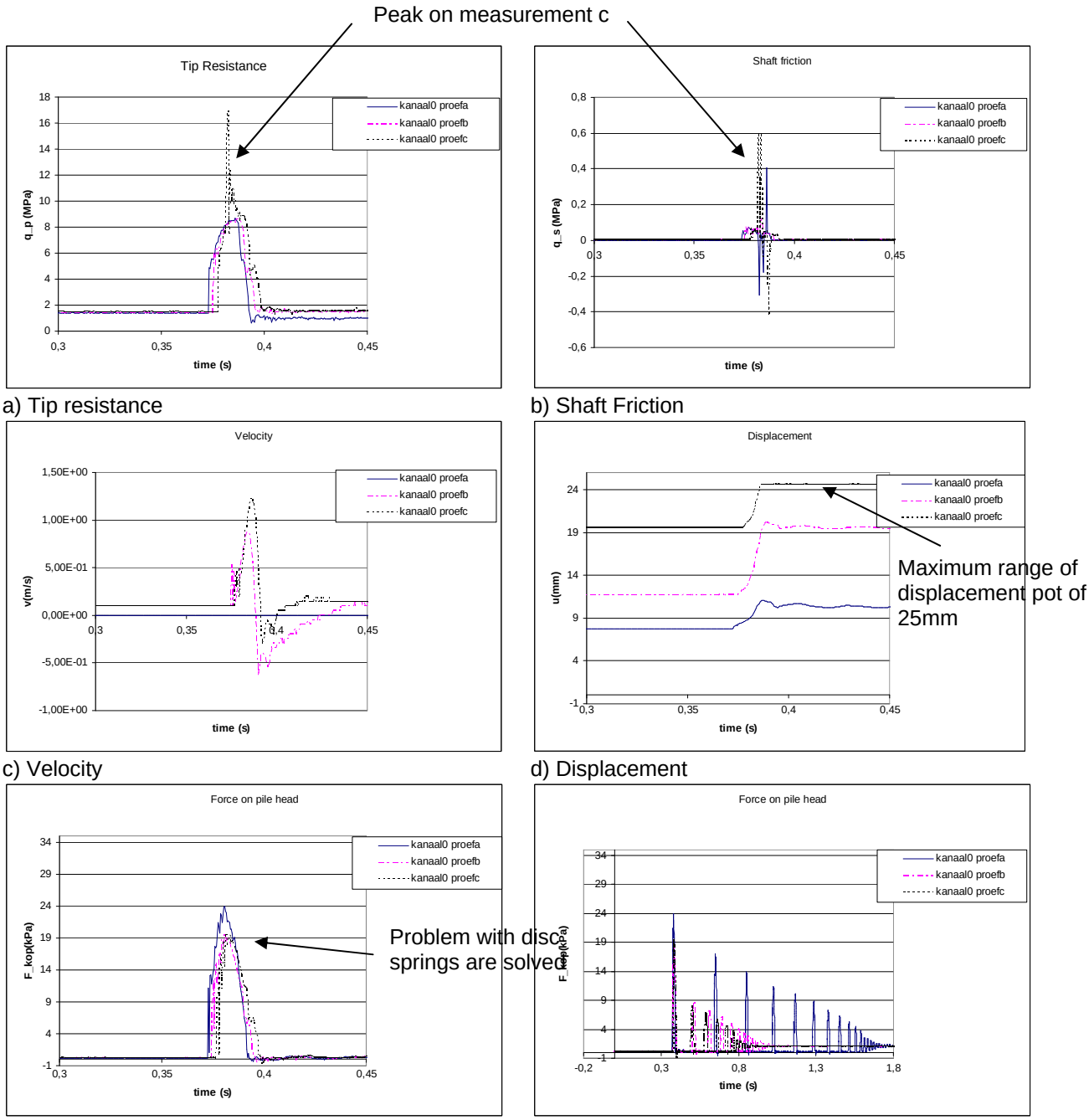

a) Tip resistance b) Shaft Friction

c) Velocity d) Displacement

e) Force on the pile head f) Rebound behaviour of force on pile head

Figure 7.3 a-f Results of three consecutive tests on location III

Fewer problems occurred, as seen in the Figure above. Only the peaks on the tip resistance and shaft friction do return in the second series. In both cases (location I and III) the loading pulse is similar to the other pulses applied on the pile, so the reason of the appearance of the peak is unclear. But it has to be soil related.

One of the main issues in § 5.2.6 was the possible problem of the rebound, as can be seen in Figure 7.2f and Figure 7.3f the rebound occurs after at least 20 ms, so is of no concern.
But clearly can be seen that the 2nd and 3rd consecutive test show a less stiff more damped soil reaction, because the rebound occurs sooner.

7.3 Comparing results with theory

7.3.1 Compare theoretical model with measuring data

To verify the measurements the results are compared with the theory as described in chapter four.

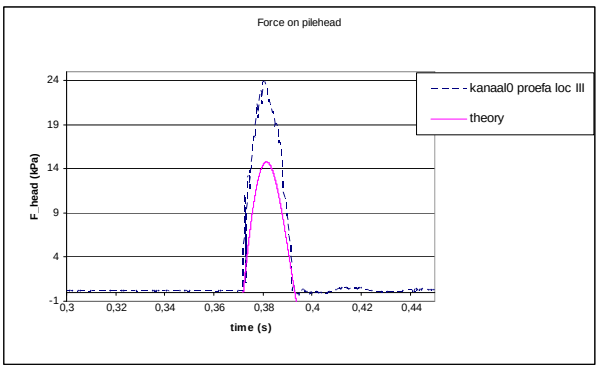

a) Force on the pile head

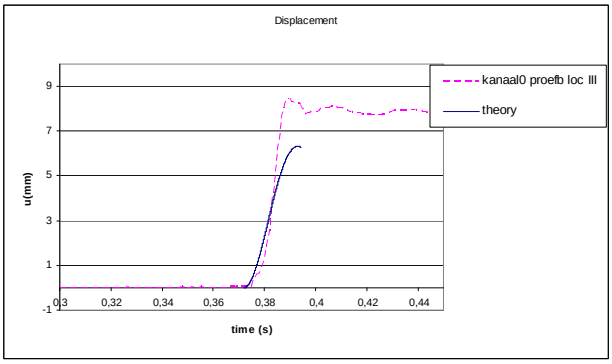

b) Displacement

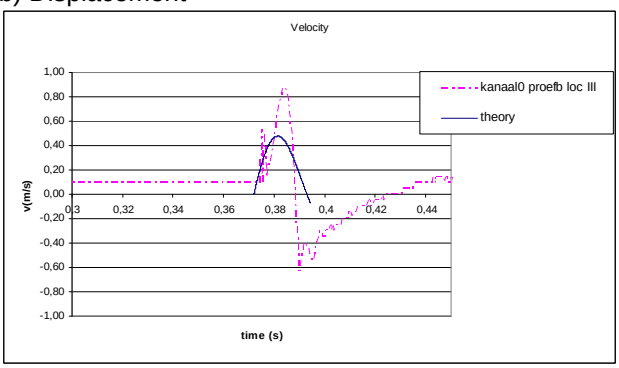

c) Velocity

Figure 7.4 Comparing measuring data with the theoretical model

The pulse width of the force on the pile head (fig. 7.4a) correlates with the expected value of ~22ms. However the magnitude in this case is ~60% larger. This difference differs from test to test the typical difference is about 40% and could be induced by boundary effects. The static test results are also showing a large soil resistance and therefore a large force on the pile head.
The difference in magnitude does return in the displacement and velocity graphs. The velocity graph is still not right it seems that the pile is moving up instead of down. It's difficult to say if the analytical model is erroneous or the measured data, because of the uniformity of the curves

together with the substantiated anomalies the measured data with exception of the velocity is supposed to be right.

7.3.2 Physical relationship

Of course some basic relationships have to hold. The displacement differentiated with respect to time has to give the velocity. As seen in the following Figure this is not the case for the second part of fig. 7.5.

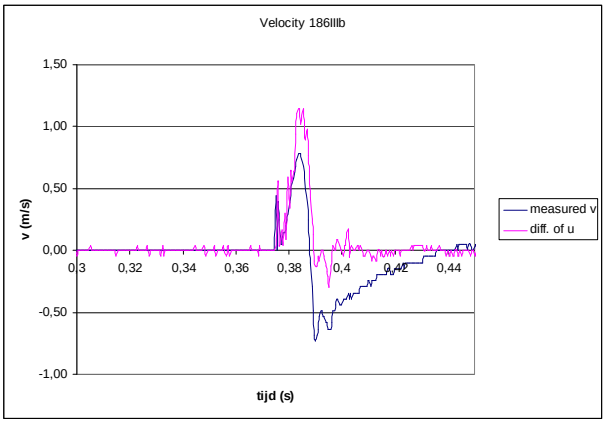

Figure 7.5 physical relationship between u and v

When the measured signal is studied closer the pile is moving upwards instead of downwards (area under the second peak is larger then the first peak). Out of the displacement info can be seen that this is simply not the case.

7.3.3 Improving the velocity data

To further investigate the quality of the measured velocity the analog integration of the load amplifier is shut off and the acceleration is measured. The acceleration is measured and plotted in fig. 7.6 (another test on location II same preparation used) also the data is converted to the frequency domain (see Appendix J FFT) and can be seen in fig. 7.7.

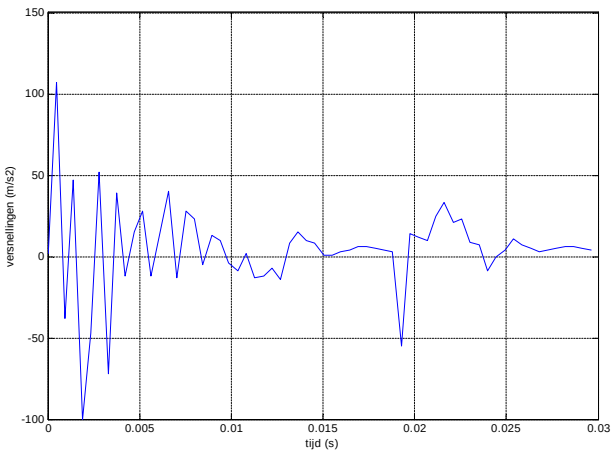

Figure 7.6 The measured acceleration against time

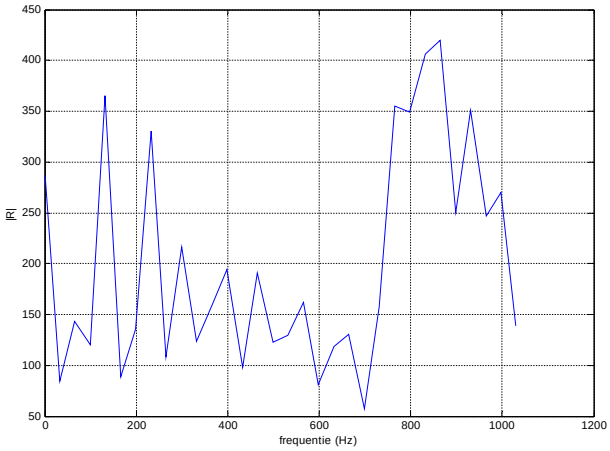

Figure 7.7 Frequency range of the measured acceleration signal

Something is oscillating in the 800-900 Hz range. This is the reflection of the pile tip. Because the total length of the pile is 2.65 m and the $c_{w;steel}$=~5000 m/s The reflection has a frequency of:

$$\left.\begin{array}{l} L = cT \\ f = \dfrac{1}{T} \end{array}\right\} f = \frac{c}{L}$$

$$\left.\begin{array}{l} L = 2 \cdot l_{pile} = 5.3m \\ c = 5000 \dfrac{m}{s} \end{array}\right\} f = 943Hz$$

When this frequency is filtered out of the signal the resulting acceleration becomes as depicted in Figure 7.8:

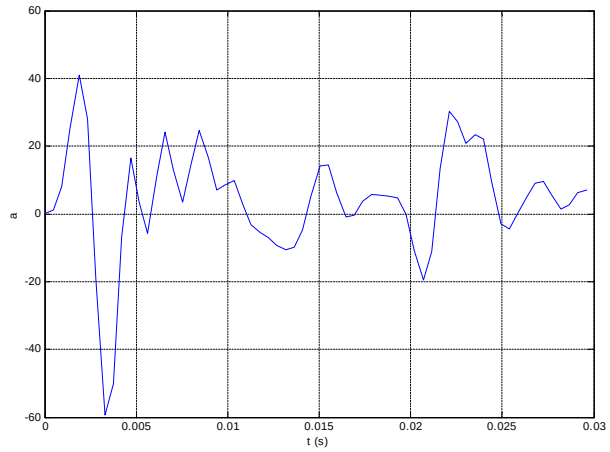

Figure 7.8 a-t after the filter is applied

Still the pulse width of the first peaks of the acceleration signal is about 3 ms or a velocity with a pulse width of 6 ms. Instead of the 10 ms pulse width of the velocity out of the displacement data as seen in Figure 7.5.

The nature of the digital conversion prohibits the use of filtering of frequencies which are higher then the Nyquist frequency. So filtering of these frequencies before the data is converted to the digital domain is mandatory. To achieve that an analog filter is designed to cut all frequencies above 500 Hz. This filter is placed between the load amplifier and the AD-converter the physical implementation is given in appendix H.

Another problem with the acceleration transducer still existed. The electrical load generated by displacement of the cable which connected the transducer to the amplifier is of O(pC). Therefore a small movement of the cable did hamper the results by as much as 50%. The only way to solve this is by using a transducer with a higher output load, so the noise (which is still of the same magnitude) is less harmful to the transported signal.

The results which are presented in the next chapters are done with the new transducer, the analog filter between the acceleration amplifier and A/D card and the acceleration transducer set to measure accelerations instead of integrating to velocities.

8. Test Regime

8.1 Introduction

In this chapter is dealt with the test regime. Besides the type and amount of tests also the choice for a certain test is substantiated. Which tests are carried out and which quantities are measured is also discussed. Also the test procedure of the chosen tests are elaborated.

8.2 Which tests to perform

8.2.1 Overview of tests

A lot of tests can be performed, but the tests which are actually performed depend on the objectives of this graduation project.

The main objective of this graduation project is to determine the loading rate effect on the pile capacity. Different loading rates have to be applied on a pile in the same soil conditions. The resulting test regime is therefore to do tests with three different loading rates.

Because the pulse width of the loading force is in the pseudostatic range, the same range as statnamic tests are performed, the correlation of the pseudostatic pile capacity with the static pile capacity is of interest. If besides the pseudostatic also static tests are performed the validity of the conversion method from pseudostatic to static can be made. If before and after a pseudostatic test a static test is made the change in soil conditions owing to the pseudo static test can also be seen. In that case a true comparison between static and static derived from pseudostatic can only be made if both static tests are similar.

The influence of the soil compaction is also studied. The damping properties of a dense sand layer are less then of a loose sand layer, so different pile behaviour can be expected. The soil compaction in the test tank can easily be altered; the test tank is just vibrated for a shorter time.

The effect of the pore water pressures is also a major concern. Thus comparing results in dry sand with the results of the same test in wet sand is also a topic of interest. Besides the rate effect in saturated soil is a rather unknown phenomenon and also of major importance on the bearing capacity.

Concluding in the following topics of interest:
1. Influence of soil strength on the static and pseudostatic response (different $T_{vibration}$)
2. Influence of loading rate on the pseudostatic results (different spring stiffness')
3. Influence of the pore water on pseudostatic results (saturated soil)
4. Influence of the rate on the pore water (pore water reaction on different loading rates)

8.2.2 Resulting data

Out of the tests not only pseudostatic pile capacity, static pile capacity, loading rate effects and the correlation between pseudostatic and static capacity for dry and wet sand can be gathered.
Sidelines as in-situ capacity (up scaling of the results), pile interface-soil behaviour in sand and the accuracy of the shaft friction sleeve of the CPT cone can also be studied.

8.2.3 Justification of amount of tests

A total of two tank preparations can be made in one week. The major time scale of this procedure is the drainage of the sand bed in the test tank. After 40 hours only water which is molecular bonded to the grains is left in the tank. So during the weekend the tank is drained, tests are

performed on Monday and Tuesday morning. After that the tank is fluidized again and drained until Thursday the next set of tests is performed.

-Rate effect

To get insight in the rate effect, at least three different rates have to be tested. A pulse width of 22 ms corresponding with the literature value for the in-situ pseudostatic load (after up scaling to the in-situ boundaries). This pulse width is obtained by combining 5 disc springs (for details see chapter 5). A pulse width of 11 ms. is obtained when only one disc spring is used. The third point is from 6 disc springs generating a pulse width of 24 ms. Each test is consecutively performed on the same pile. The order of the tests is altered with the relocation of the pile. A total of 9 tests are performed in one prepared test tank. In the worst scenario only the three tests which are applied on the pile first are of use. If the influence of the first on the last test is minimal nine tests are acquired. A total of two preparations are made so 6-18 tests are obtained. This regime is been applied in dry and wet soil conditions. A conservative estimated of one week of work is needed for these tests in the dry and also for the wet situation.

-Static test

The static tests are made before and after each pseudostatic test series, so besides static data about CPT resistance (during installation) a static test before and after the pseudostatic test is made.

-Influence of soil compaction

To obtain some insight in the influence of soil compaction three preparations with each time a different vibration time are executed. In each tank preparation on a total of three locations pile tests are executed. On each location first a CPT reading, next a static test, then a pseudostatic test and finally again a static test are made. The total duration for three preparation cycles is 1.5 weeks.

-Test in saturated sand

In one tank preparation of saturated sand on three test locations tests are executed in the same manner as the influence of the soil compaction is studied.

8.2.4 Test scheme

The tests mentioned in paragraph 8.2.3 are summarized in Table 8.1

type of test	preparation	# tests	# tank preps	# weeks
static (CPT) - pseudostatic - static	1,5F; 10V; 'dry'	3	1	0.5
static (CPT) - vary k 3 tests on 1 pile*	1,5F; 10V; 'dry'	18 (6)	2	1
static (CPT) - pseudostatic - static	1,5F; 5V; 'dry'	3	1	0.5
static (CPT) - pseudostatic - static	1,5F; 15V; 'dry'	3	1	0.5
static (CPT) - pseudostatic - static	1,5F; 10V; 'saturated'	3	1	0.5
static (CPT) - vary k 3 tests on 1 pile	1,5F; 10V; 'saturated'	18 (6)	2	1
	total	48 (24)	8	4

*each time in different order

legend:	
1F =	1 hour of fluidization
1V =	1 minute of vibration

Table 8.1 Overview of tests

When more tests on a single pile are applied the first test on the pile is seen as an high quality test in undisturbed soil (in brackets the amount of HQ tests is given). When complications arise during the testing procedure, the saturated tests will be omitted firest from the test regime.

8.3 Pseudostatic Test Procedure

8.3.1 Introduction

In this section is dealt with the pseudostatic test procedure. This type of test is used to research the effect of the loading rate on the pile capacity. All procedures involved are clarified in this section. Five phases are considered: Preparation of the test-tank, set-up of the constant rate (CR) loading device, execution of the CR test, dismantle of the CR-setup and build up of the pseudostatic setup (PS), pseudostatic testing.

8.3.2 Preparation of the test-tank

First the tank at Geotechniek is fluidized, during this operation water flows from the bottom of the tank to the top. In this way the grains redistribute to a very loose undisturbed soil structure.
After the sand in the test tank at Geotechniek is fluidized the soil does not have enough compaction, so the wall of the tank is vibrated to obtain a greater compaction of the sand. This operation is executed immediate after fluidization while the water is still in the tank. In this condition the vibration is more effective, because the water is transporting the energy to the core of the tank. As mentioned in one of the previous chapters two major difficulties occur during tank preparation, namely:

1) The vibration and fluidization method used gives different soil compaction and soil structures even when all boundary conditions are held constant (i.e. vibration time, soil type, fluidization parameters)
2) Vertical deviations in stratification after each tank preparation.

The first problem is induced by the wanted soil conditions. Shaft resistance and tip bearing capacity only occur in sand of certain porosity, if the porosity is too large, there will be too little shaft resistance mobilized. After fluidization the porosity is not low enough, thus vibration is introduced to compact the soil. The achieved porosity is a function of the vibration-time, but in practice the range of the results is quite big. The range in the results (problem 2) is mainly caused by the vibration procedure, after fluidization the upper limit of the porosity is consistently achieved, on the other hand after the vibration procedure (to decrease the porosity of the sand) the results aren't consistent enough. See appendix G for preliminary results of CPT-tests in the calibration chamber.

To work around this problem the following option is chosen:

An alternative perspective is to perform all the wanted tests in one tank. The horizontal consistency of the soil in the tank is tolerable see the results in appendix G, only when a location is close to the vibration motor differences occur. Thus each test with a different loading rate has to be executed in the same tank in that case comparisons can be made without preparation induced differences.

On each location of the rate tests also the static resistance on the depth of interest is made to determine the actual soil conditions. This value helps also to correlate the results between two tank preparations or even two different locations in the test-tank.

The apparent cohesion will still be a problem it takes time to get a complete dry soil sample after the fluidization procedure. If all the remaining water has to be expelled out of the sample a lot of energy is needed. See appendix F for a short feasibility calculation

8.3.3 The CR-test

The constant rate tests or CPTs are executed with the constant rate device. The hydraulic device pushes the cone into the ground with a constant velocity of 20 mm/s. The rod is extended each meter with another rod, so total lengths of more then 30 m can be reached. This is the same apparatus as utilized by Broere (2001). To counter the reaction force the device is bolted on the beams which lie across the test tank. The cone is standardized by the Dutch code.

The test consists of nothing more than installing the rod into the sand. The tip resistance and shaft friction of the last 60 cm is registered. This value indicates the maximum force which is needed to install the sounding rod into the sand. The depth info is not registered; the system is not compatible with the measuring computer.

After the installation of the pile the CR-device is moved and the sounding rod above the surface is replaced by the instrumented one.

8.3.4 The pseudostatic test

If the pile (actually the CPT cone) is installed properly the pile head is about 15 cm above the level of the beams. The displacement pot is installed. All electrical connections are installed to the amplifiers.

The guidance tube is aligned with the pile head and bolted against the beams. The mass is hoisted in position and the release mechanism is installed. After the installation of the loading mechanism the electrical connections are checked again.

The test itself is just a matter of pulling of the release mechanism and let the mass drop on the pile head.

The personal computer with A/D converter card is configured in such a way that after the pile is hit just the right time-frame is stored without human intervention. A detailed description of this configuration is given in Appendix H. During the test the force on the pile head, the velocity (analog integration of the acceleration) the tip resistance and shaft friction are recorded.

8.4 The static test

8.4.1 Introduction

In this section the static test is elaborated. Only the differences with the pseudostatic tests are given. Most of the initial procedures are the same.

8.4.2 The static test

The static tests are performed with the same CPT-device as the rods are installed; only in this case the loading pulse on the pile head is also measured. The pulse applied has a duration of approximately one second or fifty times the time of a pseudostatic test. The control of the test duration is hard to get right. The loading speed differs each time (it is not possible to load the pile instantly with the maximum force) because it's done manual. Also the duration of the pulse is not trivial to get right. This results in a loading pulse of different widths and steepness of the initial slope. The test is applied after the installation of the pile and after the pseudostatic test is performed. A total of two tests is executed on each pile.

8.4.3 The static test mk. II

At the end of the test series during the static test also the displacement is registered. Because the stroke of the displacement transducer is limited only displacements up to 20 mm can be measured. The load-settlement graph of these tests gives the ultimate bearing capacity in more detail.

9. Test Results Part 1: Static tests

9.1 Introduction

In this chapter the results of all performed static tests, executed before as well after the pseudostatic test, are presented. Also the results of the mk. II tests (static test with displacement registration) are used to improve the interpretation of the tests without displacement information. The general soil behaviour is also closer studied. The relation between the static results and the results of the CPT (c_p) is also discussed.

9.2 Multicycle calibration chamber preparation consistency

9.2.1 Introduction

In this paragraph the influence of the preparation procedure is studied closer. The variance between the several preparations is of main concern, if differences occur can they be explained and can these explanations lead to improvements in the preparation method.

9.2.2 Variance in time

A total of three test locations are available in the soil calibration chamber of geotechniek, these are called location i till iii. When more tests are executed the calibration chamber is prepared as described in paragraph 8.3.2. To look into the consistency of this preparations the readings of the point resistance and shaft friction for both the CPT and static test (see description in chapter 8) are plotted against the total test period (2 months). This is shown in Figure 9.1, the results are split in an overall picture (fig. 9.1a-b) and the changes over time at each location (fig 9.1c-h).

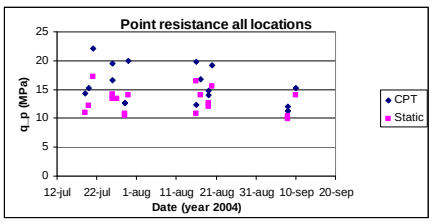

a) point resistance over time all locations

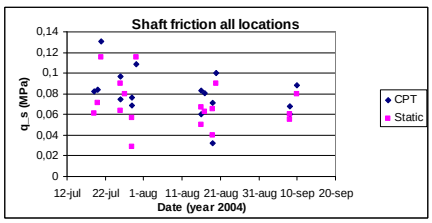

b) shaft friction over time all locations

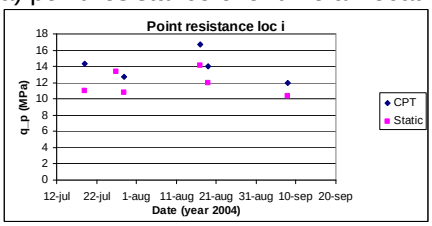

c) point resistance over time loc i

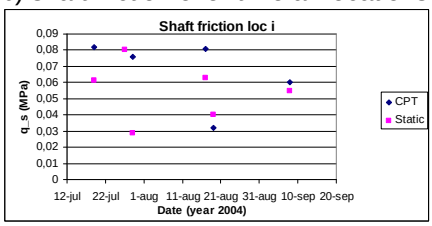

d) shaft friction over time loc i

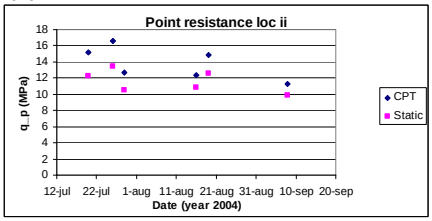

e) point resistance over time loc ii

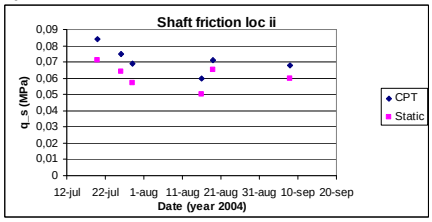

f) shaft friction over time loc ii

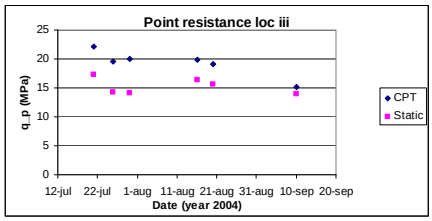

g) point resistance over time loc iii

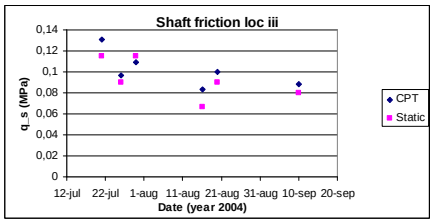

h) shaft friction over time loc iii

Figure 9.1a-h Overview of preparation consistency

At first sight (fig. 9.1 a-b) the variation of the point resistance and shaft friction is huge, but when the results are split into the different locations (fig. 9.1c-h) clearly a more consistent soil condition can be seen. One exception can be made though, the shaft friction at location i shows a lot of scatter. Because several points measured during the CPT test as well the static test show large deviations in their readings the scatter in the results is most likely induced by the soil conditions. Also at location i and iii an increase of the mobilized resistance is recognizable.

The lower values for the point resistance and shaft friction at 8 September are deliberately forced. Because on location i and iii (the locations closest to the vibration motors) a certain increase in soil resistance was found, resulting in elastic instead of plastic displacements during pseudostatic tests. This increase in soil resistance is thought to be due to the inability of the fluidization system to fully loosen the soil around location i and iii.

Therefore the calibration chamber was fluidized and not vibrated to check the soil resistance, after solely the fluidization process. This result is shown in Figure 9.2 for location i.

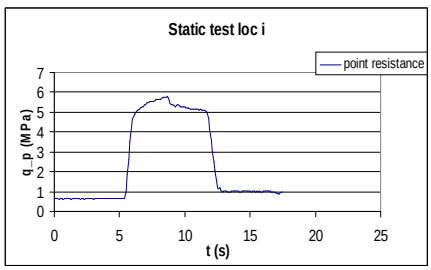

a) point resistance against time

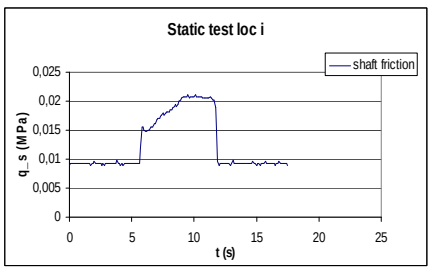

b) shaft friction against time

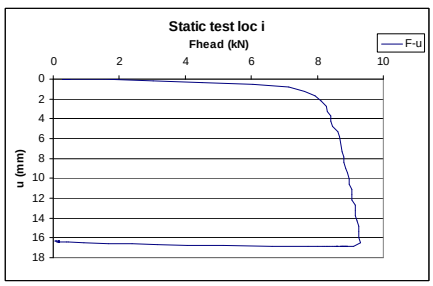

c) force on pile head against displacement

Figure 9.2 Static results for loose sand, directly after fluidization at location i

The force is almost 1/3 of a typical force in conditions with 10 minutes of vibration time (these can be seen in appendix P). Although during the preliminary tests (appendix G) the soil resistance after fluidization was far less (2 MPa point resistance and 0.015 MPa shaft friction, the force on the pile head couldn't be measured with the device).

So after several preparation cycles the fluidization system works less efficient. This fall of efficiency is caused by the situation that 1.5 hours fluidization after a preparation with vibration

time of 10 minutes (more dense) gives other results then 1.5 hours of fluidization of loose sand. This effect is relative benign during one test, but several consecutive tests strengthen this effect. Resulting in a increase of soil resistance and even a permanent higher resistance, which needs several hours of fluidization to take care of. Because the preparation after the test of the fluidization system gives less resistance (see fig. 9.1 on 8 September) this hypothesis seems be applicable.

Overall can be concluded that the results differentiated to the several locations are comparable, however some improvements can be made.

9.2.3 Possible improvements

To improve upon the utilized method (chapter 8) to obtain better consistency the fluidization time needs to be increased. This can be done in two ways, namely:

- for each preparation increase the fluidization time, but the system available for the calibration chamber is limited to 1.5 hours when fresh water needs to be supplied. In case the water is recycled and thus pumped around, the filters, valves and other systems need some maintenance in order to get the system properly working.

- after each two preparations with a quite large vibration time (say $T_{vibration}$ > 10 minutes) only fluidize and drain the tank. Execute a CPT or static test to obtain the actual soil conditions and start the next fluidization cycle. The CPT helps to determine the actual amount of consecutive tests which can be performed.

9.3 Static tests with load-settlement information

9.3.1 Introduction

During static loading of the pile (actually force controlled loading) the displacement is also recorded and the load-settlement curve can be plotted. Unfortunate several tests of this type are only performed after the testing scheme mentioned in chapter 8 was completed. Thus the results of these tests are used to improve the interpretation of the static tests as performed for the general testing scheme. Also some insight is given in the general soil behaviour and the influence of the drainage time compared to the static loading capacity and soil stiffness. The plots of all tests executed are listed in appendix P.

9.3.2 Improvement of interpretation

When displacement information is given it's quite straightforward to determine the ultimate loading capacity. According to Dutch standards (NEN 6743:1991, NEN 6745:2002) a pile has failed if the displacement of the pile is larger then 10% of the pile diameter. In Figure 9.3 a typical load-settlement curve for the calibration chamber is given (5 minutes of vibration time, 1.5 hours of fluidization). The Dutch standards are used to obtain the ultimate loading capacity out of the data. In this case $F_{ultimate}$= 32.9 kN.

When this value is plotted in the F-t plot (the typical presentation of the outcome of the static tests which do not incorporate displacement information) this point corresponds with the first change in steepness in the unloading branch (see Figure 9.3b cross-section of s1 and s2). This holds for all tests where this comparison can be made and also applies for the determination of the point resistance and shaft friction.

From now on if is referred to the value for the maximum static load, point resistance or shaft friction this method is followed to determine it out of the F-t plot.

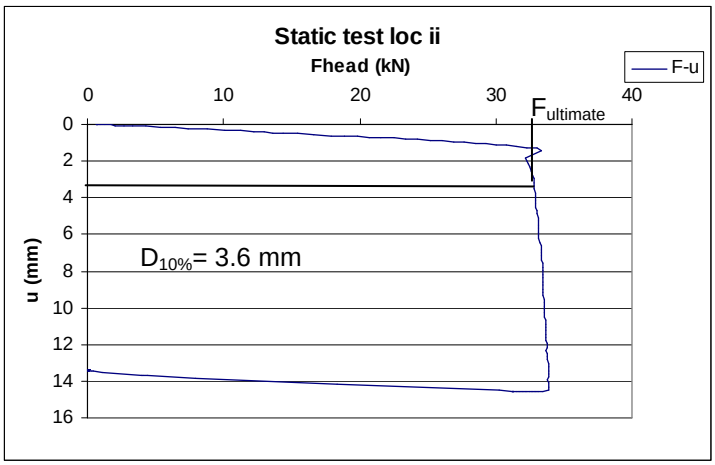

a) Deriving $F_{ultimate}$ out of the load-settlement plot

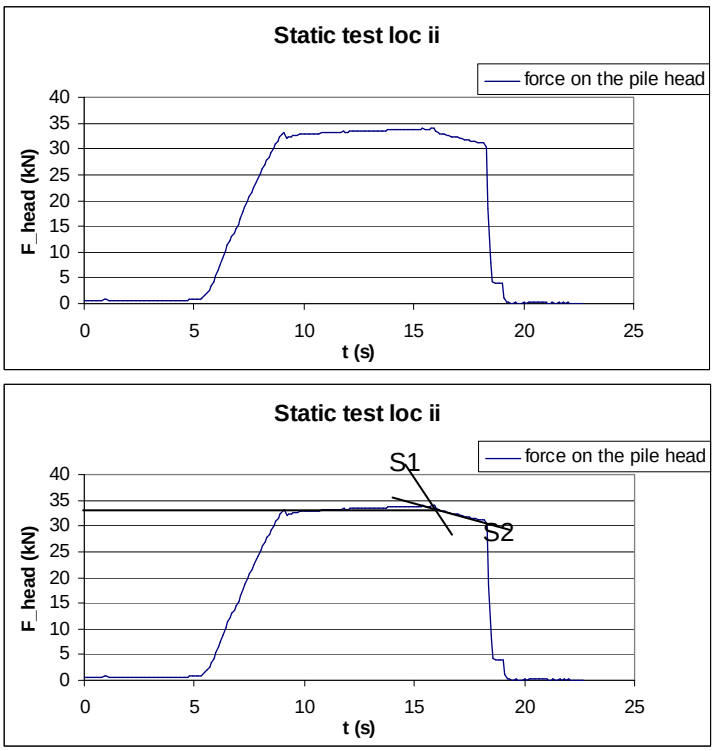

b) Searching for failure in F-t plot

Figure 9.3 Determination of $F_{ultimate}$ out of load settlement plot and F-t plot

9.3.3 Influence of $T_{drainage}$

After the preparation the tank drains for several days, after this period this phenomenon continues. The effect is studied by executing four consecutive tests with a time interval of several hours. The results for the point resistance, shaft friction and force on the pile head can be seen in Figure 9.4.

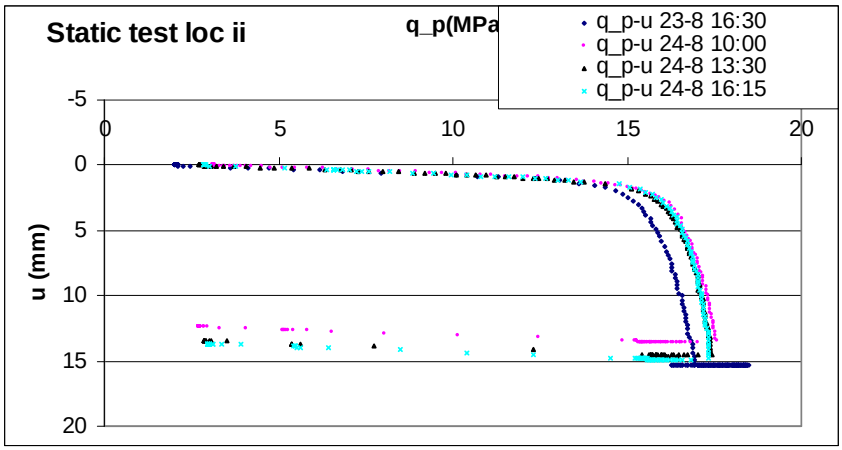

a) Point resistance against displacement for several consecutive tests

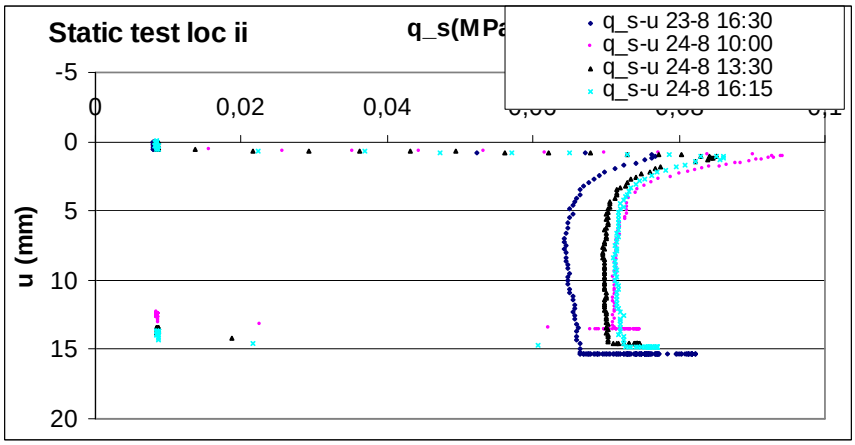

b) Shaft friction against displacement for several consecutive tests

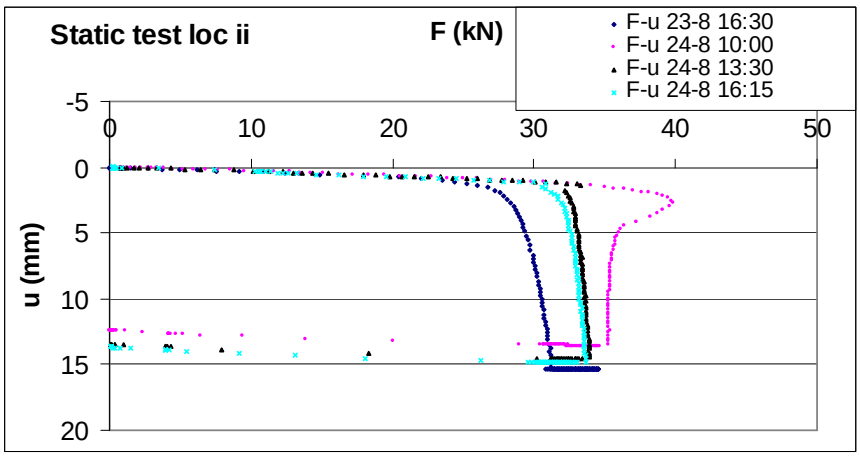

c) Force on pile head against displacement for several consecutive tests

Figure 9.4 Influence of $T_{drainage}$

After the first 16 hours the increase in soil strength is apparent, the last three tests give more or less the same results for the point resistance and shaft friction. The elastic stiffness of the soil or F/u is in all cases similar, also the unloading branch is parallel to the loading branch.

One conclusion is that if the static tests are performed on the same day the influence of the drainage process is negligible. The pre and post pseudostatic static tests can therefore be compared to give a judgment about the change in soil conditions induced by the pseudostatic test.

The difference between several preparation cycles as described in paragraph 9.2 gives more insight in the differences between several set-ups and preparations.

9.3.4 Soil stiffness and failure

A closer look at Figures 9.3 and 9.4 reveals a very abrupt transition from elastic to plastic deformation. A small variation of loading force can have great consequences in soil behaviour. A variation of +/- 10 % on the total load gives a variation of displacement of 1 up to 10 mm. Or to put it differently: it is easy to get an elastic soil reaction when an elastoplastic soil reaction is wanted. Unfortunate this behaviour is also observed in the pseudostatic test results.

The pseudostatic results can therefore be split in elastic behaviour (displacement < 3 mm) and plastic behaviour (displacement > 3 mm). In chapter 10 the results of the pseudostatic tests with primarily plastic soil behaviour are elaborated. The tests where only elastic soil behaviour has occurred are only interesting for the study of the loading rate effect on the stiffness.

9.4 Comparing pre and post static results

9.4.1 Introduction

In this part the static tests which are performed before the pseudostatic tests and after the pseudostatic tests are statistically compared. In this case the influence on the soil condition by performing a pseudostatic test can be checked. The feasibility of performing more then 1 pseudostatic test on the same pile can be tested.

9.4.2 Pre / Post

The check is performed for two data series. The first data series consists of all tests where only one pseudostatic test is performed. The second data series consists of all tests where the number of consecutive tests is larger then 1. The statistical comparison is executed with the paired student-t test.

$$\hat{X}_i = \left(X_i - \overline{X}\right)$$
$$\hat{Y}_i = \left(Y_i - \overline{Y}\right)$$
$$t_{\exp} = \left(\overline{X} - \overline{Y}\right)\sqrt{\frac{n(n-1)}{\sum_{i=1}^{n}\left(\hat{X}_i - \hat{Y}_i\right)^2}}$$

where $\overline{X}$ is the mean value of the values for q_p, q_s or F_{head} of the static test before the pseudostatic tests and $\overline{Y}$ for the values of the static tests which are executed after the pseudostatic test. n is the total number of pairs (a combination of a pre and post test).

This t is tested according the following Hypotheses:
H_0: $\overline{X} = \overline{Y}$
H_a: $\overline{X} \neq \overline{Y}$

When $t_{exp} < t_{2.5\%;n-1}$ the mean values are the same. The value for $t_{2.5\%;n-1}$ depends on the amount of degrees of freedom (n-1), the type of student-t distribution (two tailed) and the confidence interval (95% confidence gives 2.5% limit for the two tailed distribution).

In the following Table the results of this analysis are given for the static tests executed before and after 1 pseudostatic test (1 PS) and after 3 pseudostatic tests (3 PS). A more detailed outcome is given in appendix N. The results are for the soil conditions of 10 minutes of vibration time and 1.5 hours of fluidization. The results are split for the point resistance (q_p), shaft friction (q_s) and force on the pile head (F_{head}).

Type of test	Soil conditions	Number of pairs n	t_exp	$t_{2.5\%;n-1}$	post = pre
1 PS q_p	10V 1.5F	14	1.73	2.160	true
1 PS q_s	10V 1.5F	14	0.33	2.160	true
1 PS F_{head}	10V 1.5F	14	2.21	2.160	false
3 PS q_p	10V 1.5F	4	5.37	3.182	false
3 PS q_s	10V 1.5F	4	0.536	3.182	true
3 PS F_{head}	10V 1.5F	4	0.709	3.182	true

Table 9.1 Results of the paired student-t test

The result is that for the force on the pile head, which gives at first sight the most coherent results, statistically a better proof can be given that the results differ! This is caused by the relative small variance of the dataset. Because the value for $\hat{X}_i - \hat{Y}_i$ is large for most of the pairs in the shaft friction data the confidence interval is very wide, resulting in the situation that with the paired student-t method the H_0 hypothesis cannot be falsified. Not enough proof is found to reject the hypothesis.

Because the results of the pre and post static results are comparable in almost every case (and more important at least for the point resistance and shaft friction in the case of one pseudostatic test, which is needed for the calculation of the ST/CPT ratio c_p) all these results are combined to show that these are normally distributed.

This can be proven bij plotting the normal probability plot. On the x-axis the normal order statistic medians are plotted and on the y-axis the ordered response values. The normal order statistic medians can be calculated out the percent point function of the normal distribution. Figure 9.5a-c shows the results for the combined data sets (thus a total of 36 points for the point resistance, shaft friction and force on the pile head). When the data points are located on one line, the result of this analysis is that the data set is normal distributed. Which is the case.

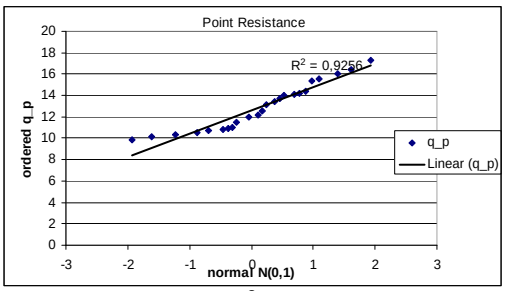

a) Point resistance; R^2=0.9256

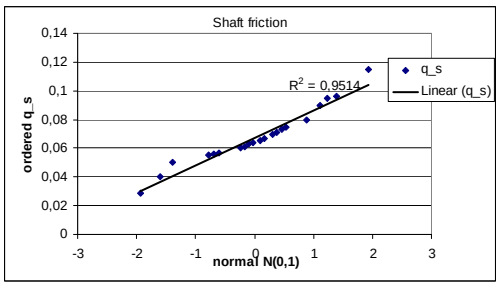

b) Shaft friction; R^2=0.9514

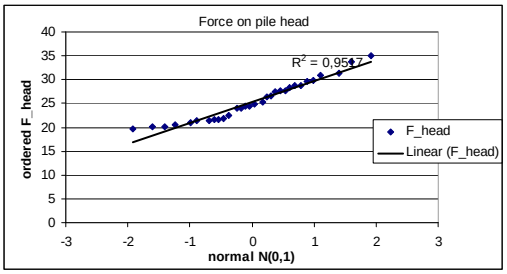

c) Force on pile head; R^2=0.9517
Figure 9.5 Prove of normal distributed experimental data

Thus the 95% confidence limit values for the normal distribution can be calculated, so deviations can also be statistically recognized.

9.5 CPT results, static test results and their coefficient c_p.

9.5.1 Introduction

Because the static test results are a good reflection of the ultimate bearing capacity (see § 9.2.2), and the results are comparable for the pre and post static tests only the pre static tests are compared with the CPT results.

9.5.2 Results of the comparison

When for 10 minutes of vibration time and 1.5 hours of fluidization the results of the CPT, see appendix O, are compared to the results of the first static test Table 9.2 is obtained. The CPT is executed at 20 mm/s while the static test is executed at ~1 mm/s.

The difference in resistance induced by the difference in velocity during the CPT and the static test is accounted for by the introduction of a factor

$$c_p = \frac{F_{static-test}}{F_{CPT}}$$

where F_{CPT} is the force calculated out of the cone resistance data by multiplying the resistance with the cone area, the $F_{static-test}$ is derived out of a static pile test as described in the same manner. Of course a similar ratio can be separate made for the point resistance and shaft friction. The c_p is split for the point resistance and the shaft friction and also listed in Table 9.2. Because of the comparison of the first static with the CPT the results of the > 3 PS are also considered in the comparison.

Point resistance			Shaft friction		
Static	CPT	c_p	Static	CPT	c_p
10.8	12.7	0.85	0.029	0.076	0.38
10.5	12.7	0.83	0.057	0.069	0.83
14.1	20	0.71	0.115	0.109	1.06
11	14.3	0.77	0.061	0.082	0.74
12.2	15.2	0.80	0.071	0.084	0.85
17.3	22.1	0.78	0.115	0.131	0.88
13.4	-	-	0.080	-	-
13.4	16.6	0.81	0.064	0.075	0.85
14.2	19.5	0.73	0.090	0.097	0.93
14.1	16.7	0.84	0.063	0.081	0.78
10.8	12.4	0.87	0.050	0.060	0.83
16.4	19.8	0.83	0.067	0.083	0.81
12	14	0.86	0.038	0.033	1.15
12.6	14.84	0.85	0.065	0.071	0.92
15.6	19.15	0.81	0.090	0.100	0.90
10.3	12.0	0.86	0.055	0.060	0.92
9.9	11.3	0.88	0.060	0.068	0.88
14	15.2	0.92	0.080	0.088	0.91

Table 9.2 Comparison of the CPT (v_{CPT} = 20 mm/s) and static results (v_{stat} = 1 mm /s)

In this case for the point resistance the c_p is ranging from 0.7 to 0.85 and for the shaft friction it's ranging from 0.74 to 1.25 (with exception of the first value). The mean value and standard deviations for c_p are listed in Table 9.3:

	Mean	Std. Dev.
$c_{p;point}$	0.82	0.05
$c_{p;shaft}$	0.86	0.16

Table 9.3 Mean and std deviation of c_p.

Out of this results can be concluded that a significant rate effect is found for the point resistance and a non-significant (caused by the large scatter in the results of the shaft friction) effect for the shaft friction.

The values for the resistance at the end of the CPT are determined to be the peak value before the gentle roll of in the q-T plot. For an example see Figure 9.6.

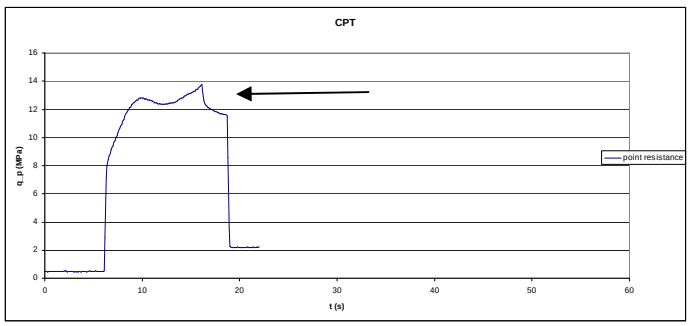

Figure 9.6 Determination of the peak CPT value

This gentle roll of is caused by the elastic response of the soil after is stopped with the displacement of the pile (the soil gives a reaction force on the loading device directly after is stopped with the pile loading). After several seconds the jack is moved upward and the pile is unloaded. Notice the residual stresses (see chapter 10.2.4 for elaboration on that topic).

9.6 Conclusions

- Acceptable soil consistency of the soil in the geotechniek calibration chamber is met when the results are differentiated to the several locations in the calibration chamber, however some improvements with regard to the soil preparation and the fluidization procedure in particular can be made.
- The improved static loading tests with additional displacement measurements can be used to improve the interpretation of the experimental data from the pseudostatic tests which do not incorporate displacement information.
- If the static tests are performed on the same day the influence on the test results of the alteration of the soil conditions by the drainage process is negligible (chapter 9).
- The Static (1 mm/s) - CPT (20 mm/s) ratio or c_p is 0.82 for the point resistance and 0.86 for the local shaft friction. Only for the point resistance this result is significant and therefore can be concluded that a rate effect exist. The results of the shaft friction show a too large scatter
- The load displacement plot is almost bilinear.
- The static result of the test before the pseudostatic test is in agreement with the static test performed after the pseudostatic test.
- The experimental static data is proven to be normal distributed.

10. Test Results Part 2: Loading rate

10.1 Introduction

A series of tests is made to investigate the influence of the loading rate on the pseudostatic loading capacity in non saturated wet sand. Three different loading pulses are applied in the pseudostatic test. Also the results of the static tests are added in the comparison to obtain the PS/ST ratio. The soil preparation is in all cases the same, namely 1.5 hours of fluidization and 10 minutes of vibration.

10.2 Influence on loading capacity

10.2.1 Introduction

On three different locations in each tank preparation with 10 minutes vibration time a pile is installed, statically tested, 1 or more times pseudostatically tested and again statically tested. So a total of 14 pseudostatic tests are executed. During the installation the tip resistance and shaft friction are recorded, while during the static tests also the force on the pile head is recorded. All quantities with a time step of 0.1 s. During the pseudostatic test the time step was 470 μs. An overview of all tests and the accompanying data and results files is given in Appendix K

On the contrary of the planning as presented in § 8.2.4 not in all cases a series of 3 consecutive tests on 1 pile are executed. After the first 3 (9) tests a closer look at the static tests (Table 9.1) revealed a substantial difference in bearing capacity, more tests on the same pile does influence the soil behaviour. Therefore in the next series of tests the amount of pseudostatic tests on each pile was reduced to one, with exception of location ii. On that location three pseudostatic tests were executed and the static test was postponed to the following day, resulting in a time difference between the last pseudostatic test and the static test of >16 hours. As discussed in § 9.3.3 this clearly influences the result of the static test as can be seen in Appendix P.

After those two series of testing a series of tests is repeated to obtain plastic soil failure. In these tests the drop height is doubled to force large displacements. Thus totaling three series of tests with a total of 3 different pile locations and 4 different preparations unfortunate a lot of tests are discarded or simply failed, so nine proper results are left which reacted plastic.

The discarded tests are tests which reacted elastic during the pseudostatic test, the reason for this behaviour can be found in the sharp transition of the soil strength as illustrated in § 9.3.4. A small variation in the load results in a mainly elastic soil reaction instead of a plastic soil reaction. The pile does not fail during the pseudostatic test and the results are not of use in the determination of the influence of the loading rate on the loading capacity.

Therefore the influence of the rate effect on the loading capacity is studied only for the tests which deformed plastic during the pseudostatic tests (8). The influence on the soil stiffness is studied for both the tests which showed plastic as well elastic soil deformation and of which during both the static as well the pseudostatic test a displacement is recorded can only be considered (2). For a total overview of all performed tests and their suitability for the loading rate analysis or stiffness analyses is referred to Table 10.1.

test series	date (2004)	loc	pseudostatic test elastic or plastic	static test with displacement	in consideration for comparison rate effect bearing capacity	quality q-u data during PS	in consideration for comparison rate effect stiffness
series1	19-jul	i	elastic	no	no	sufficient	no
	20-jul	ii	plastic	no	yes	sufficient	no
	21-jul	iii	n/a (no displ)	no	no	insufficient	no
series2	27-jul	i	plastic	no	yes	insufficient	no
	26-jul	ii	elastic	no	no	insufficient	no
	26-jul	iii	elastic	no	no	sufficient	no
hernieuwd	17-aug	i	plastic	no	yes	insufficient	no
	16-aug	ii	n/a (no displ)	no	no	insufficient	no
	16-aug	iii	n/a (no displ)	no	no	insufficient	no
hernieuwd2	19-aug	i	plastic	no	yes	insufficient	no
	19-aug	ii	plastic	no	yes	sufficient	no
	20-aug	iii	elastic	no	no	insufficient	no
hernieuwd3	8-sep	i	plastic	yes	yes	insufficient	no
	8-sep	ii	plastic	yes	yes	sufficient	yes
	10-sep	iii	plastic	yes	yes	sufficient	yes
Test with succesors	18-oct	iii	plastic	yes	yes	sufficient	No (test completed after finishing of 98 % of the report
					a total of 9 suitable results		a total of 2 suitable results

Table 10.1 Overview performed tests and their relevance for analysis

All these tests are performed in the same soil conditions (10 minutes of vibration time 1.5 hours of fluidization).

10.2.2 Influence of inertia component

In the view of the big differences in the static results during the >1 consecutive pseudostatic tests, only the first of a series of three are considered. The execution order of the three tests is changed on every location, so for each type of loading pulse a first test is present. The other tests are not taken in consideration; however the results of all tests, including the compromised ones, are listed in appendix Q.

Because this test is of the dynamic variety the inertia term has to be considered. Although the test procedure is called pseudostatic, the soil behaviour is dynamic. When an axially loaded pile supported on linear springs is considered. The following differential equation is obtained out of the equilibrium equation and Hooke's Law for the pile material and addition of the inertia term (Verruijt 1994).

$$EA\frac{\partial^2 w}{\partial z^2} - cOw = rA\frac{\partial^2 w}{\partial t^2}$$ where:

E is the Young's modulus of the pile
A is the cross sectional area of the pile
w is the pile displacement
c the subgrade modulus, the ratio of the shear stress and the displacement w so just a sort of spring stiffness spread across the pile.
O is the circumference of the pile
ρ is the density of the pile material

When a cyclic load, the loading pulse is in fact one cycle, with angular frequency ω is substituted ($w = \tilde{w}e^{iwt}$) the expression becomes

$$EA\frac{d\tilde{w}}{dz^2} - cO(1 - \frac{rAw^2}{cO})\tilde{w} = 0$$

The term $\frac{rAw^2}{cO}$, or I, is a dimensionless parameter which gives a measure for the importance of the inertia term. In the case of the model pile the period is 46 ms and thus the angular velocity is ~136 1/s The c is estimated at $q_{shaftt}/u_{plastic}$ = ~20 MPa/m. Together with the pile diameter of 36 mm this results in a value for I of ~0.14. This means that inertia does play a role.

10.2.3 Results of model tests

In Table 10.2 an overview is given for the plastic tests. The location, amount of springs, drop height, pile displacement, pile velocity, pulse duration and the pseudostatic/static ratio are given. The velocity is derived numerically by integrating the acceleration data. The focus is on the soil reaction, because in that case the inertia of the pile is already accounted for.

	series 1	**series 2**	**hernieuwd**						
location	ii	i	i	i	ii	i	ii	iii	iii
# disc springs	1	1	6	6	5	5	5	6	6
drop height (cm)	18.5	20.9	29.9	30	32.5	29,3	32	27,5	23
pile displacement (mm)	5.4	3.5	5.9	>3	6.5	>6	13	>9	8
pulse width (ms)	13	14	23.5	23	22	21	22	22,5	24
pile velocity (m/s)	0.35	0.32	0.3	0.2	0.25	0.3	0.25	0.28	0.25
PS tip resistance	13.9	14.5	14	12.7	13.9	10.6	10.6	14	12.1
ST tip resistance	12.2	13.4	14.1	12	12.6	10.3	9.9	14	11.8
PS/ST tip resistance	1.14	1.08	0.99	1.06	1.10	1.03	1.07	1.00	1.03
PS shaft friction	0.081	0.09	0.064	0.042	0.08	0.06	0.061	0.08	0.07
ST shaft friction	0.071	0.08	0.063	0.04	0.065	0.055	0.06	0.08	0.068
PS/ST shaft friction	1.14	1.13	1.02	1.05	1.23	1.09	1.02	1.00	1.03

Table 10.2 Overview plastic pseudostatic test results

When the PS/ST ratio for the shaft friction and tip resistance is plotted in a graph together with the static results, which de facto have a ratio of one and a velocity of 0.001 m/s, and the results of the CPT, actually CPT/ST = $1/\alpha_p$ at the standardized velocity of 0.02 m/s, Figure 10.1a-b can be compiled. The scale on the y-axis is curtailed, therefore the differences are exaggerated.

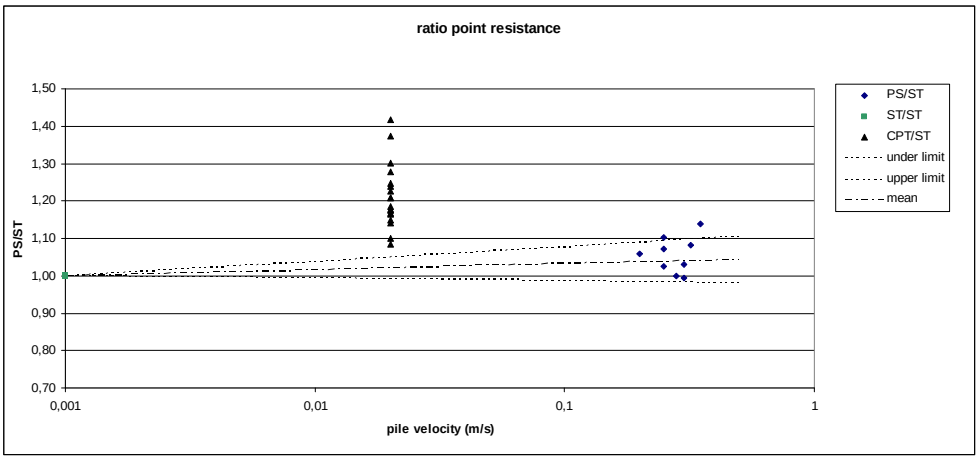

a) Tip resistance ratio pseudostatic/static against pile velocity

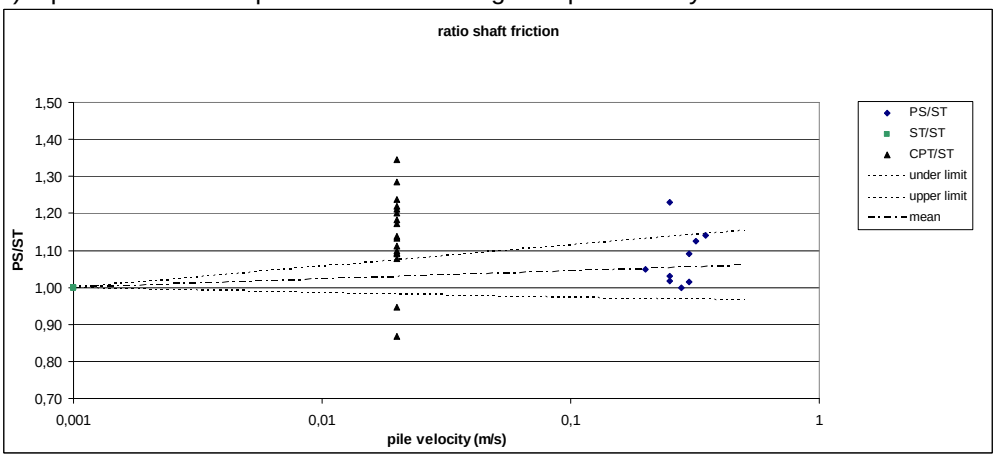

b) Shaft friction ratio pseudostatic/static against pile velocity

Figure 10.1a-b Influence of loading rate on the tip resistance & shaft friction during pseudostatic test. The pseudostatic results are normalized to the static results and plotted against the velocity.

In each graph three lines are plotted. Of the pseudostatic data between each point and the point (0.001;1.00) a function of type $y = a\ln(x) + b$ is fitted. Of all constants a and b the mean and standard deviation are calculated. With this information the 95% confidence limits are calculated. To put it schematically:

$$\bar{x}_n = \frac{\sum x}{n}$$

$$s = \sqrt{\frac{\sum x^2 - \left(\sum x\right)^2}{n(n-1)}}$$

$$P\left(m \in \left[\bar{x}_n - rs\ ,\ \bar{x}_n + rs\ \right]\right) = 1 - a$$

$$a = 10\%$$

$$r = f^{-1}\left(1 - \frac{1}{2}a\right) = 1.645$$

Of course a relationship between a and b exists this relationship introduces a certain correlation coefficient thus resulting in another probability calculation but because the standard deviation in b (the vertical shift) is small this can be neglected.

The use of the normal distribution is permitted, because the data is normally distributed see Figure 10.2a-b:

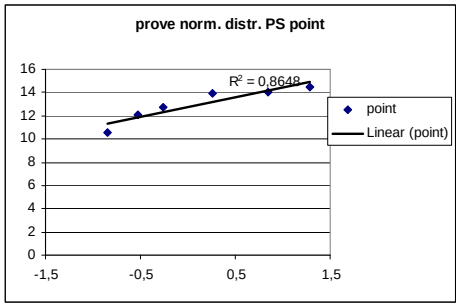

a) PS results tip resistance: $R^2 = 0.86$

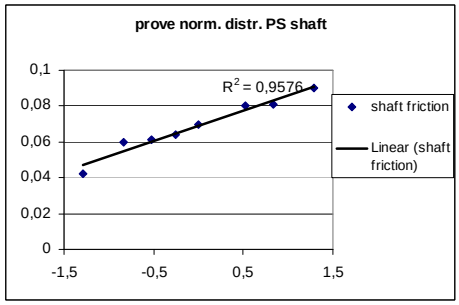

b) PS results shaft friction $R^2 = 0.96$

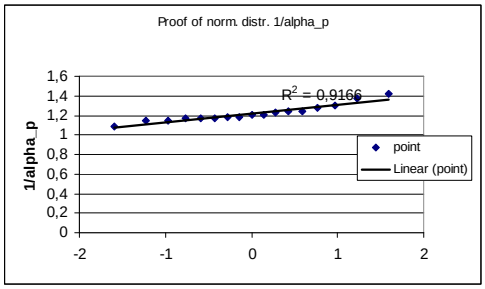

c) $1/c_p$ results tip resistance: $R^2 = 0.95$

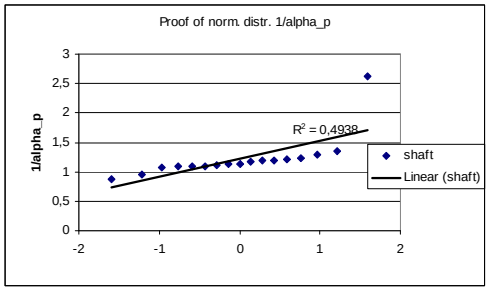

d) $1/c_p$ results shaft friction $R^2 = 0.49$

Figure 10.2 Proof of distribution results of pseudostatic tests

Out of the loading rate analysis can be concluded that the loading rate effect in non saturated wet sand in scaled conditions is a small (tip resistance 4 %; shaft friction 6%), but not significant effect, because values of the PS/ST ratio of <1 are in the confidence interval the findings aren't significant. These findings are in line with literature for example Eiksund & Nordal (1996) who also found a small not significant effect.

The CPT data is not considered because of the very large displacements (several diameters) which occur during installation, therefore the failure mechanism is a bit difference. The mean CPT/ST ratio is 1.22 for the tip resistance and 1.16 for the shaft friction (see § 9.5 for the mean value of c_p). Therefore the CPT readings are affected by the loading rate. The data of $1/c_p$ is normally distributed see Figure 10.2c-d. thus that is not explaining the big scatter.

When for the last PS test and the accompanying static test the individual components are plotted (tip resistance shaft friction of the whole pile, inertia term and the total measured PS force) then Figure 10.3 is obtained.

The inertia term is calculated out of the acceleration data and the mass of the pile $F_i(t) = m_p \cdot a(t)$ with m_p = 21 kg. The force on the pile head, $F_{head;PS}(t)$, is directly measured during the pseudostatic test (PS) and during the static test $F_{head;static}$. The tip resistance $F_{p;PS}(t)$ is calculated out of $q_p(t)$ by multiplying with the tip surface $A_p = 10^{-3}$ m^2. The shaft friction during the PS test is derived by subtracting $F_i(t)$ and $F_{p;PS}(t)$ from $F_{head;PS}(t)$. During the static test the tip resistance $F_{p;static}$ can be directly derived out of q_p in the same way as in the PS case. However no inertia term is present thus the shaft friction along the whole pile is simply the measured force on the pile head ($F_{head;static}$) minus the tip resistance q_p multiplied with A_p resulting in $F_{p;static}$.

In short:

pseudostatic

$$F_{s;PS}(t) = F_{head;PS}(t) - F_{i;}(t) - F_{p;PS}(t)$$

static

$$F_{s;static} = F_{head;static} - F_{p;static}$$

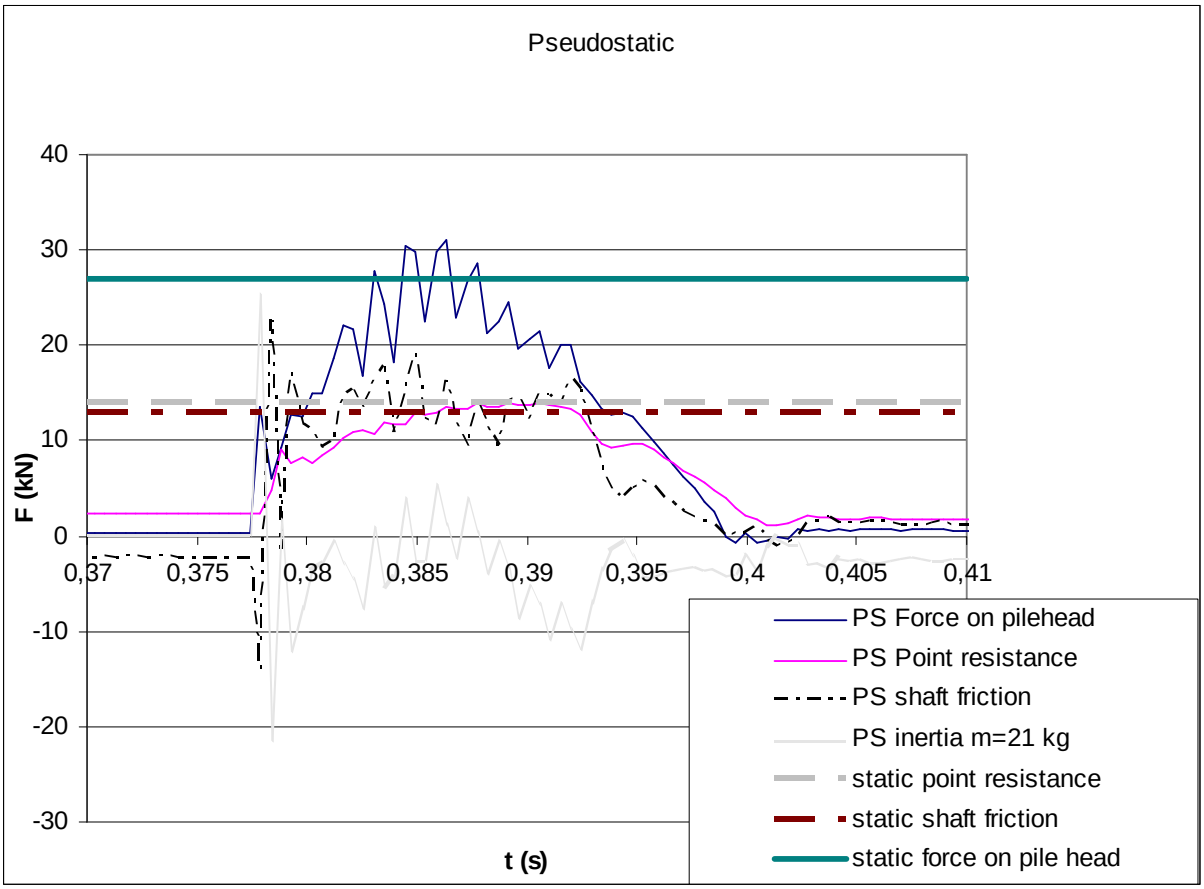

Figure 10.3 Individual force components during static and pseudostatic test

Clearly can be seen that in all cases the results of the static test are similar to the results of the PS test. No rate effect is present at all. It is important to notice that at a higher loading rate no shift from tip bearing into shaft bearing is present. The division in shaft friction and tip resistance is similar.

When the actual measured sleeve friction is scaled up with the ratio $A_{pilecircumference}/A_{sleeve}$ (with $A_{pilecircumference} = \pi DL_{pile}$ and $A_{sleeve} = \pi DL_{sleeve}$) = 0.15 m^2 / 0.015 m^2 = 10. The force in the static case becomes $F_{measured;static;scaled} = q_{s;static} \cdot A_{sleeve} \cdot 10$ = 11.6 kN. And during the PS case: $F_{measured;PS;scaled}$ $q_{s;PS} \cdot A_{sleeve} \cdot 10$ = 10.1 kN.

When the values for the upscaled measured shaft friction and the shaft friction out of equilibrium are compared (see Table 10.3) the upscaled measured PS value does differ most from the actual value (25%), the difference during the static test are also there, but only 10%.

ST out of equilibrium (kN)	$F_{measured;static;scaled}$ (kN)	PS out of equilibrium (kN)	$F_{measured;PS;scaled}$ (kN)
13	11.6	13.6	10.1

Table 10.3 Differences in measured shaft friction and actual shaft friction

Where this discrepancy comes from is uncertain, because both the friction sleeve and the rough upscaling can be erroneous.

10.3 Influence of rate effect on soil stiffness

10.3.1 Introduction

As mentioned in the introduction of §10.2 tests which reacted elastic can be added to the data set, but none of the elastic tests have also a static test with recorded displacements. The addition of those tests gives a total number of fifteen tests. Unfortunate the amount of static tests with recorded displacement is by far not as large so that amount is thus the limiting factor. In Table 10.1 an overview is given.

The q/u ratio is the only quantity which directly can be derived from the q_p-displacement plot and the q_c-displacement plot, thus giving a spring constant for the tip resistance and a spring constant for the shaft friction. Or to put it schematically in Figure 10.4:

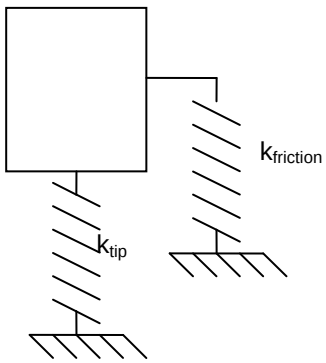

Figure 10.4 Spring stiffness

Those two springs are in parallel so $1/k_{shaft} + 1/k_{tip} = 1/k_{total}$ or the soil reaction, the second spring in a two mass spring system.

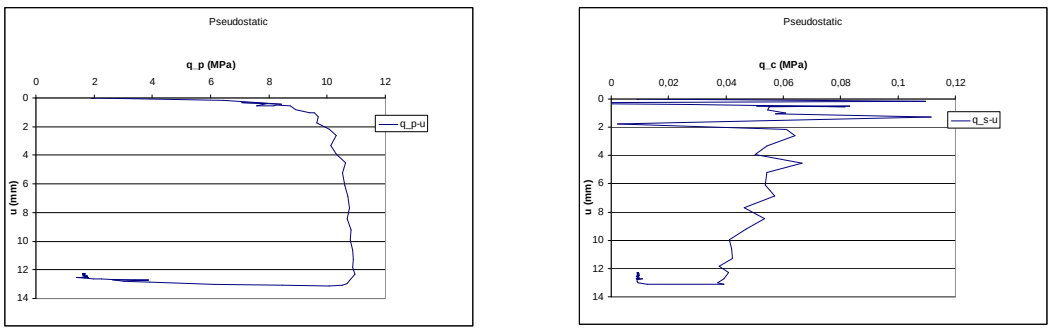

Figure 10.5 Typical q_p-u and q_s-u plots

In Figure 10.5 a typical graph is given of the load-displacement plot of a pseudostatic test. Because the analysis of the loading branch is very difficult (e.g. a lot of peaks on the signal of the

shaft friction), in that case the unloading branch is taken. Loading and unloading behaviour is most similar. For both the static as well the pseudostatic this is done unless the displacement pot reached it's maximum before loading was ended (in case of very large deformations).

Also when is looked at the experimental data keep in mind that some elastic shortening of the pile does occur. This shortening will be calculated first in §10.3.2 after that the true soil stiffness will be discussed in §10.3.3.

10.3.2 Elastic shortening of the pile

The elastic shortening of the pile is not trivial to calculate. In general two major factors are in play:

1) Decreasing normal force in the pile below ground level caused by the shaft friction
2) Residual load in the pile after installation

1) Influence of shaft friction on normal forces

With increasing depth the shaft friction becomes larger, each increment in the shaft friction give a decrease in normal force.

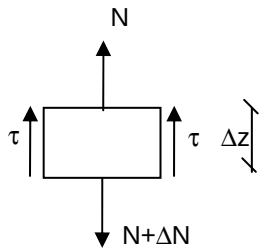

Or in math:

$$\frac{dN}{dz} = tO$$

N = normal force (N)

dz = height of increment (m)

t = shaft friction

O = circumference pile (m)

Figure 10.6 Element of axially loaded pile

This equation can be extended (see e.g. Verruijt 1994) with force stress relation ($N=\sigma A$) and Hooke's Law ($\sigma=E_{pile}\varepsilon$), and displacement strain relationship ($\varepsilon=du/dz$) and linear behaviour of the shear stress ($\tau=c\cdot u$ with c the subgrade modulus) to acquire the basic differential equation for an axially loaded pile supported by springs.

$$EA\frac{d^2u}{dz^2} - cOu = 0$$

The solution for this problem for z = 0; N = -P and z=L; N = 0 (no tip resistance) is elaborated by Verruijt and is of the form:

$$N = -P\frac{\sinh\left[(L-z)/h\right]}{\sinh(L/h)}$$

Where P is the applied force and h the characteristic length defined as:

$$h = \sqrt{EA/cO}$$

If h is small compared to the total length L, the pile is considered infinite long and the solution reduces to:

$$N = -Pe^{-\frac{z}{h}}$$

But of course we do have tip resistance, thus at z = L; N = Y the solution then becomes (see appendix L for derivation)

$$N = -\frac{e^{-\frac{l}{h}}\left(Pe^{-\frac{l}{h}} - Y\right)e^{\frac{z}{h}} - \left(P - Ye^{-\frac{l}{h}}\right)e^{-\frac{z}{h}}}{EA\left(\left(e^{\frac{-l}{h}}\right)^2 - 1\right)}$$

P = loading force

Y = m*easured* tip resistance

l = pile length

The main problem is that this analysis is used to find the stiffness of the soil, thus the subgrade modulus is unknown. For the estimated subgrade reaction out of § 10.2.3 (20 MPa/m), L = 1.25 m (embedded length), A = 10^{-3} m^2, O = 0.11 m, P = 24 kN and E_{pile} = 210 GPa the solution becomes as depicted in Figure 10.7. The results are fitted on a tip resistance of 12 kN. The k_p becomes in this situation a relatively high value of $1.7 \cdot 10^7$ N/m. All these values are in the proper range, resulting in some confidence in the model.

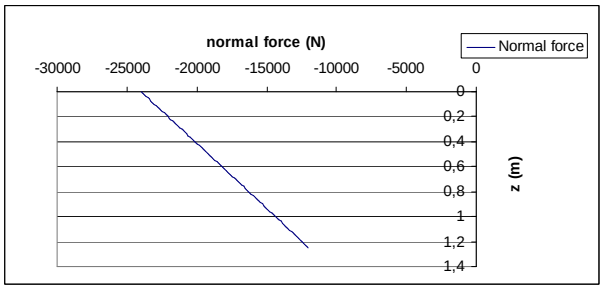

Theoretical normal force

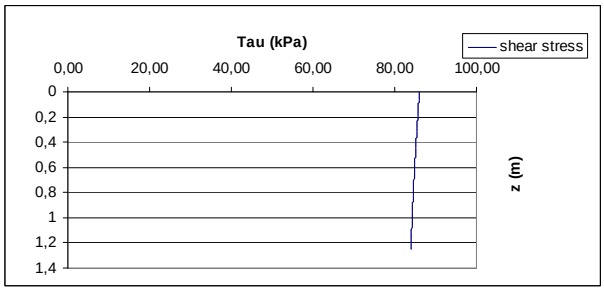

Theoretical shear stresses

Figure 10.7 Results of elastic model

The calculated value gives more or less a linear distribution, this is a reasonable approximation from the model, when an even more simple view is maintained this is also expected:

$t = s'_n \tan j$

$t = s'_h \tan j$

$t = l_0 s'_v(z) \tan j$

$t = l_0 g z \tan j$

$t = C \cdot z$

with

$C = l_0 g \tan j$ (independent of z)

l = lateral earth pressure coefficient

g = volumetric weight

j = angle of internal friction

Therefore the following normal force distribution (see Figure 10.8 not to scale) is a good representation for the normal forces during compressive loading, in this case installation, because out of the measurements it becomes apparent that F_p is of the same magnitude as F_s and the normal force in the rod above ground level is constant.

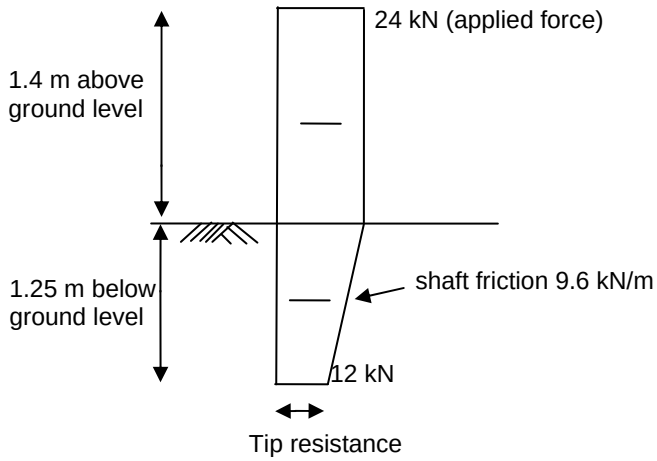

Figure 10.8 Normal forces of pile during installation

2) Influence of residual load on normal forces

After installation some stresses are still recorded by the CPT cone, these so called residual stresses are still acting on the pile. This means that not all elastic shortening during installation is reversed. And therefore the pile is already shorter resulting in an overestimation of the pile shortening.

When residual stresses in the pile are considered (see e.g. Briaud (1985), Poulos (1987), Maiorano (1996), Fellenius (2002) for more information about the topic) immediate after installation the normal forces plot depicted in Figure 10.8 will change in the plot as shown in Figure 10.9a. the forces above ground level are not shown (calculated with the same elastic schematization, boundary value of 2 kN at the pile tip). The more sophisticated elastic model gives a more or less linear tendency of the normal forces during installation as well the residual normal forces.

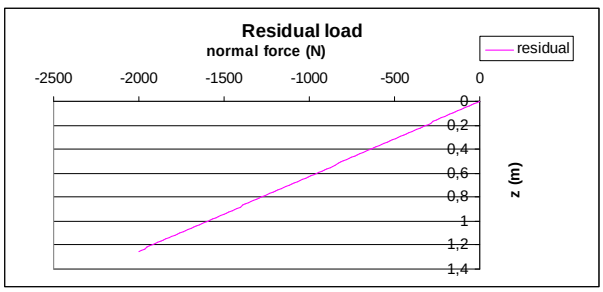

a) Residual load

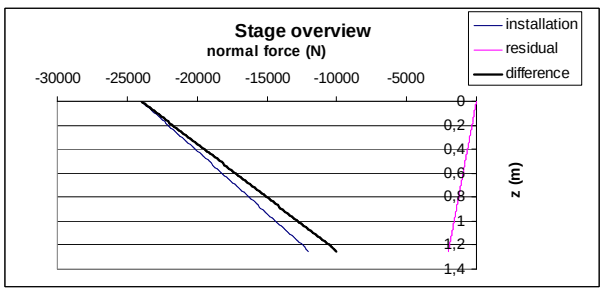

b) Stage overview

Figure 10.9 Residual force in the pile

What happens is the fact that during the unloading the pile moves upward and mobilizes friction. So the lower levels couldn't be unloaded properly because of the shaft friction higher up the pile. The mobilization of friction needs less displacement in comparison to tip resistance, the tip is not fully unloaded when the shaft is unloaded. Equilibrium is met before the complete unloading of the tip is finished.

When the residual normal force is subtracted from the initial normal load the resulting load plot is the actual load distribution during reloading of the pile see Figure 10.9b. This difference between

the normal force during installation and the residual loads is used to calculate the elastic shortening of the pile.

A total of two areas are considered, the normal force above ground level (I) and the normal force below ground level (II). The rod with strain gauges and acceleration transducer has a different cross sectional area also the normal forces do not decrease. For situation (II) the shortening is calculated in increments of 0.01 m. out of Figure 10.9b. The other data is given below.

I F_n= 24 kN; L = 1.4 m; $A_p = 4.84 \cdot 10^{-4}$ m^2; E_{steel} = 210 GPa
II F_n= varies; $L_{increment}$ = 0.01 m; L_{total} = 1.25 m; $A_p = 8.41 \cdot 10^{-4}$ m^2; E_{steel} = 210 GPa

The elastic shortening is calculated with the following well known expression:

$$\Delta L = \frac{F_n L_i}{E_{steel} A_p}$$

And gives a total elastic shortening of $\Delta L_{pile} = \Delta L_I + \Delta L_{II}$ = 0.33 mm + 0.10 mm = 0.43 mm.

10.3.3 Incorporating elastic shortening in derivation of soil stiffness

The pile displacements are measured in the rod above ground level. Therefore the actual displacement of the pile tip should be calculated by subtracting the amount of elastic shortening from the total displacements.

An assumed linear relationship of the displacement with an increasing force can be plotted in the force-displacement plot. The pile is assumed to behave static during the pseudostatic tests, therefore the static expression for the elastic shortening is also used for the PS tests.

When first the elastic pile behaviour is plotted in the static and the pseudostatic F-u graphs (Figure 10.10a-d) (in PS case inertia effects are accounted for by subtracting $F_i = m_p \cdot a$) a very interesting phenomenon can be noticed. During the pseudostatic tests the initial stiffness is fully accounted by the elastic shortening of the pile.

The schematized stiffness for the shaft friction as well the tip resistance are connected in parallel, thus for both the displacement is similar. The ratio F_{shaft} : F_{tip} is approximately 1:1 and the elastic pile shortening is known, thus the shortening can also be incorporated in the q_p-u and q_c-u plots, by plotting the line through ($u_{shortening}$; $q_{failure}$).

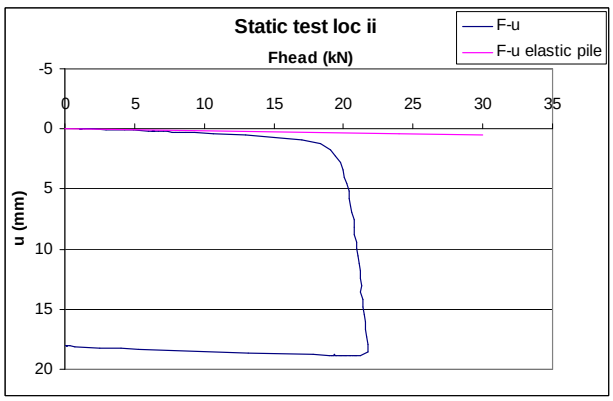

a) F-u plot Static test location ii

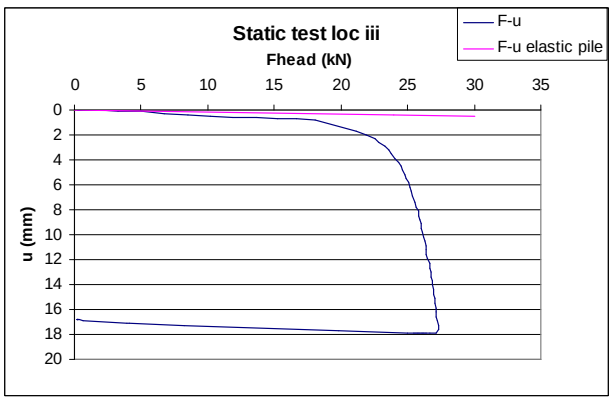

b) F-u plot Static test location iii

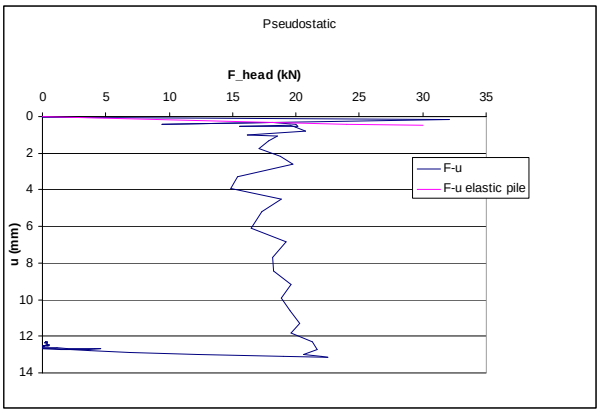

c) F-u plot PS test location ii

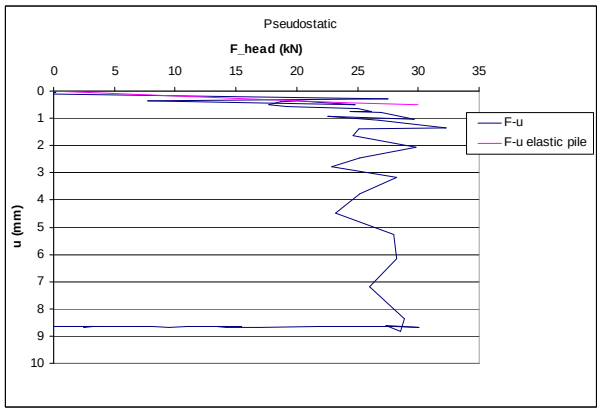

d) F-u plot PS location iii

Figure 10.10a-d F-u plots with elastic pile behaviour for static and pseudostatic test (inertia effect in PS test is accounted for)

A more accurate method to acquire pile shortening requires displacement measurements at the pile head as well the pile tip. When for the existing two cases the rate effect is studied the following Table is obtained:

	stiffness out of q_p-u (GPa/m)		stiffness out of q_s-u (GPa/m)		tip	shaft
	ST	PS	ST	PS	PS/ST	PS/ST
loc ii	37	Inf.	0.16	Inf.	-	-
loc iii	35	18	0.36	Inf.	0.51	-

Table 10.4 Effect of loading rate on soil stiffness

An infinite stiff reaction is found when for the PS test the stiffness is acquired. Or to put it differently: the theoretical value for the pile reacts less stiff then the complete measured pile + soil reaction. So no value for the soil can be determined.

10.3.4 Comparison of stiffness of pile-soil system

When the stiffness of the pile-soil system as a whole is considered, this has great practical relevance, the comparison is easier to make. Only the measured reaction force on the pile head plotted against the measured displacement are considered (see appendix P and Q for the data). Both tests are performed in the same soil conditions (in the same tank preparation). In the case of the pseudostatic test the result of the force is corrected for inertia. Table 10.5 shows the results.

	stiffness out of F-u (MN/m)		Rate
	ST	PS	PS/ST
loc ii	23	58	2.5
loc iii	21	65	3.1

Table 10.5 Effect of loading rate on soil stiffness

Both the static and pseudostatic tests show good consistency in stiffness (within 10 %) and the rate effect is >>1, more research is needed to come to a better conclusion.

10.3.5 Closing remarks about the measured signal

A general remark about the quality of the force and displacement signal can be made. During the execution of the PS tests it is observed that in the first three data points the increase in resistance

is huge. In the following Figure (fig. 10.11) for two typical tests a zoomed view of the response of the tip resistance and shaft friction is given. Also the data points are shown.

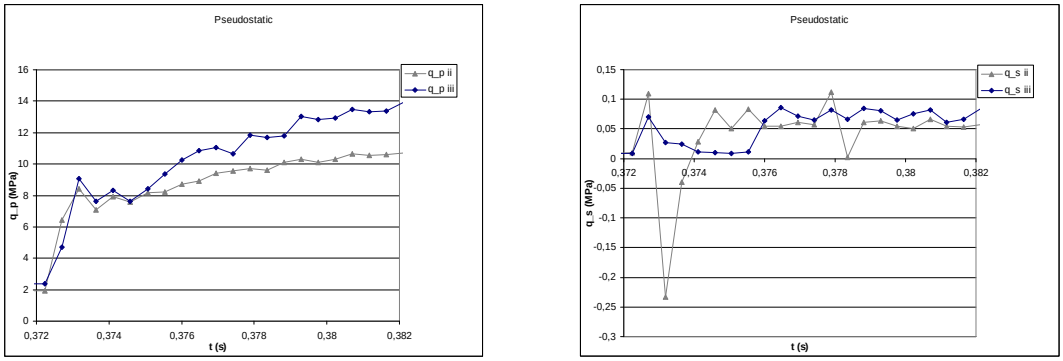

a) Tip resistance b) Shaft friction

Figure 10.11 Close up of response of the tip resistance and shaft friction 1 data point corresponds with T_s of 470 ms.

This behaviour does partly elucidate the extreme stiff reaction found during the stiffness analysis.

Another difference can be found in the intrinsic behaviour of the measuring system. The analog to digital conversion of the system is done on the data acquisition card. This card has only one A/D conversion chip and one multiplexer chip. Therefore the different channels are sequential written into the buffer during the sampling time. Also some overhead needs to be accounted for this overhead time is estimated at 70 μs. In Figure 10.12 a schematic view is shown. Therefore an offset in time of at least 80 μs is found between the results of the different channels.

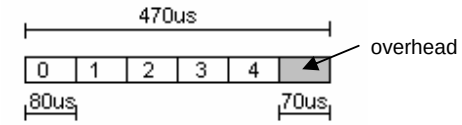

Figure 10.12 Sequential sampling of the channels

The offset depends not only on the data acquisition card and the amount of channels monitored, but also the speed of the computer and the efficiency of the measuring software are of great importance (the overhead).

The sampling time of 470 μs is already the limit of the system (experimentally determined by the measuring department of CT) when a shorter sampling time is chosen the incoming signals are corrupted. Thus the offset cannot be decreased by shortening the sampling time.

This means that the final data needs to be corrected by an offset. Though a problem arises, what is exactly the offset. The only way to acquire this information is to test the system. Feed a known delta voltage simultaneously on all channels (a block function hampers the interpretation, because it's steep flanks are difficult to consistently produce by the A/D converter) of the A/D card and compare the data.

Another problem is to incorporate this offset in the measuring data if the offset is not precizely one sampling period. Because for the F(t)-u(t) or q_p(t)-u(t) both signals have to be defined on the same time! But the individual signals have a shifted discretisatie. Therefore the functions need to be interpolated between the points, so both functions are known on a arbitrary time, before a proper comparison can be made.

When all this is accounted for, still some changes have to be made for the relative distance between the sensors. The displacement is registered 2.5 meters above the sensor of the tip resistance. When the pile head is moving the tip does not move immediate it takes some time, namely the distance between the sensors divided by the wave velocity in the pile (for steel 5000 m/s) or 0.5 ms. Thus the tip resistance is lagging behind for about one times the sampling time. In other words: the pile head moves first and after 0.5 ms the reaction of the tip resistance is registered.

But when all this is incorporated, clearly can be seen that the difference is very small (Figure 10.13).

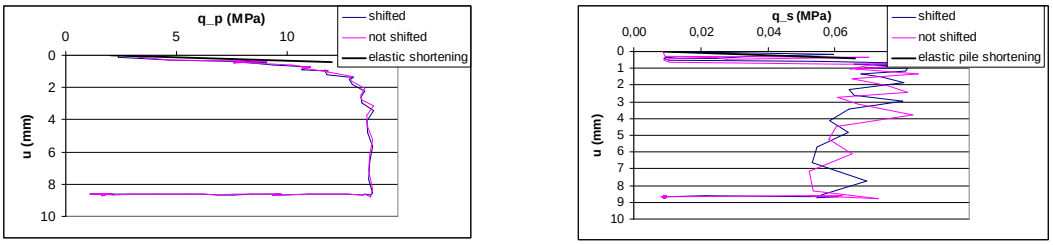

a) Tip resistance b) Shaft friction

Figure 10.13 Comparison in interpretation of the same test

10.4 Conclusions

- In general can be said that with a velocity increase from 1 mm/s to ~250 mm/s the increase in bearing capacity found during the execution of pseudostatic model tests is a non-significant increase of ~ 4% for the tip resistance and also a non-significant increase of ~ 6% for the shaft friction.
- The ratio of the total shaft friction and tip resistance is the same during the static test and the pseudostatic test, no shift in the share of each component is found when the loading rate is increased.
- If more then one consecutive pseudostatic model test is performed on a pile the soil conditions do alter.
- During the pseudostatic test the initial stiffness of the soil-pile system is completely accounted for by the theoretical elastic shortening of the pile, even when an attempt is made to get a proper calculation for the elastic shortening of the pile and the incorporation of the time shift in the measuring data.
- When only the stiffness of the pile soil system is considered both the static and pseudostatic tests show good consistency in stiffness (2 tests within 10 %) and the rate effect is >>1, more research is needed to come to a better conclusion.

11. Discussion of the results

11.1 Introduction

In this chapter some general remarks are made about the results in this report. Three major topics can be distinguished:

1) Variance in preparation and loading which leads to a lot of discarded tests
2) Changes in soil resistance after the PS test.
3) Shape of loading pulse

11.2 Amount of suitable tests results

The preparation problems of the tank are influencing the amount of proper test data. During the initial tests (chapter 7) the displacement was sufficiently large (plastic deformations of the soil), but when the official testing regime was started the displacements were too small. The consistency of the preparation method is thus not as good as expected, although this is location dependent, because the middle location had good consistency (Figure 9.1e-f)

Some variance in the force on the pile head during the pseudostatic load is also found. Partly this is due to the variance in drop height. When a closer look is given at the expression for the initial velocity the influence of the force variance is ~5 % when the drop height is decreased and almost non existing when the drop height is increased. Thus a decrease of 1 cm in drop height gives a decrease of about 1 kN in load. While an increase of 1 cm does not give an increase at all. This can all be accounted for by the square root in the expression for the initial velocity.

Also the friction mobilized in the tube may be still too high. Traces of wear in the tube and on the rim of the drop weight indicate some contact between the two objects.

Therefore additional test series (hernieuwd1 – hernieuwd3) were needed to get enough data points to be able to study the loading rate effect on the bearing capacity of the model piles.

The influence of these varying conditions on the loading rate is not large, because the static and pseudostatic tests are executed on the same pile in the same conditions. Thus the PS/ST ratio is not affected by the difference in conditions during static and pseudostatic tests. But by comparing the ratio with another one some variance is introduced, actually this variance can also be seen in different pile velocities.

11.3 Change in soil resistance

The expected amount of tests on one pile was not reached, because the difference between the static tests which are performed before the pseudostatic test and the static tests which are performed after the pseudostatic test is quite large.

If the quality of the measurements is high (i.e. the measurements of the force on the pile head and the readings of the point resistance) and therefore the variance is small, differences are almost statistically significant (point resistance) or are statistically significant for the case with only one loading cycle.

The pseudostatic test is thus possibly affecting the soil conditions. This matter of fact needs further research, because during a PLT test several loading cycles are successively performed. And even during a statnamic test with only one loading cycle the soil is possibly altered and thus affecting the future loading capacity.

11.4 Shape of loading pulse

A closer look at the results of the pseudostatic tests revealed a very large increment of force / resistance / friction. This is also depicted in Figure 10.11. The loading rate is defined as the steepest slope dF/dt of the loading pulse on the pile head. The reproduced slope of the pseudostatic model tests (appendix Q) is considerably larger then of a typical in-situ prototype test (Figure 4.1). Actually it is a loading rate which resembles more of a dynamic test then a pseudostatic test. See Figure 11.1 for a comparison between the prototype dynamic and statnamic test and an up scaled model test.

After the pile is hit a stress wave is traveling through the pile. When this stress wave is sufficiently long in comparison to the length of the pile (e.g. during a pseudostatic or static test) both the pile head and the pile tip are moving in phase therefore in the same direction on the same time. This is called the rigid body assumption. It simplifies the analysis of the results, because the stress waves are out of the equation. And only the inertia of the pile and the soil response are of interest for the pseudostatic case while during a true static test the inertia can also be neglected.

During a dynamic test the stress wave is short in comparison with the length of the pile. The wave is traveling to the pile tip and back for several times, the amplitude is dampened by the internal friction of the pile and the shaft friction and in the end the waves are dampened out. The system becomes far more complex, because the stress waves in the pile cannot be neglected in the interpretation of the results. This behaviour is called dynamic in this report.

The scaling of the model to the prototype situation is calculated with the scale rules as given in appendix B:

$$t_p = \sqrt{n} \cdot t_m$$
$$F_{\max;\,point;\,p} = n^3 \cdot F_{\max;\,point;\,m}$$
$$F_{\max;\,shaft;\,p} = n^3 \cdot F_{\max;\,shaft;\,m}$$

The results of the model pile test of 8 September at location ii are used in the comparison. For the dynamic case a pulse with a time base of 6 ms is used with a F_{max} of ~25 MN (thus the dynamic pulse as given by Middendorp (1992) only with a larger F_{max}). The statnamic test is taken from Lin, et al (2004).

The loading rate dF/dt for these cases is $6.25 \cdot 10^9$ N/s for the results of the dynamic prototype and the scaled model. For the results of the statnamic prototype test a value for dF/dt of $4.0 \cdot 10^8$ N/s is found. A difference between the prototype statnamic test and the scaled model test of one order is found.

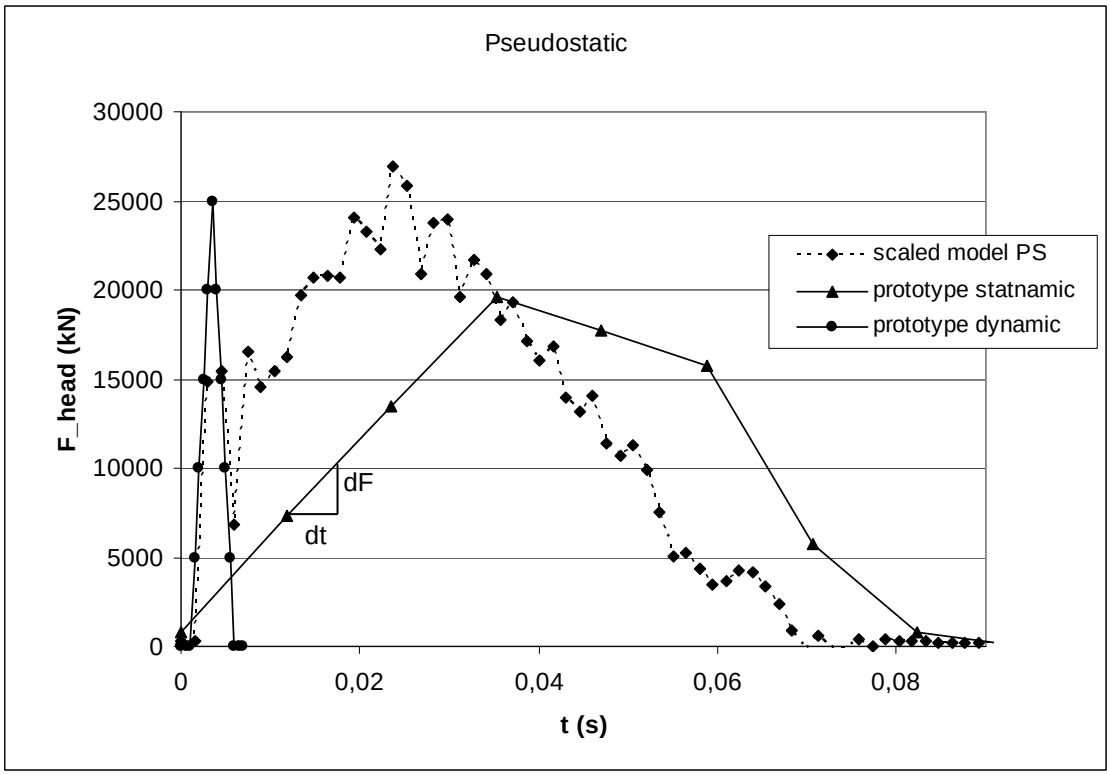

Figure 11.1 Comparison of loading pulses

The pile is still behaving dynamic during the beginning of the model test even when the pulse width and peak force are comparable with the prototype.

The first peak on the pseudostatic pulse from the model is thought to be caused by the steel on steel contact of the drop mass and pile head. This causes a stress wave with very large amplitude, which seems to affect the overall loading pulse which is induced by the springs.

Although all performed tests are situated in the velocity and pulse duration range (after scaling) of a pseudostatic/statnamic test the results can not be compared so easily. Therefore the tests can be classified as a high loading rate test and not necessarily as a pseudostatic test.

12 Conclusions and recommendations

12.1 Conclusions

- The model pile tests (scale 1:10) are performed at 1g conditions in unsaturated wet sand.
- All pseudostatic tests considered in the comparison showed failure of the soil.
- Inertia effects of the model pile are taken out of the equation, thus only the soil reaction is considered for the investigation of the rate effect.
- Acceptable soil consistency of the soil in the geotechniek calibration chamber is met when the results are differentiated to the several locations in the calibration chamber, however some improvements with regard to the soil preparation and the fluidization procedure in particular can be made (chapter 9).
- The improved static loading tests with additional displacement measurements can be used to improve the interpretation of the experimental data from the pseudostatic tests which don't incorporate displacement information (chapter 9).
- If the static tests are performed on the same day the influence on the test results of the alteration of the soil conditions by the drainage process is negligible (chapter 9).
- The Static (1 mm/s) - CPT (20 mm/s) ratio or c_p is 0.82 for the point resistance and 0.86 for the local shaft friction. Only for the point resistance this result is significant and therefore can be concluded that a rate effect exist. The results of the shaft friction show a too large scatter (chapter9).
- In general can be said that with a velocity increase from 1 mm/s to ~250 mm/s the increase in bearing capacity found during the execution of pseudostatic model tests is a non-significant increase of ~ 4% for the point resistance and also a non-significant increase of ~ 6% for the shaft friction (chapter 10).
- The ratio of the total shaft friction and point resistance is the same during the static test and the pseudostatic test, no shift in the share of each component is found when the loading rate is increased (chapter 10).
- If more then one consecutive pseudostatic model test is performed on a pile the soil conditions do alter (chapter 10).
- During the pseudostatic test the initial stiffness of the soil-pile system is completely accounted for by the theoretical elastic shortening of the pile, even when an attempt is made to get a proper calculation for the elastic shortening of the pile and the incorporation of the time shift in the measuring data (chapter 10).
- When only the stiffness of the pile soil system is considered both the static and pseudostatic tests show good consistency in stiffness (2 tests within 10 %) and the rate effect is >>1, more research is needed to come to a better conclusion (chapter 10).
- The initial steepness of the loading pulse which is applied on the model pile is important to classify the behaviour of the pile (chapter 11).

12.2 Recommendations

Static loading system

Improve the loading set-up for the static tests in such a way that a preset force-displacement curve can be met at very low velocities of O(10^{-4} m/s). In that case a true static benchmark can be set, without introducing rate effects. A computer controlled hydraulic jack system seems the solution.

Pseudostatic loading system

To get a smaller variance in applied load, the loading system can be optimized by decreasing the friction of the mass – guidance tube system. Also the spring system needs to be revised to incorporate a less steep initial slope.

Measuring set-up

In order to improve the measured acceleration signal the computer + A/D conversion needs to be improved. The sampling rate which is 470 μs or f_s = ~2 kHz (effective range ¼ * 2 kHz = 500 Hz) has to be increased to accommodate the high frequencies of the acceleration signal. All amplifiers and sensors in the chain are properly working.

Soil preparation

After several preparation cycles the fluidization system is not able to loosen the soil, this is partly due to the fluidization time, but also the sand fraction used is too coarse. Further more the system needs a lot of time to fluidize, a higher flow rate (an increase of pump capacity) shortens the fluidization time considerably. So another type of sand and to a lesser extent an improved fluidization system is recommended.

The densification method of the soil needs to be improved to obtain a more homogenous soil distribution.

Also the influence of apparent cohesion needs to be further researched; all tests presented in this paper are executed in soil conditions with apparent cohesion (unsaturated wet sand).

Extend the velocity range

Repeat the tests for shorter and longer loading pulse durations (higher velocities and lower velocities). So extent the boundaries to the dynamic case O(ms) to the pseudostatic-static case O($1{\cdot}10^2$ - $7{\cdot}10^2$ ms). In that case the loading rate behaviour can be mapped for a wider range. And the whole spectrum from 0.1 mm/s until 1000 mm/s is studied. For high velocities and short pulse durations the measuring system also needs to be improved.

Saturated soil response

For the typical Dutch case the influence of pore water on the loading rate is of great importance, therefore the effect needs to be studied.

Investigate the influence of the location of the shaft friction sleeve

The shaft friction is measured with a standard CPT cone; in that case the location of the friction sleeve is close to the point. The fail mechanism and soil displacement around the pile tip is influencing the stresses around the pile, thus the measured shaft friction can be too high. Those mechanisms are expected to be rate dependent. Or to put it simple: the rate is affecting the reliabilty of the shaft friction measurements.

Scaling of the model to the prototype

Investigation in the scale rules is necessary to come to a proper (non-geometric) scaling of the prototype. Are the results of the model tests a true representation of the prototype as implicitly expected in this report.

Residual stresses

After pile installation residual stresses are left in the soil, the effect of these stresses on static soil behaviour is already complex, but the effect of these stresses on the pseudostatic or dynamic response is unknown and needs to be investigated further.

Pile mass during pseudostatic testing

By calculating the inertia of the pile only the mass of the pile is accounted for. The soil directly around the pile (say ~1-2D_{pile}) also have a certain mass. When this additional mass is incorporated the derived shaft friction does alter and also the rate effect is influenced. Further research is needed to investigate the influence zone during pseudostatic testing.

Influence of the pile test on the soil conditions

No conclusive proof is found about the soil conditions. Do they alter during a pseudostatic test or not. This could be important for the PLT tests which rely on several test cycles. And could also be important for the application of tests on piles which after testing are incorporated in the construction.

Appendix

Appendix A: Considerations about the choice of model tests

There are several methods possible to study the influence of loading rate on pile capacity, to make things clear, first I present the different approaches to consider this problem. Then I choose the method which will be used in the continuation of the graduation project.

1) Investigate the loading rate dependable soil parameter (i.e. Young's modulus), for example by means of constant rate tests (CRT). So a theoretical model has to be developed to correlate the acquired loading rate dependable soil parameter to the results of dynamic and statnamic tests. This correlation has to be verified with in-situ dynamic and statnamic test results. (or representative model tests[1]) During the execution of the CRT a cpt-cone is installed with different predefined velocities (loading rates), in this case the cpt-cone is primarily a measuring device to measure the loading rate dependable soil parameters.

2) Investigate the effect of the loading rate on pile capacity on a model pile which is already installed and measure the relevant parameters (acceleration, displacement etc.) these tests are modeling pile-soil interaction. The results are easier to compare with the results of in-situ dynamic and statnamic test results. As these tests are scaled representations. In this case the pile will be loaded with different time dependable loading profiles (variation of loading rate), to model constant rate, dynamic and pseudo static loads or even a gale on a building.

Of course each method gives different problems. For (1) the theoretical model is necessary to correlate the results, and the loading mechanism has to be capable of large displacements. Another aspect is that higher loading rates require more time to get on speed, during this acceleration phase valuable physical distance is wasted (measurements are made during constant velocities). While in case (2) the short term loading of the pile and the measuring of the sub-millisecond phenomena are more difficult then in case (1), the results are easier to correlate with the in-situ tests.

I opt for case 2, to execute tests on model piles, because I think it will lead to the more specific case of researching the effect of the loading rate on pile-soil interaction. Therefore it is a better fit on the main objective. In my view case 1 is the PhD study of Mr. Huy. And case 2 is a more specific subject which can be embedded in the PhD study.

[1] Actually the kind of tests presented in option 2

Appendix B: Derivation of prototype-model scale when g can not be scaled

In this appendix is looked at the scaling of the in situ problem (prototype) to the model test (model). When the acceleration of gravity can not be linearly scaled and the dimensions are linearly scaled, the resulting model problem is not behaving like the in-situ problem in all means, because of the stress dependent behaviour of the soil. The effect of this scaling on other quantities e.g. the force, the damping coefficient and the spring-stiffness have to be determined to be able to scale the problem. The derivations are made for a homogenous drained sand layer. The relation between the prototype and the model situation will be derived. The following scale rules are applied:

Scale 1:n is adopted for the dimensions → $r_p = nr_m$

The maximum point resistance and shaft friction
The ultimate bearing capacity is a function of the shear stress (τ) and the surface of the pile tip (A_p) and the pile shaft (A_s).

$$F_{\max} = A_p \tau_{\max;point} + A_s \tau_{\max;shaft}$$
$$F_{\max} = \pi r^2 \tau_{\max;point} + 2\pi r L \tau_{\max;shaft}$$

The basic shear equation is $\tau = \sigma_0^{'} \tan\phi$ where $\sigma_0^{'}$ is the normal stress and ϕ the angle of internal friction. The shear stress can be split into a specific expression for the shaft and for the point:

$$\tau_{\max;point} = \sigma_v^{'} \tan\phi$$
$$\tau_{\max;shaft} = \sigma_h^{'} \tan\delta$$

The shaft shear stress is depending on the interface strength, while the point shear is depending on soil-soil shear. Also the normal stress differs for both situations. The equation for F_{max} becomes:

$$F_{\max} = \pi r^2 \sigma_v^{'} \tan\phi + 2\pi r L \sigma_h^{'} \tan\delta$$

First the scaling of the point resistance $F_{\max;point} = \pi r^2 \sigma_v^{'} \tan\phi$:

When the scale rules are applied on $\sigma_v^{'}$ this results in a prototype – model relationship of:

$$\left.\begin{aligned} \sigma_{v;p}^{'} &= \gamma_p z_p \\ \gamma_p &= \gamma_m \\ z_p &= n z_m \\ \sigma_{v;m}^{'} &= \gamma_m z_m \end{aligned}\right\} \sigma_{v;p}^{'} = (\gamma_m)(n z_m) = n\gamma_m z_m = n\sigma_{v;m}^{'}$$

Therefore the force becomes

$$F_{\max;point;p} = \pi (n r_m)^2 (n\sigma_{v;m}^{'}) \tan\phi$$
$$= F_{\max;point;p} = n^3 \pi r_m^2 \sigma_{v;m}^{'} \tan\phi$$

with $F_{\max;point;m} = \pi r_m^3 \sigma'_{v;m} \tan\phi$ this results in :

$$F_{\max;point;p} = n^3 F_{\max;point;m}$$

therefore the scaling of the volumetric weight is correct:

$$\left.\begin{aligned} \gamma_p &= \frac{F_p}{V_p} = \frac{n^3 F_m}{n^3 V_m} \\ \gamma_m &= \frac{F_m}{V_m} \end{aligned}\right\} \gamma_p = \gamma_m$$

Second the scaling of the shaft friction $F_{\max;shaft} = 2\pi r L \tau_{\max;shaft}$:

The horizontal effective stress is linear dependent on the vertical effective stress so for the horizontal stress the following expression also holds:

$\sigma'_{h;p} = n\sigma'_{h;m}$

resulting in:

$$F_{\max;shaft;p} = 2\pi(nr_m)(nL_m)(n\sigma'_{h;m})\tan\delta$$
$$= F_{\max;shaft;p} = n^3 2\pi r_m L_m \sigma'_{h;m} \tan\delta$$

with $F_{\max;shaft;m} = 2\pi r_m L_m \sigma'_{h;m} \tan\delta$ this results in :

$$F_{\max;shaft;p} = n^3 F_{\max;shaft;m}$$

The combined point resistance and shaft friction, the total force $F_{max;p}$, is therefore:

$$F_{\max;p} = n^3 F_{\max;m}$$

The mass

The magnitude of the mass as function of the dimensions is:

$m = \rho V$ where ρ is the volumetric mass and *V* the volume of the mass.

Because $V_p = n^3 V_m$ and ρ doesn't alter ($\rho_p = \rho_m = \rho$), m_p becomes:

$$\left.\begin{aligned} m_p &= \rho V_p = \rho(n^3) V_m \\ m_m &= \rho V_m \end{aligned}\right\} m_p = n^3 m_m$$

The velocity of the mass at t=0

For the following expression is derived: $v_0 = \sqrt{2gh}$, in this expression only h is scaled $h_p=nh_m$ and $g_p = g_m$ Therefore $v_{0;p}$ becomes:

$$\left.\begin{aligned} v_{0;p} &= \sqrt{2gh_p} = \sqrt{2gnh_m} \\ v_{0;m} &= \sqrt{2gh_m} \end{aligned}\right\} \; v_{0;p} = \sqrt{n}v_{0;m}$$

The loading pulse and time

The loading pulse $F \cdot t = m \cdot v$ has to be the same in the prototype and the model situation, the relations $v_p = \sqrt{n}v_m$, $m_p = n^3 m_m$ and $F_p = n^3 F_m$ still hold so the resulting relationship for the time is:

$$\left.\begin{aligned} t_p &= \frac{m_p v_p}{F_p} = \frac{n^3\sqrt{n}m_m v_m}{n^3 F_m} \\ t_m &= \frac{m_m v_m}{F_m} \end{aligned}\right\} \; t_p = \sqrt{n}t_m$$

When the time is derived in another way:

$v = \frac{u}{t}$ in the linear case where $v_p = \sqrt{n}v_m$ and $u_p=nu_m$ the resulting t_p becomes:

$$\left.\begin{aligned} t_p &= \frac{u_p}{v_p} = \frac{nu_m}{\sqrt{n}v_m} \\ t_m &= \frac{u_m}{v_m} \end{aligned}\right\} \; t_p = \sqrt{n}t_m$$

The relationship is consistent!

The spring stiffness

The spring stiffness has to be scaled as well, for a spring the following expression exists:
F=ku, where k is the spring stiffness and u is the displacement.
Because $F_p=n^3F_m$ and $u_p=nu_m$ are applicable the resulting expression for k_p is:

$$\left.\begin{aligned} k_p &= \frac{F_p}{u_p} = \frac{n^3 F_m}{nu_m} \\ k_m &= \frac{F_m}{u_m} \end{aligned}\right\} \; k_p = n^2 k_m$$

Damper coefficient

The damper coefficient is scaled as well, F=cv where c is the damper coefficient and v is the pile velocity. $F_p=n^3F_m$ still holds, also $v_p = \sqrt{n}v_m$ is still applicable. This results in the following expression for c_p:

$$\left.\begin{aligned} c_p &= \frac{F_p}{v_p} = \frac{n^3 F_m}{\sqrt{n}v_m} \\ c_m &= \frac{F_m}{v_m} \end{aligned}\right\} \quad c_p = n^2\sqrt{n}c_m$$

But when the other legitimate expression for the damper coefficient is scaled, with $E_{s;p}=E_{s;m}$ and $\rho_{s;p}=\rho_{s;m}$ The following is the case:

$$\left.\begin{aligned} c_p &= A_{p;p}\sqrt{E_{s;p}\rho_{s;p}} = n^2 A_{p;m}\sqrt{E_{s;m}\rho_{s;m}} \\ c_m &= A_{p;m}\sqrt{E_{s;m}\rho_{s;m}} \end{aligned}\right\} \quad c_p = n^2 c_m$$

Both derivations give different answers. A choice has to be made, this is relatively easy because the model pile is already available (an old CPT-cone) thus the young's modulus and the volumetric weight are quantities determined by this CPT-cone. So the 2nd method will be adopted, because this derivation incorporates the chosen boundary conditions in a more direct way. Therefore the scaling of the damper coefficient isn't as optimal as wanted.

Appendix C: Derivation of prototype-model scale when g can be scaled as well

In this appendix the prototype – model relationship is derived again, with one important difference, namely the acceleration of gravity is also scaled (in practice this can be done by a geocentrifuge). As a result all scale rules are consistent. The following rules are applied.

Scale 1:n is adopted for the dimensions → $r_p = n r_m$ and

$g_p = \frac{1}{n} g_m$ for the acceleration of gravity [lecture notes 4370].

The maximum point resistance and shaft friction

The ultimate bearing capacity is a function of the shear stress (τ) and the surface of the pile tip (A_p) and the pile shaft (A_s).

$$F_{\max} = A_p \tau_{\max;point} + A_s \tau_{\max;shaft}$$
$$F_{\max} = \pi r^2 \tau_{\max;point} + 2\pi r L \tau_{\max;shaft}$$

The basic shear equation is $\tau = \sigma_0^{'} \tan\phi$ where $\sigma_0^{'}$ is the normal stress and ϕ the angle of internal friction. The shear stress can be split into a specific expression for the shaft and for the point:

$$\tau_{\max;point} = \sigma_v^{'} \tan\phi$$
$$\tau_{\max;shaft} = \sigma_h^{'} \tan\delta$$

The shaft shear stress is depending on the interface strength, while the point shear is depending on soil-soil shear. Also the normal stress differs for both situations. The equation for F_{max} becomes:

$$F_{\max} = \pi r^2 \sigma_v^{'} \tan\phi + 2\pi r L \sigma_h^{'} \tan\delta$$

First the scaling of the point resistance $F_{\max;point} = \pi r^2 \sigma_v^{'} \tan\phi$:

When the scale rules are applied on $\sigma_v^{'}$ this results in a prototype – model relationship of:

$$\left.\begin{aligned} \sigma_{v;p}^{'} &= \gamma_p z_p \\ \gamma_p &= \frac{1}{n}\gamma_m \\ z_p &= n z_m \\ \sigma_{v;m}^{'} &= \gamma_m z_m \end{aligned}\right\} \sigma_{v;p}^{'} = \left(\frac{1}{n}\gamma_m\right)(n z_m) = \gamma_m z_m = \sigma_{v;m}^{'}$$

This gives in an ideal situation of increased gravity a scale independency for the stresses. Therefore the force becomes

$$F_{\max;point;p} = \pi (n r_m)^2 (\sigma_{v;m}^{'}) \tan\phi$$
$$= F_{\max;point;p} = n^2 \pi r_m^2 \sigma_{v;m}^{'} \tan\phi$$

with $F_{\max;point;m} = \pi r_m^2 \sigma_{v;m}^{'} \tan\phi$ this results in :

$$F_{\max;point;p} = n^2 F_{\max;point;m}$$

therefore the scaling of the volumetric weight is correct:

$$\left.\begin{aligned} \gamma_p &= \frac{F_p}{V_p} = \frac{n^2 F_m}{n^3 V_m} \\ \gamma_m &= \frac{F_m}{V_m} \end{aligned}\right\} \gamma_p = \frac{1}{n}\gamma_m$$

Second the scaling of the shaft friction $F_{\max;shaft} = 2\pi r L \tau_{\max;shaft}$:
The horizontal effective stress is linear dependent on the vertical effective stress so for the horizontal stress the following expression also holds:
$\sigma'_{h;p} = \sigma'_{h;m}$

resulting in:

$$F_{\max;shaft;p} = 2\pi(nr_m)(nL_m)(\sigma'_{h;m})\tan\delta$$
$$= F_{\max;shaft;p} = n^2 2\pi r_m L_m \sigma'_{h;m} \tan\delta$$

with $F_{\max;shaft;m} = 2\pi r_m L_m \sigma'_{h;m} \tan\delta$ this results in :

$$F_{\max;shaft;p} = n^2 F_{\max;shaft;m}$$

The combined point resistance and shaft friction, the total force $F_{max;p}$, is therefore:

$$F_{\max;p} = n^2 F_{\max;m}$$

The mass
The magnitude of the mass as function of the dimensions is:
$m = \rho V$ where ρ is the volumetric mass and *V* the volume of the mass.
Because $V_p = n^3 V_m$ and ρ doesn't alter ($\rho_p = \rho_m = \rho$), m_p becomes:

$$\left.\begin{aligned} m_p &= \rho V_p = \rho(n^3)V_m \\ m_m &= \rho V_m \end{aligned}\right\} m_p = n^3 m_m$$

The velocity of the mass at t=0

For the following expression is derived: $v_0 = \sqrt{2gh}$, in this expression h is scaled $h_p=nh_m$ and $g_p = \frac{1}{n} g_m$

Therefore $v_{0;p}$ becomes:

$$\left.\begin{aligned} v_{0;p} &= \sqrt{2gh_p} = \sqrt{2\frac{g_m}{n} nh_m} \\ v_{0;m} &= \sqrt{2gh_m} \end{aligned}\right\} v_{0;p} = v_{0;m}$$

The loading pulse and time

The loading pulse $F \cdot t = m \cdot v$ has to be the same in the prototype and the model situation, the relations $v_p = v_m$, $m_p = n^3 m_m$ and $F_p = n^2 F_m$ still hold so the resulting relationship for the time is:

$$\left.\begin{aligned} t_p &= \frac{m_p v_p}{F_p} = \frac{n^3 m_m v_m}{n^2 F_m} \\ t_m &= \frac{m_m v_m}{F_m} \end{aligned}\right\} t_p = nt_m$$

When the time is derived in another way:

$v = \frac{u}{t}$ in the linear case where $v_p=v_m$ and $u_p=nu_m$ the resulting t_p becomes:

$$\left.\begin{aligned} t_p &= \frac{u_p}{v_p} = \frac{nu_m}{v_m} \\ t_m &= \frac{u_m}{v_m} \end{aligned}\right\} t_p = nt_m$$

The relationship is consistent!

The spring stiffness

The spring stiffness has to be scaled as well, for a spring the following expression exists:
F=ku, where k is the spring stiffness and u is the displacement.
Because $F_p=n^2F_m$ and $u_p=nu_m$ are applicable the resulting expression for k_p is:

$$\left.\begin{aligned} k_p &= \frac{F_p}{u_p} = \frac{n^2 F_m}{nu_m} \\ k_m &= \frac{F_m}{u_m} \end{aligned}\right\} k_p = nk_m$$

Damper coefficient
The damper coefficient is scaled as well, F=cv where c is the damper coefficient and v is the pile velocity. $F_p=n^2F_m$ still holds, also $v_p = v_m$ is still applicable. This results in the following expression for c_p:

$$\left.\begin{aligned} c_p &= \frac{F_p}{v_p} = \frac{n^2 F_m}{v_m} \\ c_m &= \frac{F_m}{v_m} \end{aligned}\right\} \quad c_p = n^2 c_m$$

But when the other legitimate expression for the damper coefficient is scaled, with $E_{s;p}=E_{s;m}$ and $\rho_{s;p}=\rho_{s;m}$ The following is the case:

$$\left.\begin{aligned} c_p &= A_{p;p}\sqrt{E_{s;p}\rho_{s;p}} = n^2 A_{p;m}\sqrt{E_{s;m}\rho_{s;m}} \\ c_m &= A_{p;m}\sqrt{E_{s;m}\rho_{s;m}} \end{aligned}\right\} \quad c_p = n^2 c_m$$

Yes both derivations give the same relationship!

Conclusion

When both the dimensions and the acceleration of gravity are scaled linearly, all scale rules are consistent.

Appendix D: Pile-drivability

The calculated value for the displacement is based on a model the chosen parameters are substantiated by theory but still based on a simplified schematization. Therefore an empiric relation is utilized to verify the order of magnitude of the displacement.

The following empiric relationship is used:

$$c = \frac{m_b + m_p}{m_b + \alpha^2 \cdot m_p}$$

$$r = \frac{m_b \cdot h \cdot \xi}{c}$$

$$z = \frac{r}{F} - \frac{F \cdot L_p}{2 \cdot E_p \cdot A_p}$$

with:

quantity	dimension
m_b= mass of the ram	[kg]
m_p= mass of the pile	[kg]
h = drop height	[cm]
F = calculated bearing capacity	[kg]
L_p= length of the pile	[cm]
A_p= cross-section	[cm^2]
E_p= young's modulus	[kg/cm^2]
α= empiric constant 1	[-]
ξ= empiric constant 2	[-]

With the in table D1 listed values for the dynamic and the statnamic case the displacement (z) of the pile is calculated. As seen in the table, the order of magnitude of the dynamic case is $O(10^{-3}m)$ and is about 3 times higher relative to the value for the dynamic case calculated out of the theoretical assumptions. When the empiric value of the statnamic case is compared to the theoretical value the value differs about two times. Because the empiric value is higher no problems during pile drivability are expected. Only the range of maximum displacement has to be adjusted to 15 mm.

	dynamic	statnamic	dimension
m_b	10	70	kg
h	35	15	cm
Es	2100000	2100000	kg/cm2
rho	0.00785	0.00785	kg/cm3
Ap	7.63E+00	7.63E+00	cm2
L_p	2.00E+02	2.00E+02	cm
m_p	1.20E+01	1.20E+01	kg
F	7.00E+02	7.00E+02	kg
alpha	7.50E-01	7.50E-01	
ksi	9.00E-01	9.00E-01	
c	1.31E+00	1.07E+00	
r	2.40E+02	8.85E+02	
z	0.34	1.3	cm
theory	0.1	0.6	cm

Table D1: Empiric calculations for the displacement

Appendix E: Two-masses-spring-system

A two-masses-spring-system (figure E1) is first choice to incorporate the finite length of the pile. The first mass is the drop mass, the second mass the pile. The first spring represents the pile cap; the second spring does describe the soil behavior.

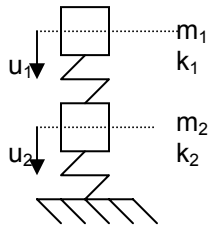

$$\begin{bmatrix} m_1 & 0 \\ 0 & m_2 \end{bmatrix}\begin{bmatrix} \ddot{u}_1 \\ \ddot{u}_2 \end{bmatrix}+\begin{bmatrix} k_1 & -k_1 \\ -k_2 & (k_1+k_2) \end{bmatrix}\begin{bmatrix} u_1 \\ u_2 \end{bmatrix}=\begin{bmatrix} F_1 \\ F_2 \end{bmatrix}$$

The system of equations is given above. The stiffness matrix is derived out of the equilibrium of forces. To obtain the eigen frequencies and the solution for the displacement of m_1 and m_2 the following holds:

$$\begin{bmatrix} k_1-\lambda & -k_1 \\ -k_2 & (k_1+k_2)-\lambda \end{bmatrix}\begin{bmatrix} u_1 \\ u_2 \end{bmatrix}=\begin{bmatrix} 0 \\ 0 \end{bmatrix}$$

$$\lambda^2-(2k_1+k_2)\lambda+k_1^2=0$$

The eigenvalues become:

$$\lambda_1=\frac{2k_1+k_2+\sqrt{4k_1k_2+k_2^2}}{2}$$

$$\lambda_2=\frac{2k_1+k_2-\sqrt{4k_1k_2+k_2^2}}{2}$$

The eigenvectors:

$$\vec{e}_1=\begin{bmatrix} 1 \\ \dfrac{k_2}{k_1\lambda_1} \end{bmatrix}$$

$$\vec{e}_2=\begin{bmatrix} 1 \\ \dfrac{k_2}{k_1\lambda_2} \end{bmatrix}$$

The two eigen frequencies become:

$$\omega_1=\sqrt{\frac{\lambda_1}{m_1}}$$

$$\omega_2=\sqrt{\frac{\lambda_2}{m_2}}$$

Trying the general solution u(t)=Asin(ωt+ϕ) with following conditions on t=0:
u_1=0
u_2=0
$du_1/dt = v_0 = \sqrt{(2gh)}$
du_2/dt = 0
gives:

$$A_1 \sin\phi_1 + A_2 \sin\phi_2 = 0$$
$$A_1\left(\frac{k_2}{k_1\lambda_1}\right)\sin\phi_1 + A_2\left(\frac{k_2}{k_1\lambda_2}\right)\sin\phi_2 = 0$$
$$\omega_1 A_1 \cos\phi_1 + \omega_2 A_2 \cos\phi_2 = v_0$$
$$\omega_1 A_1\left(\frac{k_2}{k_1\lambda_1}\right)\cos\phi_1 + \omega_2 A_2\left(\frac{k_2}{k_1\lambda_2}\right)\cos\phi_2 = 0$$

This system can be solved and gives for respectively ϕ_1, ϕ_2, A_1 and A_2:
$$\phi_1 = 0$$
$$\phi_2 = 0$$
$$A_1 = -\left(\frac{\lambda_1\sqrt{2gh}}{\omega_1\lambda_2 - \omega_1\lambda_1}\right)$$
$$A_2 = \frac{\sqrt{2gh}}{\left(\omega_2 - \frac{\omega_2\lambda_1}{\lambda_2}\right)}$$

And the final solution becomes:
$$\begin{bmatrix} u_1 \\ u_2 \end{bmatrix} = -\left(\frac{\lambda_1\sqrt{2gh}}{\omega_1\lambda_2 - \omega_1\lambda_1}\right)\vec{e}_1 \sin\omega_1 t + \frac{\sqrt{2gh}}{\left(\omega_2 - \frac{\omega_2\lambda_1}{\lambda_2}\right)}\vec{e}_2 \sin\omega_2 t$$

This analytical model does not describe the damping properties of the soil. In other words the prediction of this analytical model does not give an increase in duration and decrease in amplitude. Thus the results are very conservative if the results are favourable for this situation, the reality will be even more favourable.

The spring stiffness of both springs is affecting the period (duration) of the force. Because of the uncertainty in the soil stiffness the value of the spring k_2 is the most critical one the value of k_1 can be changed by choosing another material.

Unfortunate with the manual-CPT device of geotechniek I wasn't able to measure the stiffness of the soil. So the outcome of the calculations are not accurate, see e.g. the displacement (m/s) against the time (s) in figure:

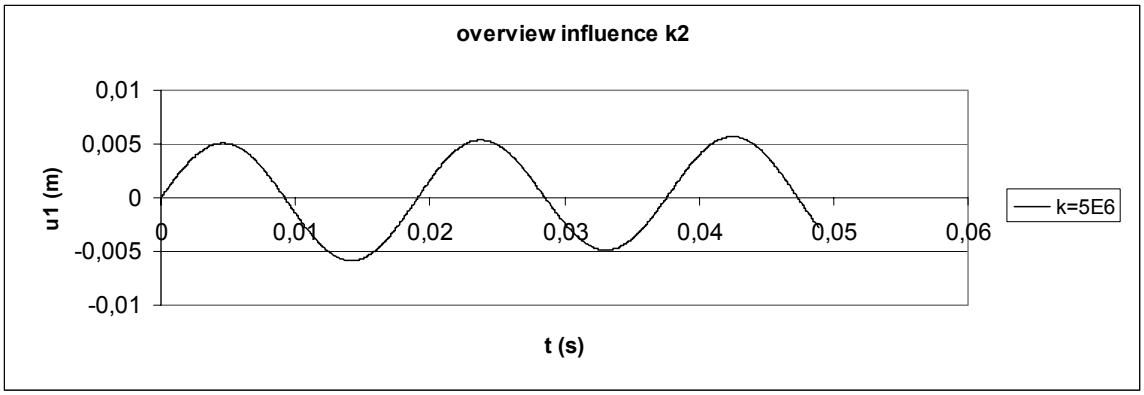

Figure E2 displacement – time diagram of the first mass.

k1	1.50E+06	N/m
k2	5.00E+06	N/m
m1	70	kg
m2	15	kg
g	9.81	m/s2
h	0.15	m
v0	1.715517415	m/s
labda1	7708099.244	
labda2	291900.7565	
omega1	331.8368627	
omega2	139.4992847	

Table E1 used parameters

When the k2 (soil stiffness) is varied the period of the rebound remains outside the 10 ms range see figure below. A stiff soil gives a shorter duration. The second positive peak is the location where the rebound occurs.

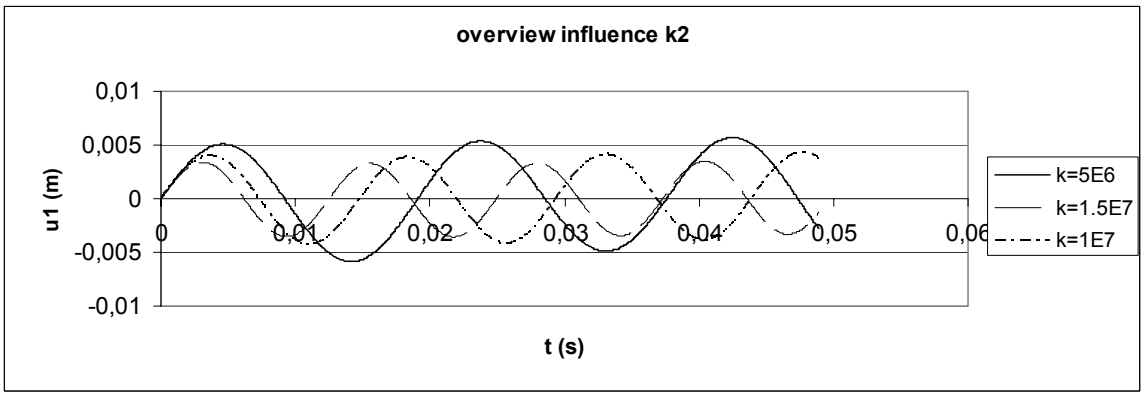

Figure E3 Influence of the soil stiffness on the rebound of the drop mass

Thus qualitative can be said that the rebound is of no influence and doesn't need to be damped. When the properties of spring k2 is chosen as infinite stiff; the loading mechanism is migrating to a 1 mass-spring system. The following holds for the displacement:

$$m\ddot{u} + ku = 0$$

trying

$$u(t) = A\cos(\omega_0 t + \phi)$$

$$t = 0; u = 0; \dot{u} = v_0$$

$$\left.\begin{aligned} A\cos\phi &= 0 \\ -\omega_0 \sin\phi &= v_0 \end{aligned}\right\} A = -\frac{v_0}{\omega_0}; \phi = \frac{1}{2}\pi$$

$$u(t) = -\frac{v_0}{\omega_0}\cos(\omega_0 t + \frac{1}{2}\pi)$$

or

$$u(t) = \frac{v_0}{\omega_0}\sin(\omega_0 t)$$

$$v(t) = \frac{du(t)}{dt} = v_0 = \cos(\omega_0 t)$$

Which in the following displacement-time diagram:

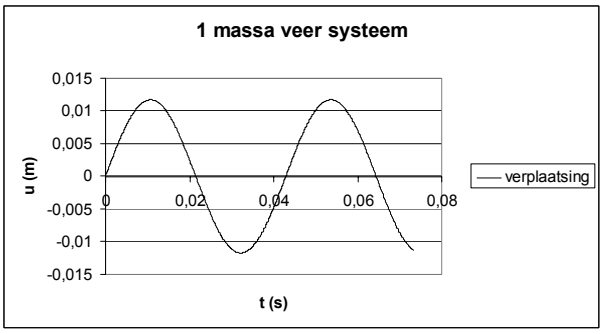

Figure E4 1 mass spring system displacement-time

Appendix F: Energy needed to get a dry sample

The apparent cohesion in the test tank is estimated at 5% of the pore volume, the pore volume is estimated at 40% of the total volume, so the amount of water which is left in the tank after drainage is about 2% of the total volume. The dimensions of the tank are 1.8 m high sandcolumn which is 1.9 m in diameter giving a total of 5.1 m^3. Thus the total volume of pore water left is about 100 l. or 100 kg. The specific heat for water is about $4.18 \cdot 10^3$ J/(kg·K). To expell the remaining water the temperature has to be increased to 100 ^oC. This means a temperature increase of 78 ^oC, because the room temperature at the geotechniek lab is about 22 ^oC.

The energy needed to boil down the remaining water is:

$$P = cm\Delta T$$

$$P = 33MJ$$

with:

c	= the specific heat
m	= mass
ΔT	= temperature difference

With a 2000 W power source, say a HR central heating boiler, this cost about 4.5 hours. In this case only the water is considered and the location of the water is neglected. The heat distribution in the tank is not ideal to do it in 4.5 hours 100% of the energy has to go into the water which is of course not the case.

Appendix G: Preliminary soil investigation test chamber

Introduction

In this chapter the actual soil conditions in the geotechniek test chamber are discussed. Also the effect of the preparation dependent parameters is taken in account. First the sieve curve is compared with old data. Then the CPTs made with the standard geotechniek manual sounding device are presented. Finally the influence of the results on the test regime is given.

Sieve curve

A sieve curve of the sand in the geotechniek test chamber is made at surface level minus 70 cm. This curve is depicted in figure G.1

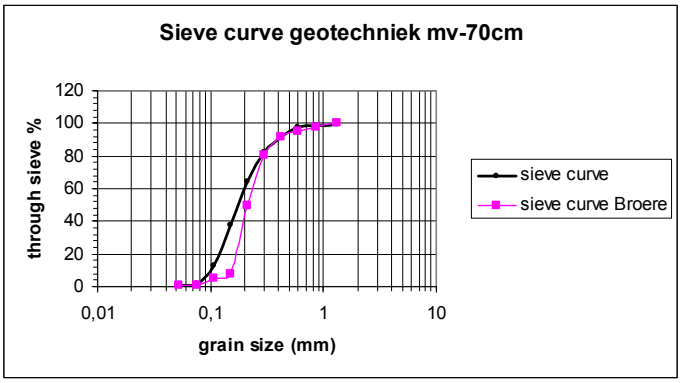

Figure G.1 Sieve curve geotechniek 28-1-04

When the result is compared with the result of Broere (2001) it is most similar with type 3 sand at 0.3 meter minus surface, although the sample consists of more fine material. This can be explained by the fact that after some fluidization-cycles fine materials are transported to the top of the tank.

CPTs

To obtain some insight in the effect of the preparation method used some CPTs are made. The CPTs are made with an electric cone equipped with sensors for point resistance and sleeve friction. Because the mechanical loading device is manual driven a maximum limit of about 10 MPa can be measured, the analog registration device however is limited to 6 MPa. This limit can be surpassed by changing the sensitivity settings of the analog registration device from 2 mV to 5 mV. CPTs with maximum values of >6MPa are registered on the 5mv range and linearly scaled up, so they have the same scale as the other CPTs. The CPTs are executed on three different locations. This can be seen in figure G.2. Location A, B and C are chosen.

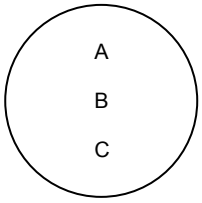

Figure G.2 CPT location

Because of the non-linearity of the geotechniek CPT-cone the following calibration curve is made. The cone is loaded with a known value this value is plotted against the measured value. In this graph a trend line is fitted to obtain a conversion to the corrected values. See figure G.3 for the calibration curve with a linear trend line forced through the 0. Only three points are taken so the accuracy is only moderate, but enough for the preliminary phase.

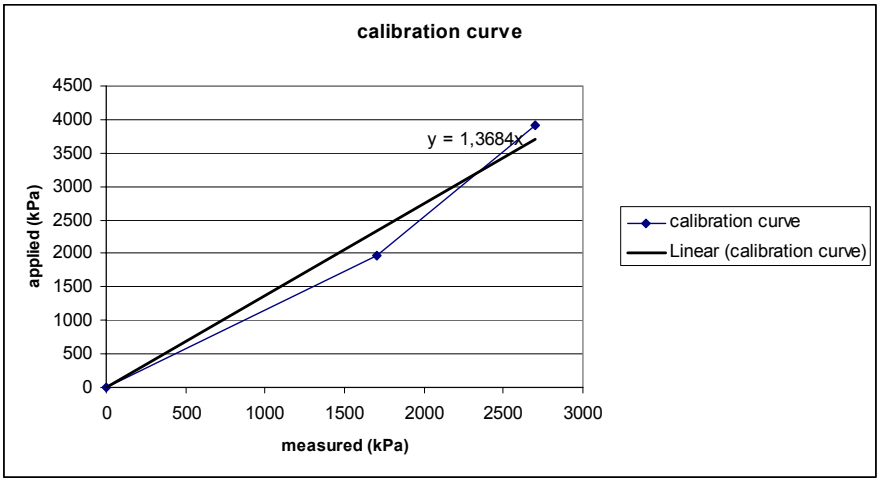

Figure G.3 calibration curve with trend.

The geotechniek test chamber is first fluidized and afterwards during drainage vibrated. The occurrence of water increases the effectiveness of the vibrating process, because the energy is transferred by the water into the core of the chamber. The water cannot dissipate energy while it can't mobilize shear stresses, so all the energy is dissipated in the friction between the grains.

Vibration time

The influence of the vibration time is considered first. In the case of no vibration figure 7.3 is obtained. When 5 minutes is vibrated the figure G.4 is obtained. And the cone resistance in the tank after 10 minutes is depicted in 7.5.

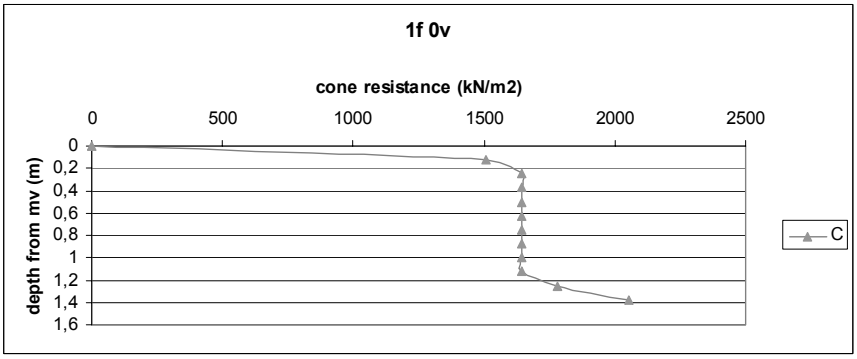

Figure G4 1 hour of fluidization (1f) 0 minutes of vibrating (0v)

Clearly is seen in figure 7.3 that no cone resistance is present after fluidization, the last 0.5 meters is caused by the influence of the bottom of the test chamber. When the soil is vibrated for 5 minutes the soil strength increases and begins to depend on the depth as seen in in-situ conditions.

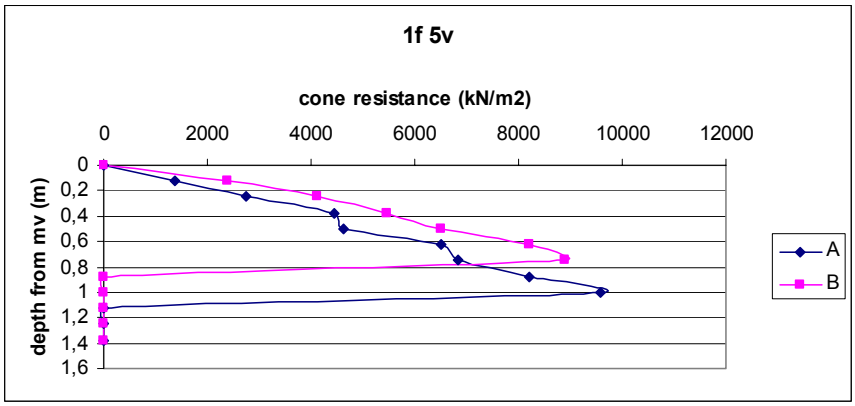

Figure G5 1 hour of fluidization (1f) 5 minutes of vibrating (5v)

Increasing of the vibrating time does increase the strength even further.

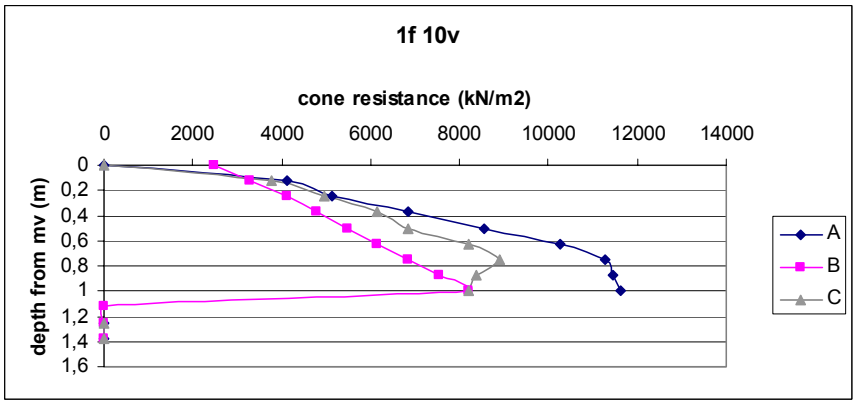

Figure G6 1 hour of fluidization (1f) 10 minutes of vibrating (10v)

Horizontal variance

When the horizontal variance is considered location A and location C, which are close to the rim of the test chamber, give consequently higher values than the B location which is positioned in the middle of the tank. The differences are larger when the vibrating duration is increased. One possible explanation might be that some compressed hotspots are created around the vibrators. Location A is very close to one of the vibrators, and therefore it is registering the highest values.

Appendix H: Additional data of the measuring setup

Equipment data

The acceleration transducer is from Bruel & Kjær type 4367 nr. 628202 with a sensitivity of 2.13 pC/ms^{-2} and a resonance frequency of f_{res} = 39 kHz. This is the intrinsic resonance frequency of the transducer. The mounting of the transducer is also affecting the resonance, this influence is negative, so the real life $f_{res;system}$ is smaller then of the transducer only.

The accompanying charge amplifier is also from Bruel & Kjær type 2635 with an adjustable input sensitivity of 0.01 mV to 10 V/pC and a calibrated output rating of 0.1 mV/ms^{-2} to 1 V/ms^{-2}. The frequency range of the acceleration amplifier is given as 0.2 Hz to 100 kHz.

In-between the acceleration amplifier and the acceleration transducer an additional low pass filter at 500 Hz is implemented (analog, see fig H.1) A low pass filter filters out all high frequencies.

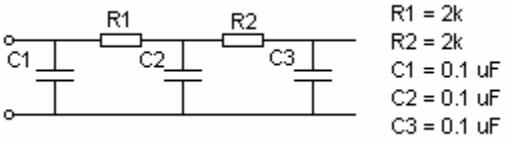

Figure H.1 schematic of analog LP filter

The displacements are measured with a Sakae S13FLP25A linear stroke potentio meter with a resistance of 1 kΩ and date code 0305. This pot is relabeled by Feteris components the supplier of the device. The potentiometer is supplied with 6V from the strain gauge amplifier.

The strain gauge amplifier is a design by the section I&A – DA (measuring group of CITG). The amplifier has sixteen input channels and has series number DA02.10. The bandwidth is sufficient for this application (2 kHz).

Calibration of the sensors

To convert the signals of the sensors to engineering quantities the following calibration parameters are used.

Point resistance
Geodelft the supplier of the sounding cone (cone number 9) states that the point resistance sensor gives 46.05 MPa/mV/V. This means that for 1 V supply voltage on the cone, the cone is giving 1mV of signal for each 46.05 MPa of measured pressure.

Because the strain gauge amplifier feeds the cone with 6V the sensitivity of the cone is 7.675 MPa/mV/6V. *This is before amplification!*

Shaft friction
Geodelft the supplier of the sounding cone states that the shaft friction sensor gives 0.3555 MPa/mV/V. Because the strain gauge amplifier feeds the cone with 6V this results in 0.05925 MPa/mV/6V. *This is before amplification!*

Force on the pile head
The rod is calibrated a tension force of 50 kN gives 1644.381 μstrain or 1kN = 32.888 μstrain. The strain gauge bridge in combination with the amplifier are calibrated in such a way that 3000 μstrain is 9V or a theoretical 3333.333 μstrain/10 V.

So 3333.333 μstrain = 10 V = 101.355 kN, this results in 0.010135 kN/mV.

Because the measurement department has calibrated the strain gauges and strain gauge amplifier together, this is *with* amplification.

Displacement
For the displacement a linear potentiometer is utilized, actually a voltage divider. When the displacement is 25 mm (the maximum stroke of the pot) a total of 6V falls across the input of the A/D card. So 1 mm is 0.24 V or: 0.0041667 mm/mV

Acceleration transducer
It depends on which quantity is measured, because the amplifier is able to integrate the acceleration signal to velocities.

All this results in (for simplicity only engineering quantity and measuring signal in the dimensions, when the supply voltage is changed alterations are necessary):

Quantity	Calibration factor
Point resistance	7.675 MPa/mV
Shaft friction	0.05925 MPa/mV
Force on pile head*	0.010135 kN/mV
Displacement	0.0041667 mm/mV
Acceleration/Velocity	differs

*Table H.1 *including amplification*

Data acquisition system and amplification
All these signals are first amplified by the strain gauge amplifier (point/shaft/force) or the load amplifier of the acceleration transducer before being fed into the data acquisition system. So every mV from the strain gauges delivers 1V at the output of the amplifier and therefore on the input of the A/D card. The 12-bit A/D converter of the data acquisition system has a range of +10 V / -10 V and a resolution of 4.88 mV.

Software of data acquisition system

The program which is installed on the data acquisition system has to be configured such that the output files are engineering quantities. Therefore some additional conversions have to be made, to incorporate the resolution of the system and the amplification.

Point resistance
The signal is amplified 1000 times Therefore the point resistance is after amplification 7.675 MPa/V. The resolution of the A/D card is 4.88mV, resulting in the calibration factor in the program of: $7.675 \cdot 4.88 \cdot 10^{-3}$ = 0.037476 MPa. (this the smallest value which can be measured)

Shaft friction
The signal is also amplified 1000 times resulting in 0.05925 MPa/V. The resolution of the A/D card is 4.88mV, resulting in the calibration factor in the program of: 0.05925 MPa/V$\cdot 4.88 \cdot 10^{-3}$ V = 0.000289307 MPa.

Force on the pile head
The signal is already amplified, thus incorporating the resolution of the A/D system:
$0.010135\ kN/mV \cdot 4.88 \cdot 10^{-3} = 0.049496\ kN$

Displacement
The same procedure, because also no amplification had to be incorporated in the calculation:
$0.0041667\ mm/mV \cdot 4.88mV = 0.02\ mm$

Summarized in a table:

Quantity	Calibration factor in program
Point resistance	0.037476 MPa
Shaft friction	0.000289307 MPa
Force on pile head	0.049496 kN
Displacement	0.02 mm
Acceleration/Velocity	differs

Table H.2

These values have to be incorporated in the measuring program.

Appendix I: The virtues of automatic post triggering

The phenomena under test are very short lasting, resulting in a high sampling frequency and therefore a huge amount of data is recorded each second. The buffer of the A/D card and the addressed memory in the PC can only hold ~ 50,000 samples. Depending on the sample size and the amount of different channels this buffer holds a certain measuring period. For normal operation the system records not all data points but takes averages, cycles or maximum or minimum values in this case test can last for days. Therefore it is important to use the values in the buffer.

In this case five channels are used and the smallest possible sample time of 470 μs is chosen. In this case a total of 4.7s / channel of data can be recorded. This time is enough to cover the problem.

But practically one person isn't able to operate the release mechanism and the triggering of the measuring device at the same time. If the start of the test is triggered manually and consecutively the test is performed at least 30 seconds have passed. The long term measuring option does not record all data points, thus isn't an option.

An advanced option of the utilized measuring program is used. An alarm function is set. This alarm is triggered by a signal at one of the channels. In this case the strain in the pile head is chosen. When the mass hits the pile head the strain increases and therefore the signal increases above a certain threshold value. This threshold have to be defined such that noise on the input does not trigger the measuring system. After a delay of 1.5 seconds the buffer which is set at a total length of 2 seconds is recorded to the hard drive.

So the system detects the start of the test and waits for 1.5 seconds and finally writes the passed 2 seconds to the disc. The total phenomenon is captured with the maximum amount of data points which the system is capable of.

Appendix J: FFT issues

When additional information about the important frequencies of a signal is needed measuring data in the time domain can be converted to the frequency domain with an algorithm called: 'Fast Fourier Transform'. Additional information about the major frequencies is important to detect the components of which the signal is built.

For discrete signals the Fourier transform is given as:

$$U_N(\omega) = \sum_{k=0}^{N-1} u_d(k) e^{-ik\omega\Delta T}$$

$$u_d(k) = \frac{1}{N} \sum_{l=0}^{N-1} U_N(\frac{l}{N}\omega_s) e^{i\frac{2\pi l}{N}k}$$

If the signal is transformed with the help of the Matlab[2] function *fft* a real input signal of N data points gives N complex numbers or 2N real numbers. With the following redundancy:
-U_1 is real (mean u(k))
-U_2 … $U_{N/2}$ consist of the amplitude and phase information of $\frac{2}{N}\omega_s \ldots \frac{N/2}{N}\omega_s$
-$U_{N/2+1}$ is real and holds the amplitude at the Nyquist frequency (half of the sampling frequency)
-$U_{N/2+2}$ … U_N consists of the amplitude and phase of the complex conjugate of the positive frequencies.

Take for example the following acceleration signal in the time domain (fig. A.x.1):

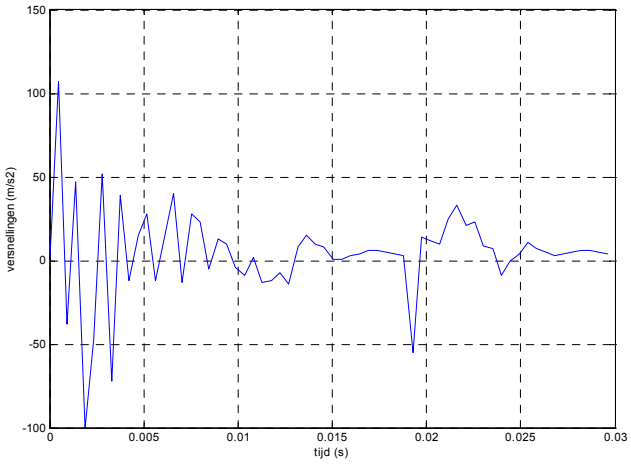

Figure J.1 a-t signal in the time domain

[2] Well known mathematical software package

After the signal is converted to the frequency domain the following graph (fig. A.x.2) is obtained:

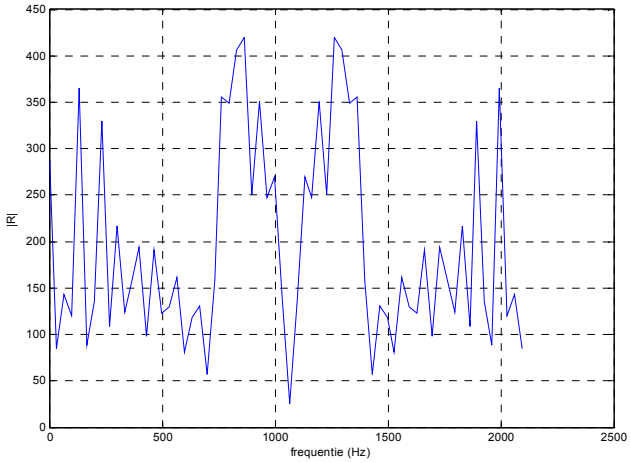

Figure J.2 frequency segmentation of the acceleration signal

The distribution of the frequencies in the measured signal of the acceleration is plotted. On the y-axis information about the magnitude of the frequency is plotted, the amplitude of the complex number which is obtained after transformation. The mirrored function is the complex conjugate and mirrors on the Nyquist frequency which is halve of the sample frequency in this case the Nyquist frequency becomes ½ of 2128 Hz is 1064 Hz. As said before this information is redundant. When neglecting this data the plot becomes as depicted in figure A.x.3:

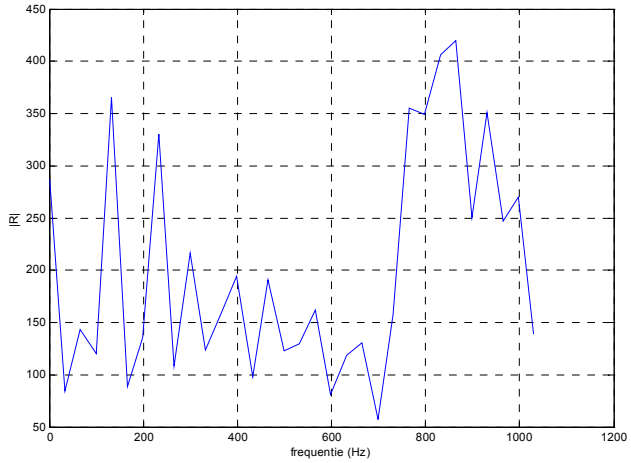

Figure J.3 R-f plot <$f_{Nyquist}$

After a closer look at figure A.x.3 it becomes apparent that frequencies in the 800-900 Hz are overrepresented. If this frequency range is not wanted in the physical data (i.e. a eigen frequency of the acceleration transducer). This can easily filtered out of the data, again with the help of Matlab.

In figure A.x.4 a 8th order Butterworth filter at ~500 Hz is depicted this is implemented as a IIR filter (Infinite Impulse Response, standard filter in the digital domain):

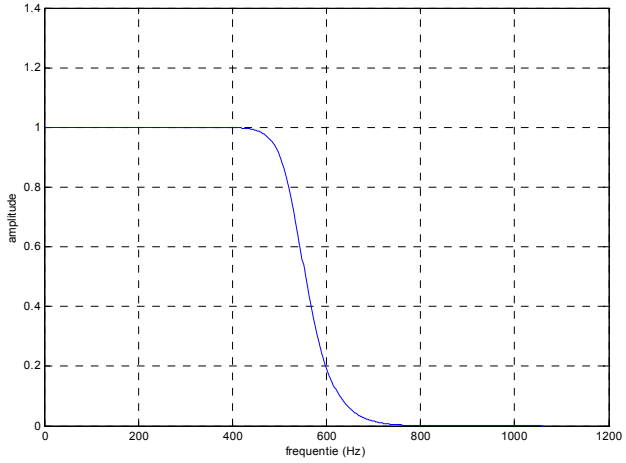

Figure J.4 8th order Butterworth filter at~ 500 Hz (halve $f_{nyquist}$)

After this filter is applied the following frequency info is obtained (see figure A.x.5):

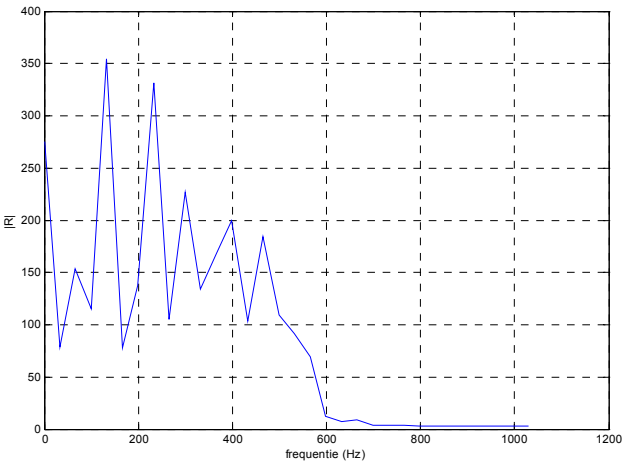

Figure J.5 |R|-f

Or with the conjugate as depicted in A.x.6, as can seen all the frequency components around the Nyquist frequency are filtered out of the signal.

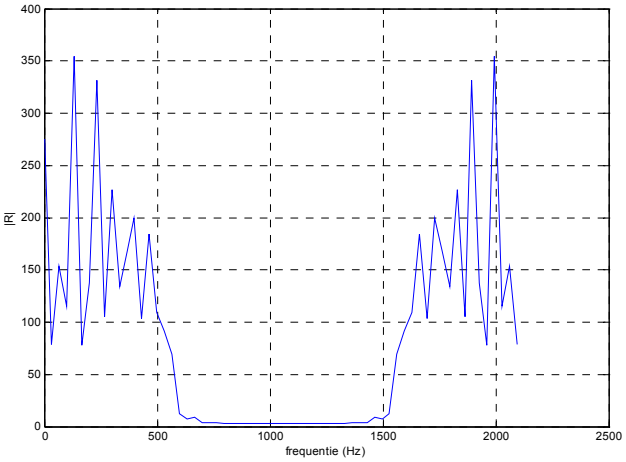

Figure J.6 |R|-f with conjugate information

When the signal is converted to the time domain (fig A.x.7), the signal doesn't contain the higher frequencies, the period of the first peak has become larger.

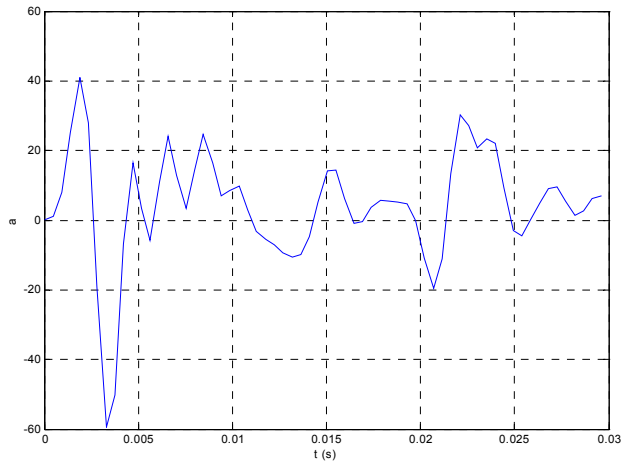

Figure J.7 a-t after the filter is applied

Appendix K Overview of performed tests

To get some insight in the amount of tests and the resulting data-files a summary is made and put in the table below:

filenaam	type file	type proef	grondgesteldheid	valhoogte (cm)	locatie	# veren	datum	opmerking	bijbehorende excel file
127CPT.dfx	dt=0.1s	q_p en q_s tijdens installeren	5T 1.5F droog		i		12-jul		
127sv.dfx	dt=0.1s	statische proef voor de PS proef	5T 1.5F droog		i		12-jul		127ioverzicht.xls
127sn.dfx	dt=0.1s	statische proef na de PS proef	5T 1.5F droog		i		12-jul		
127ia.000	bufferfile dt = 470us	pseudostatische proef (PS)	5T 1.5F droog	12.5	i	5	12-jul		
127iic.dfx	dt=0.1s	q_p en q_s tijdens installeren	5T 1.5F droog		ii		12-jul		
127iis.dfx	dt=0.1s	statische proef voor de PS proef	5T 1.5F droog		ii		12-jul		127iioverzicht.xls
137iisn.dfx	dt=0.1s	statische proef na de PS proef	5T 1.5F droog		ii		12-jul	proef volgende dag	
127iia.000	bufferfile dt = 470us	pseudostatische proef (PS)	5T 1.5F droog	12.0	ii	5	12-jul		
137iiic.dfx	dt=0.1s	q_p en q_s tijdens installeren	5T 1.5F droog		iii		13-jul		
137iiis.dfx	dt=0.1s	statische proef voor de PS proef	5T 1.5F droog		iii		13-jul		137iiioverzicht.xls
137iiisn.dfx	dt=0.1s	statische proef na de PS proef	5T 1.5F droog		iii		13-jul		
1373a.000	bufferfile dt = 470us	pseudostatische proef (PS)	5T 1.5F droog	13.5	iii	5	13-jul		
157iic.dfx	dt=0.1s	q_p en q_s tijdens installeren	15T 1.5F droog		ii		15-jul		
157iis.dfx	dt=0.1s	statische proef voor de PS proef	15T 1.5F droog		ii		15-jul		157iioverzicht.xls
1572sn.dfx	dt=0.1s	statische proef na de PS proef	15T 1.5F droog		ii		15-jul	proef mislukt	
157iia.000	bufferfile dt = 470us	pseudostatische proef (PS)	15T 1.5F droog	15.0	ii	5	15-jul		
157iiic.dfx	dt=0.1s	q_p en q_s tijdens installeren	15T 1.5F droog		iii		15-jul	proef mislukt	
157iiis.dfx	dt=0.1s	statische proef voor de PS proef	15T 1.5F droog		iii		15-jul		157iiioverzicht.xls
1573sn.dfx	dt=0.1s	statische proef na de PS proef	15T 1.5F droog		iii		15-jul		
157iiia.000	bufferfile dt = 470us	pseudostatische proef (PS)	15T 1.5F droog	14.5	iii	5	15-jul		
157ic.dfx	dt=0.1s	q_p en q_s tijdens installeren	15T 1.5F droog		i		15-jul		
167is.dfx	dt=0.1s	statische proef voor de PS proef	15T 1.5F droog		i		16-jul		167ioverzicht.xls
167isn.dfx	dt=0.1s	statische proef na de PS proef	15T 1.5F droog		i		16-jul		
167ia.000	bufferfile dt = 470us	pseudostatische proef (PS)	15T 1.5F droog	16.5	i	5	16-jul		
197ic.dfx	dt=0.1s	q_p en q_s tijdens installeren	10T 1.5F droog		i		19-jul		
197is.dfx	dt=0.1s	statische proef voor de PS proef	10T 1.5F droog		i		19-jul		
197isn.dfx	dt=0.1s	statische proef na de PS proef	10T 1.5F droog		i		19-jul		
197ia.000	bufferfile dt = 470us	pseudostatische proef (PS)	10T 1.5F droog	16.5	i	5	19-jul		197ioverzicht.xls
197ib.000	bufferfile dt = 470us	pseudostatische proef (PS)	10T 1.5F droog	13.0	i	6	19-jul		
197i1v.000	bufferfile dt = 470us	pseudostatische proef (PS)	10T 1.5F droog	12.5	i	1	19-jul		
207iic.dfx	dt=0.1s	q_p en q_s tijdens installeren	10T 1.5F droog		ii		20-jul		
207iis.dfx	dt=0.1s	statische proef voor de PS proef	10T 1.5F droog		ii		20-jul		
207iisn.dfx	dt=0.1s	statische proef na de PS proef	10T 1.5F droog		ii		20-jul		
207ii1v.000	bufferfile dt = 470us	pseudostatische proef (PS)	10T 1.5F droog	18.4	ii	1	20-jul		207iioverzicht.xls
207ii5v.000	bufferfile dt = 470us	pseudostatische proef (PS)	10T 1.5F droog	16.0	ii	5	20-jul		
207ii6v.000	bufferfile dt = 470us	pseudostatische proef (PS)	10T 1.5F droog	15.5	ii	6	20-jul		
217iiic.dfx	dt=0.1s	q_p en q_s tijdens installeren	10T 1.5F droog		iii		21-jul		
217iiis.dfx	dt=0.1s	statische proef voor de PS proef	10T 1.5F droog		iii		21-jul		
2173sn.dfx	dt=0.1s	statische proef na de PS proef	10T 1.5F droog		iii		21-jul		

21731v.000	bufferfile dt = 470us	pseudostatische proef (PS)	10T 1.5F droog	19.2	iii	1	21-jul		217iiioverzicht.xls
21735v.000	bufferfile dt = 470us	pseudostatische proef (PS)	10T 1.5F droog	16.4	iii	5	21-jul		
21736v.000	bufferfile dt = 470us	pseudostatische proef (PS)	10T 1.5F droog	15.1	iii	6	21-jul		

267iiic.dfx	dt=0.1s	q_p en q_s tijdens installeren	10T 1.5F droog		iii		26-jul	mv = BR -78 cm	
267iiis.dfx	dt=0.1s	statische proef voor de PS proef	10T 1.5F droog		iii		26-jul		267iiioverzicht.xls
2673sn.dfx	dt=0.1s	statische proef na de PS proef	10T 1.5F droog		iii		26-jul		
26735v.000	bufferfile dt = 470us	pseudostatische proef (PS)	10T 1.5F droog	19.5	iii	5	26-jul		

267iic.dfx	dt=0.1s	q_p en q_s tijdens installeren	10T 1.5F droog		ii		26-jul	mv = BR -78 cm	
267iis.dfx	dt=0.1s	statische proef voor de PS proef	10T 1.5F droog		ii		26-jul		
2672sn.dfx	dt=0.1s	statische proef na de PS proef	10T 1.5F droog		ii		26-jul	statische proef >16uur	267iioverzicht.xls
26721v.000	bufferfile dt = 470us	pseudostatische proef (PS)	10T 1.5F droog	23.5	ii	1	26-jul		
26725v.000	bufferfile dt = 470us	pseudostatische proef (PS)	10T 1.5F droog	19.5	ii	5	26-jul		
26726v.000	bufferfile dt = 470us	pseudostatische proef (PS)	10T 1.5F droog	18.7	ii	6	26-jul		

277ic.dfx	dt=0.1s	q_p en q_s tijdens installeren	10T 1.5F droog		i		27-jul	proef mislukt	mv = BR -78 cm
277is.dfx	dt=0.1s	statische proef voor de PS proef	10T 1.5F droog		i		27-jul		277ioverzicht.xls
277isn.dfx	dt=0.1s	statische proef na de PS proef	10T 1.5F droog		i		27-jul	statische proef >2 uur	
277i1v.000	bufferfile dt = 470us	pseudostatische proef (PS)	10T 1.5F droog	20.9	i	1	27-jul		

297ic.dfx	dt=0.1s	q_p en q_s tijdens installeren	10T 1.5F droog		i		29-jul	mv = BR -76 cm	
297is.dfx	dt=0.1s	statische proef voor de PS proef	10T 1.5F droog		i		29-jul		297ioverzicht.xls
297isn.dfx	dt=0.1s	statische proef na de PS proef	10T 1.5F droog		i		29-jul	statische proef >35min	
297ia.000	bufferfile dt = 470us	pseudostatische proef (PS)	10T 1.5F droog	15.9	i	5	29-jul		

297iic.dfx	dt=0.1s	q_p en q_s tijdens installeren	10T 1.5F droog		ii		29-jul	mv = BR -76 cm	
297iis.dfx	dt=0.1s	statische proef voor de PS proef	10T 1.5F droog		ii		29-jul		
2972sn.dfx	dt=0.1s	statische proef na de PS proef	10T 1.5F droog		ii		29-jul	proef mislukt	297iioverzicht.xls
2972sn2.dfx	dt=0.1s	statische proef na de PS proef	10T 1.5F droog		ii		29-jul	statische proef >45min	
297iia.000	bufferfile dt = 470us	pseudostatische proef (PS)	10T 1.5F droog	14.5	ii	5	29-jul		

307iiic.dfx	dt=0.1s	q_p en q_s tijdens installeren	10T 1.5F droog		iii		30-jul	mv = BR -76 cm	
307iiis.dfx	dt=0.1s	statische proef voor de PS proef	10T 1.5F droog		iii		30-jul		307iiioverzicht.xls
3073sn.dfx	dt=0.1s	statische proef na de PS proef	10T 1.5F droog		iii		30-jul	statische proef >45min	
307iiia.000	bufferfile dt = 470us	pseudostatische proef (PS)	10T 1.5F droog	14.4	iii	5	30-jul		

168iiic.dfx	dt=0.1s	q_p en q_s tijdens installeren	10T 1.5F droog		iii		16-aug	mv = BR -76 cm	
168iiis.dfx	dt=0.1s	statische proef voor de PS proef	10T 1.5F droog		iii		16-aug		168iiioverzicht.xls
1683sn.dfx	dt=0.1s	statische proef na de PS proef	10T 1.5F droog		iii		16-aug		
16836v.000	bufferfile dt = 470us	pseudostatische proef (PS)	10T 1.5F droog	23	iii	6	16-aug		

168iic.dfx	dt=0.1s	q_p en q_s tijdens installeren	10T 1.5F droog		ii		16-aug	mv = BR -76 cm	
168iis.dfx	dt=0.1s	statische proef voor de PS proef	10T 1.5F droog		ii		16-aug		168iioverzicht.xls
168iisn.dfx	dt=0.1s	statische proef na de PS proef	10T 1.5F droog		ii		16-aug		
168ii5v.000	bufferfile dt = 470us	pseudostatische proef (PS)	10T 1.5F droog	30.4	ii	5	16-aug		

178ic.dfx	dt=0.1s	q_p en q_s tijdens installeren	10T 1.5F droog		i		17-aug	mv = BR -76 cm	
178is.dfx	dt=0.1s	statische proef voor de PS proef	10T 1.5F droog		i		17-aug		178ioverzicht.xls
178isn.dfx	dt=0.1s	statische proef na de PS proef	10T 1.5F droog		i		17-aug		
178i6v.000	bufferfile dt = 470us	pseudostatische proef (PS)	10T 1.5F droog	29.9	i	6	17-aug		

198ic.dfx	dt=0.1s	q_p en q_s tijdens installeren	10T 1.5F droog		i		19-aug	mv = BR -75.5 cm	
198is.dfx	dt=0.1s	statische proef voor de PS proef	10T 1.5F droog		i		19-aug		198ioverzicht.xls
198isn.dfx	dt=0.1s	statische proef na de PS proef	10T 1.5F droog		i		19-aug		
198i6v.000	bufferfile dt = 470us	pseudostatische proef (PS)	10T 1.5F droog	30	i	6	19-aug		

198iic.dfx	dt=0.1s	q_p en q_s tijdens installeren	10T 1.5F droog		ii		19-aug	mv = BR -75.5 cm	
198iis.dfx	dt=0.1s	statische proef voor de PS proef	10T 1.5F droog		ii		19-aug		198iiioverzicht.xls
198iisn.dfx	dt=0.1s	statische proef na de PS proef	10T 1.5F droog		ii		19-aug		
198ii5v.000	bufferfile dt = 470us	pseudostatische proef (PS)	10T 1.5F droog	32.5	ii	5	19-aug		

208iiic.dfx	dt=0.1s	q_p en q_s tijdens installeren	10T 1.5F droog		iii		20-aug	mv = BR -75.5 cm	
208iiis.dfx	dt=0.1s	statische proef voor de PS proef	10T 1.5F droog		iii		20-aug		208iiioverzicht.xls
2083sn.dfx	dt=0.1s	statische proef na de PS proef	10T 1.5F droog		iii		20-aug		
20836v.000	bufferfile dt = 470us	pseudostatische proef (PS)	10T 1.5F droog	26.5	iii	6	20-aug		

238iiic.dfx	dt=0.1s	q_p en q_s tijdens installeren	5T 1.5F droog		iii		23-aug	mv = BR -75.5 cm	
238iiis.dfx	dt=0.1s	statische proef voor de PS proef	5T 1.5F droog		iii		23-aug	u ook gemeten!	238iiioverzicht.xls
2383sn.dfx	dt=0.1s	statische proef na de PS proef	5T 1.5F droog		iii	16:30	23-aug	u ook gemeten!	
2383a.000	bufferfile dt = 470us	pseudostatische proef (PS)	5T 1.5F droog	30	iii	5	23-aug		

248iiic.dfx	dt=0.1s	q_p en q_s tijdens installeren	5T 1.5F droog		iii		24-aug	mv = BR -75.5 cm	
248iiis.dfx	dt=0.1s	statische proef >17uur	5T 1.5F droog		iii	10:00	24-aug	u ook gemeten!	248iiioverzicht.xls
248iiis2.dfx	dt=0.1s	statische proef >20 uur	5T 1.5F droog		iii	13:20	24-aug	u ook gemeten!	
248iiis3.dfx	dt=0.1s	statische proef >23 uur	5T 1.5F droog		iii	16:15	24-aug	u ook gemeten!	

039ic.dfx	dt=0.1s	q_p en q_s tijdens installeren	5T 1.5F droog	20cm van loc	i*		3-sep		
039is.dfx	dt=0.1s	statische proef voor de PS proef	5T 1.5F droog	20cm van loc	i*		3-sep	u ook gemeten!	039ioverzicht.xls
039isn.dfx	dt=0.1s	statische proef na de PS proef	5T 1.5F droog	20cm van loc	i*		3-sep	u ook gemeten!	
039i5v.dfx	bufferfile dt = 470us	pseudostatische proef (PS)	5T 1.5F droog	20cm van loc	i*		3-sep	u ook gemeten!	

069ic.dfx	dt=0.1s	q_p en q_s tijdens installeren	0T 1.5F droog		i		6-sep		
069is.dfx	dt=0.1s	statische proef voor de PS proef	0T 1.5F droog		i		6-sep	u ook gemeten!	069ioverzicht.xls
069isn.dfx	dt=0.1s	statische proef na de PS proef	0T 1.5F droog		i	14:15	6-sep	u ook gemeten!	
069i5v.dfx	bufferfile dt = 470us	pseudostatische proef (PS)	0T 1.5F droog	u >30 mm	i	11:50	6-sep	u ook gemeten!	

089ic.dfx	dt=0.1s	q_p en q_s tijdens installeren	10T 1.5F droog		i		8-sep	mv = BR -74 cm	
089is.dfx	dt=0.1s	statische proef voor de PS proef	10T 1.5F droog		i		8-sep	u ook gemeten!	089ioverzicht.xls
089isn.dfx	dt=0.1s	statische proef na de PS proef	10T 1.5F droog		i		8-sep	u ook gemeten!	
089i5v.dfx	bufferfile dt = 470us	pseudostatische proef (PS)	10T 1.5F droog	29.3	i	5	8-sep	u ook gemeten!	

089iic.dfx	dt=0.1s	q_p en q_s tijdens installeren	10T 1.5F droog		ii		8-sep	mv = BR -74 cm	
089iis.dfx	dt=0.1s	statische proef voor de PS proef	10T 1.5F droog		ii		8-sep	u ook gemeten!	089iioverzicht.xls
089isn.dfx	dt=0.1s	statische proef na de PS proef	10T 1.5F droog		ii		8-sep	u ook gemeten!	10 mm onder PS gemeten
089ii5v.dfx	bufferfile dt = 470us	pseudostatische proef (PS)	10T 1.5F droog	32.0	ii	5	8-sep	u ook gemeten!	

109iiic.dfx	dt=0.1s	q_p en q_s tijdens installeren	10T 1.5F droog		iii		10-sep	mv = BR -74 cm	
109iiis.dfx	dt=0.1s	statische proef voor de PS proef	10T 1.5F droog		iii		10-sep	u ook gemeten!	089iioverzicht.xls
109iisn.dfx	dt=0.1s	statische proef na de PS proef	10T 1.5F droog		iii		10-sep	u ook gemeten!	bij eerste statisce proef
109iii6v.dfx	bufferfile dt = 470us	pseudostatische proef (PS)	10T 1.5F droog	27.4	iii	6	10-sep	u ook gemeten!	geen u gemeten

Table K.1 Overview of tests and accompanying files

Appendix L Derivation elastic model for normal force

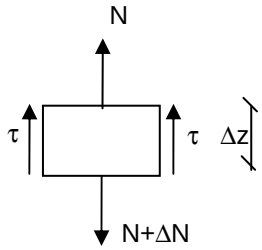

$$\frac{dN}{dz} = tO$$

N = normal force (N)

dz = height of increment (m)

t = shaft friction

O = circumference pile (m)

This equation can be extended (see e.g. Verruijt 1994) with force stress relation (N=σA) and Hooke's Law ($\sigma=E_{pile}\varepsilon$), and displacement strain relationship (ε=du/dz) and linear behaviour of the shear stress (τ=c·u with c the subgrade modulus) to acquire the basic differential equation for an axially loaded pile supported by springs.

$$EA\frac{d^2u}{dz^2} - cOu = 0 \qquad (1)$$

The general solution is of the form:

$$u = C_1 e^{\frac{z}{h}} + C_2 e^{-\frac{z}{h}} \qquad (2)$$

with for h the characteristic length:

$$h = \sqrt{EA/cO} \qquad (3)$$

When the integration constants are determined at z = 0 the load is –P and at z = L the point resistance is given by Y (the measured tip resistance).
Thus eq. 2 needs to be rewritten for normal forces:

$$N = EA\frac{du}{dz} = \frac{EA}{h}\left\{C_1 e^{\frac{z}{h}} + C_2 e^{-\frac{z}{h}}\right\} \qquad (4)$$

When both boundary conditions are put into eq. 4 the following two equations with the two unknown integration constants can be compiled:

$z = 0$:

$$-P = \frac{EA}{h}\{C_1 + C_2\} \qquad (5)$$

$z = l$

$$-Y = \frac{EA}{h}\left\{C_1 e^{\frac{l}{h}} + C_2 e^{-\frac{l}{h}}\right\} \qquad (6)$$

When eq. 5 is substituted in eq. 6 after some elaboration the constants C_1 and C_2 can be found.

$$C_1 = -\frac{e^{-\frac{l}{h}}\left(Pe^{-\frac{l}{h}} - Y\right)}{\sqrt{cOEA}\left(\left(e^{\frac{-l}{h}}\right)^2 - 1\right)}$$

$$C_2 = -\frac{\left(P - Ye^{-\frac{l}{h}}\right)}{\sqrt{cOEA}\left(\left(e^{\frac{-l}{h}}\right)^2 - 1\right)}$$

(7) & (8)

When these two constants are substituted in eq. 3 (displacement) and eq. 4 (normal force) the solution becomes:

$$u = -\frac{e^{-\frac{l}{h}}\left(Pe^{-\frac{l}{h}} - Y\right)e^{\frac{z}{h}} + \left(P - Ye^{-\frac{l}{h}}\right)e^{-\frac{z}{h}}}{\sqrt{cOEA}\left(\left(e^{\frac{-l}{h}}\right)^2 - 1\right)}$$

$$N = EA\frac{du}{dz} = -\frac{e^{-\frac{l}{h}}\left(Pe^{-\frac{l}{h}} - Y\right)e^{\frac{z}{h}} - \left(P - Ye^{-\frac{l}{h}}\right)e^{-\frac{z}{h}}}{\left(\left(e^{\frac{-l}{h}}\right)^2 - 1\right)}$$

(9) & (10)

Appendix M Drawings test set-up

guidance + drop weight + pile head

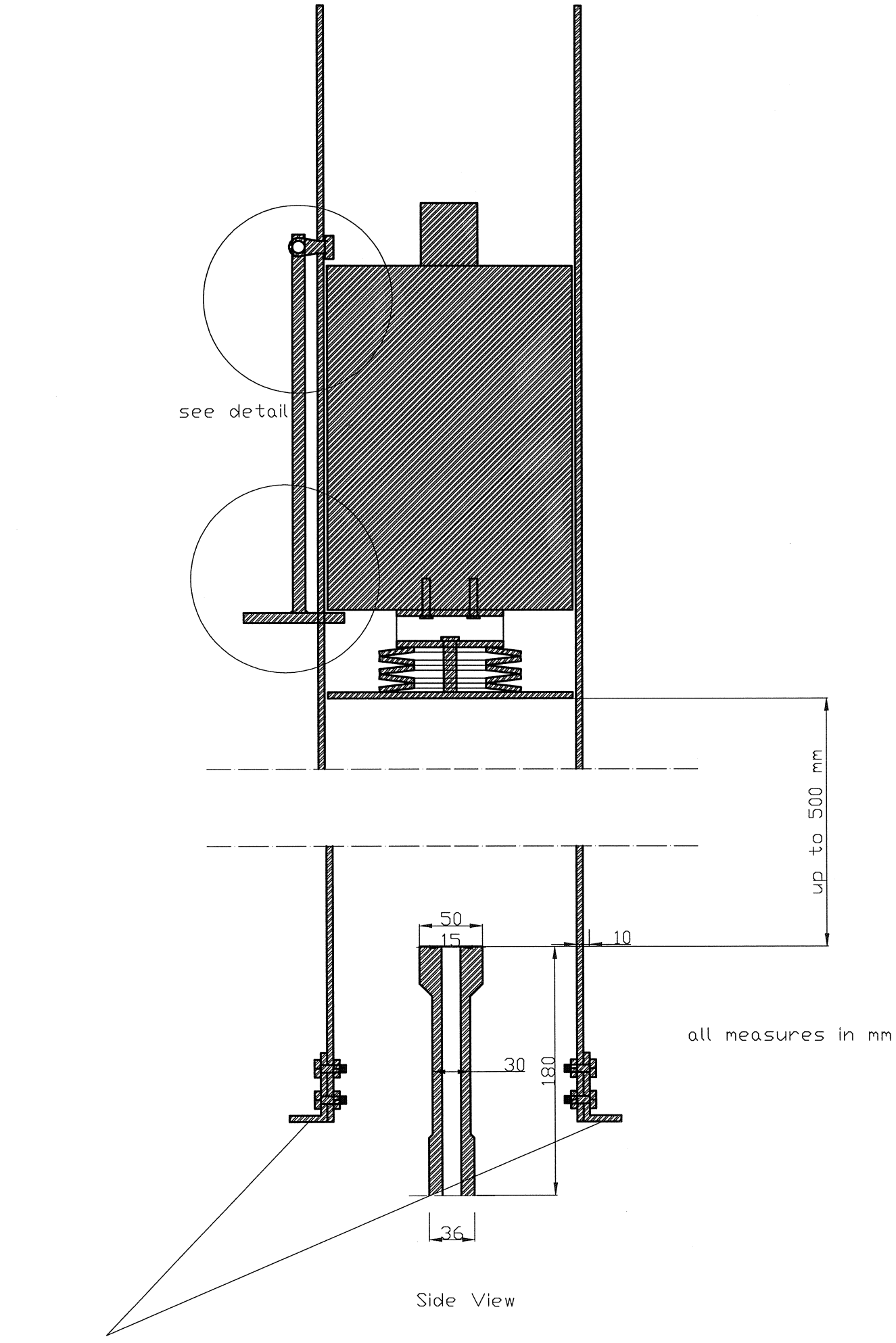

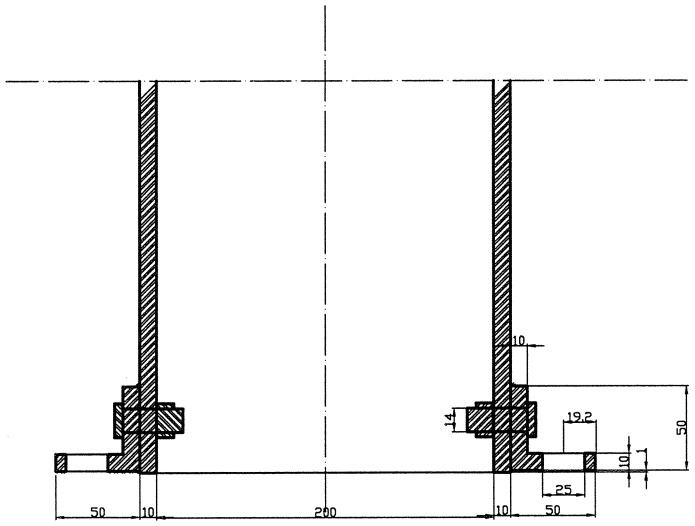

Doorsnede A-A

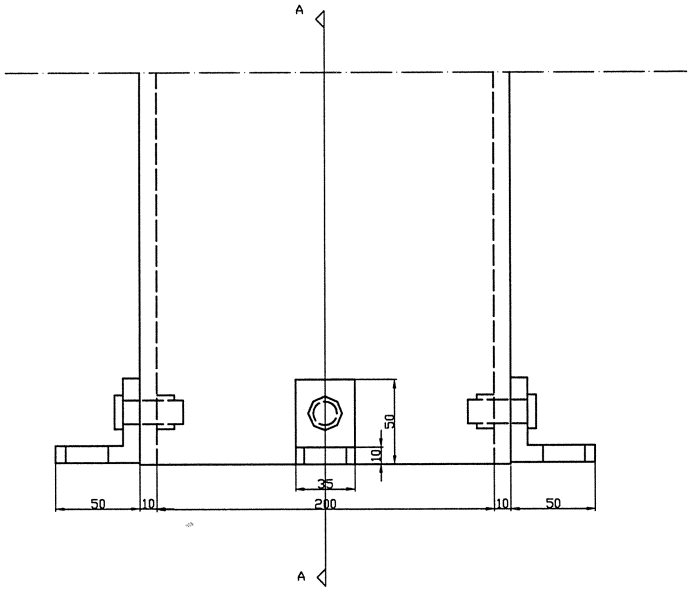

Zij-aanzicht

all measurements in mm

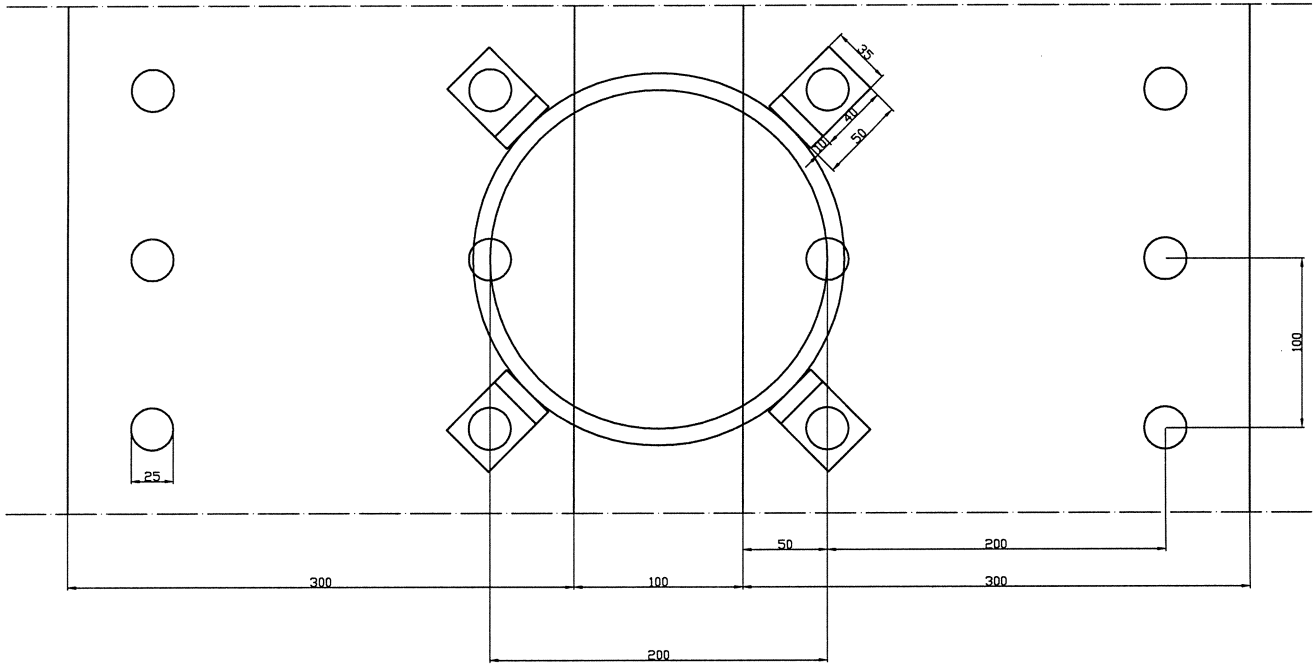

Bovenaanzicht

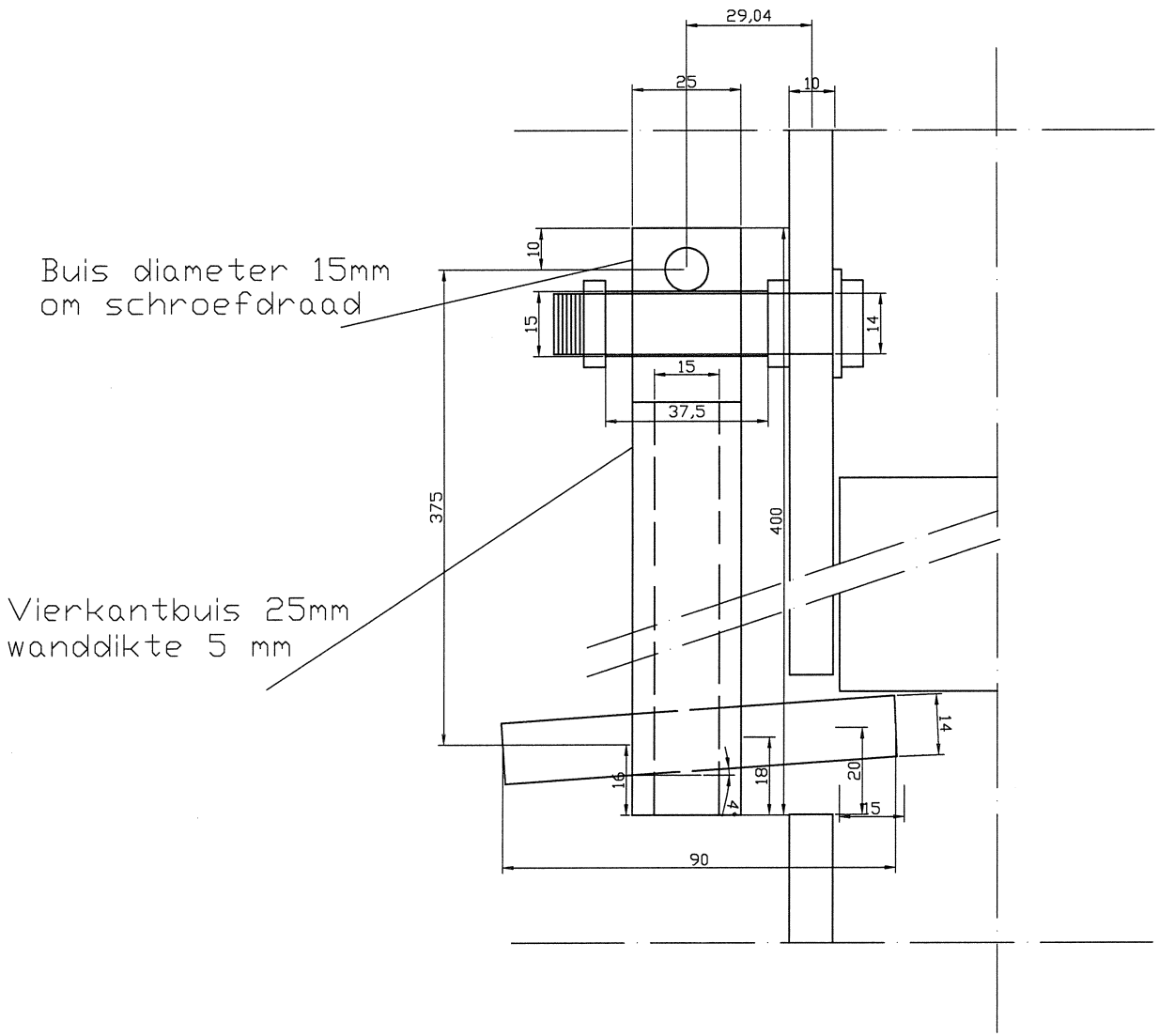

Vooraanzicht

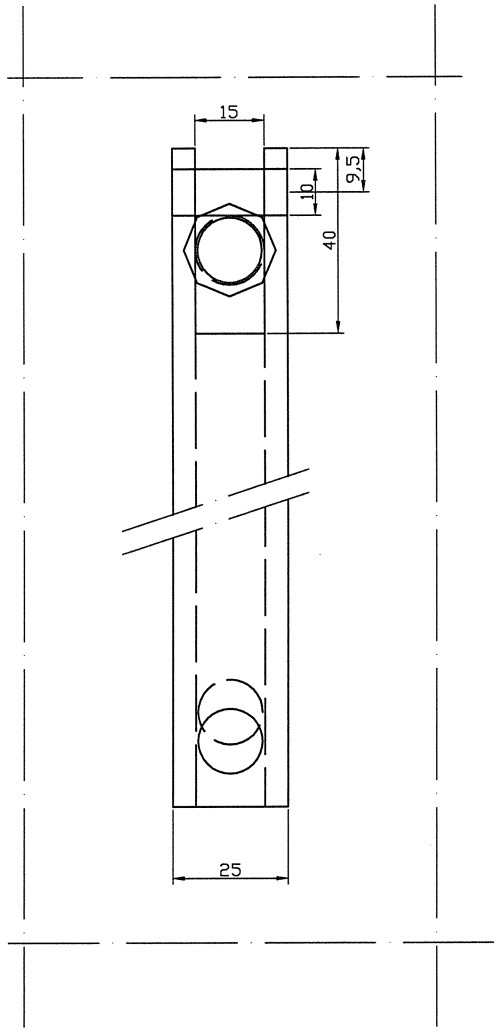

Zij-aanzicht

dropweight + disc springs

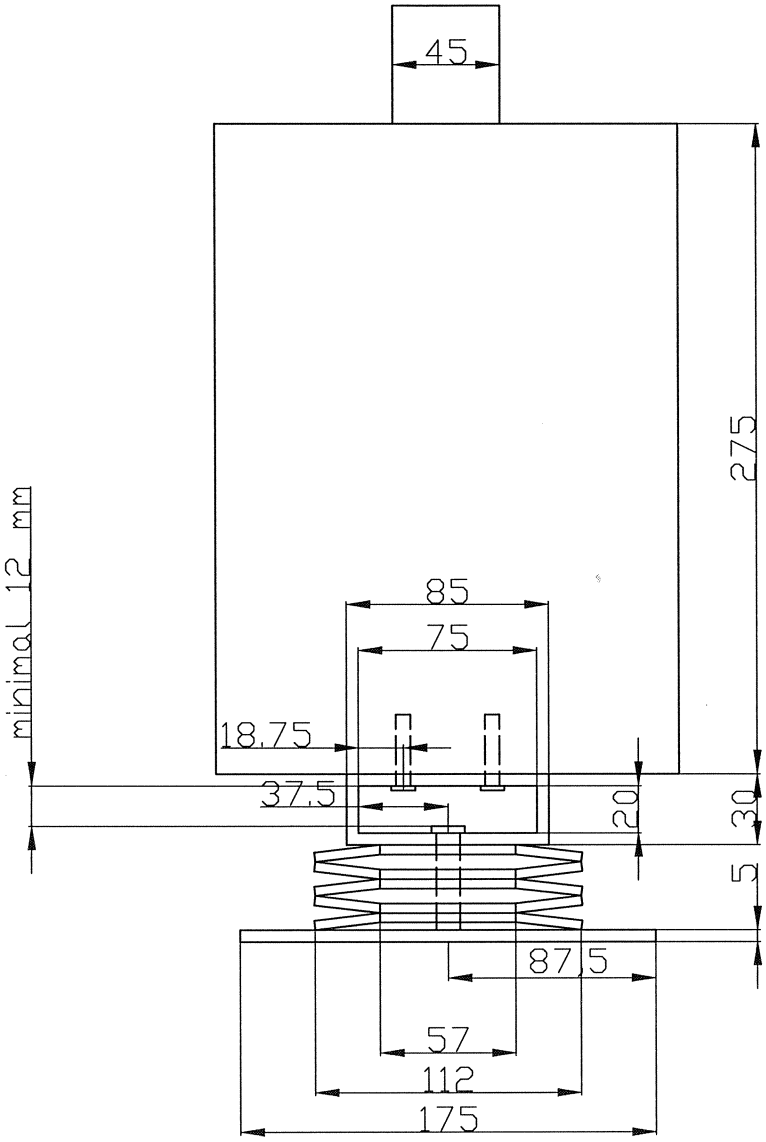

Front View

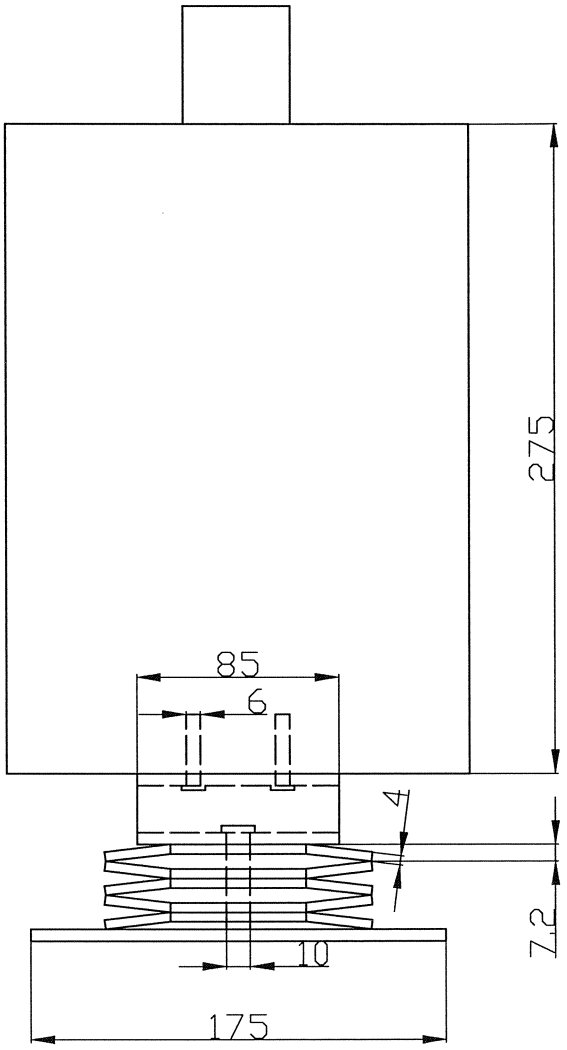

Side View

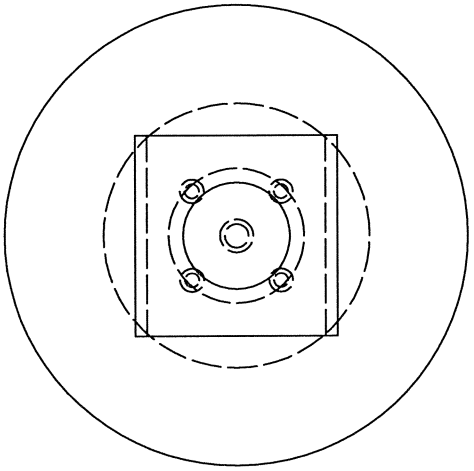

Top View

all measures in mm

detail of drop[illegible] + disc springs

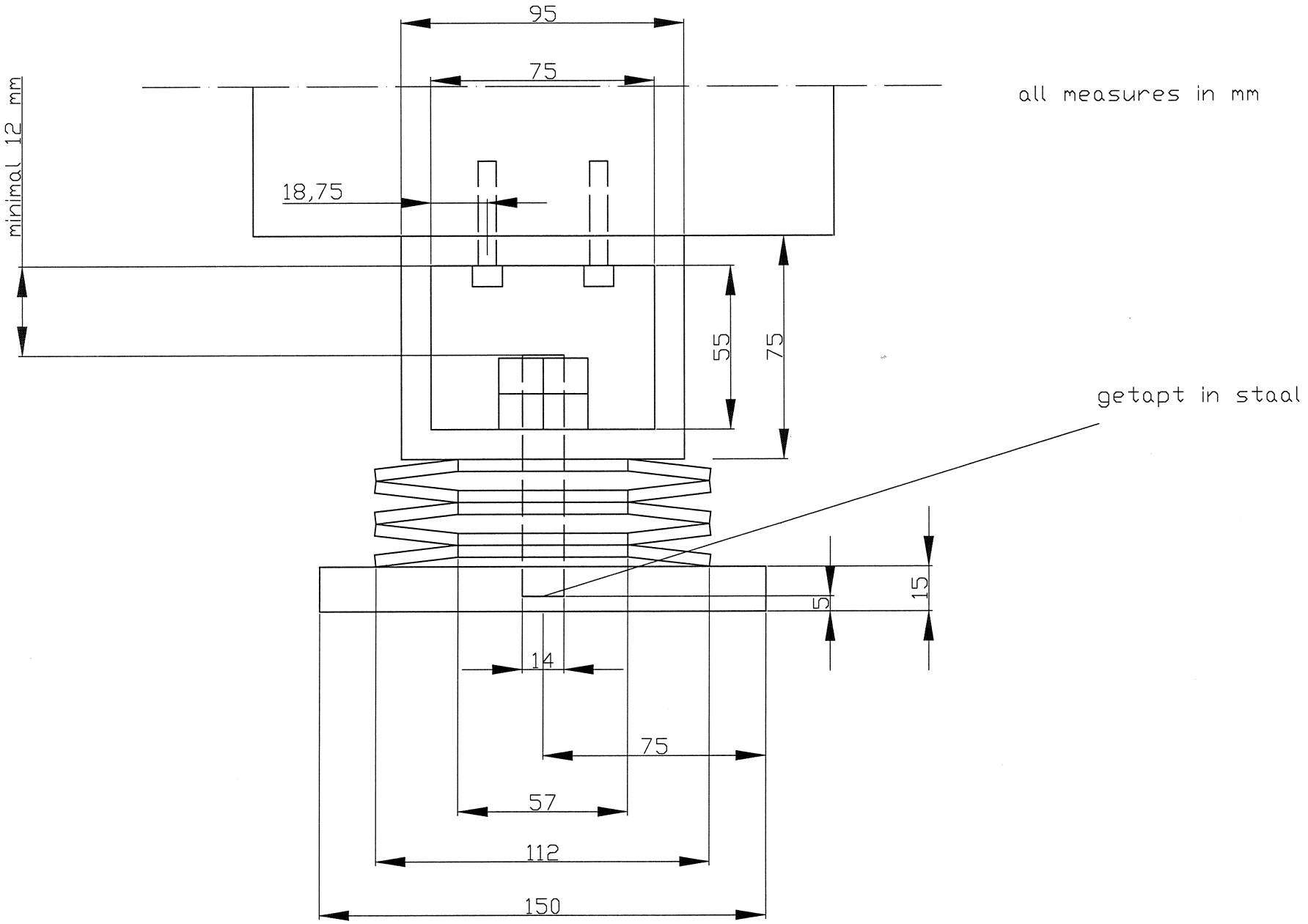

all measures in mm

Front View

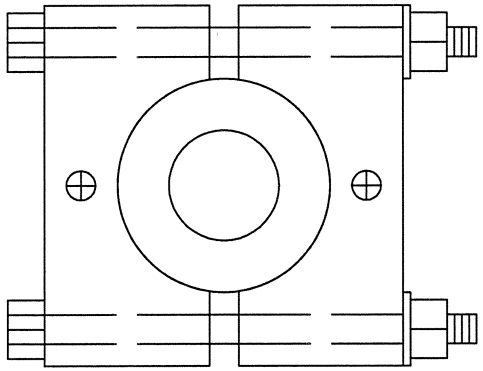

Top View

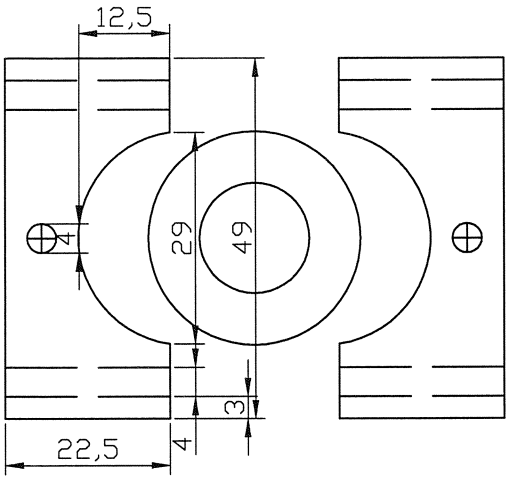

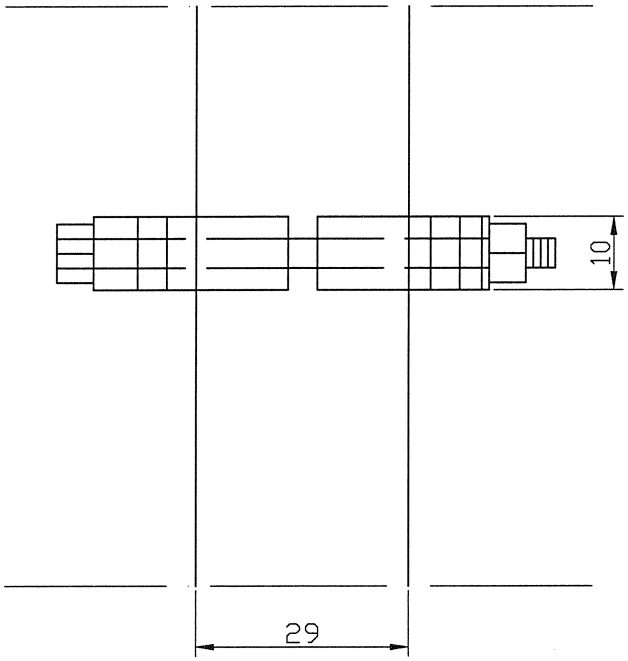

Side View

All measures in mm

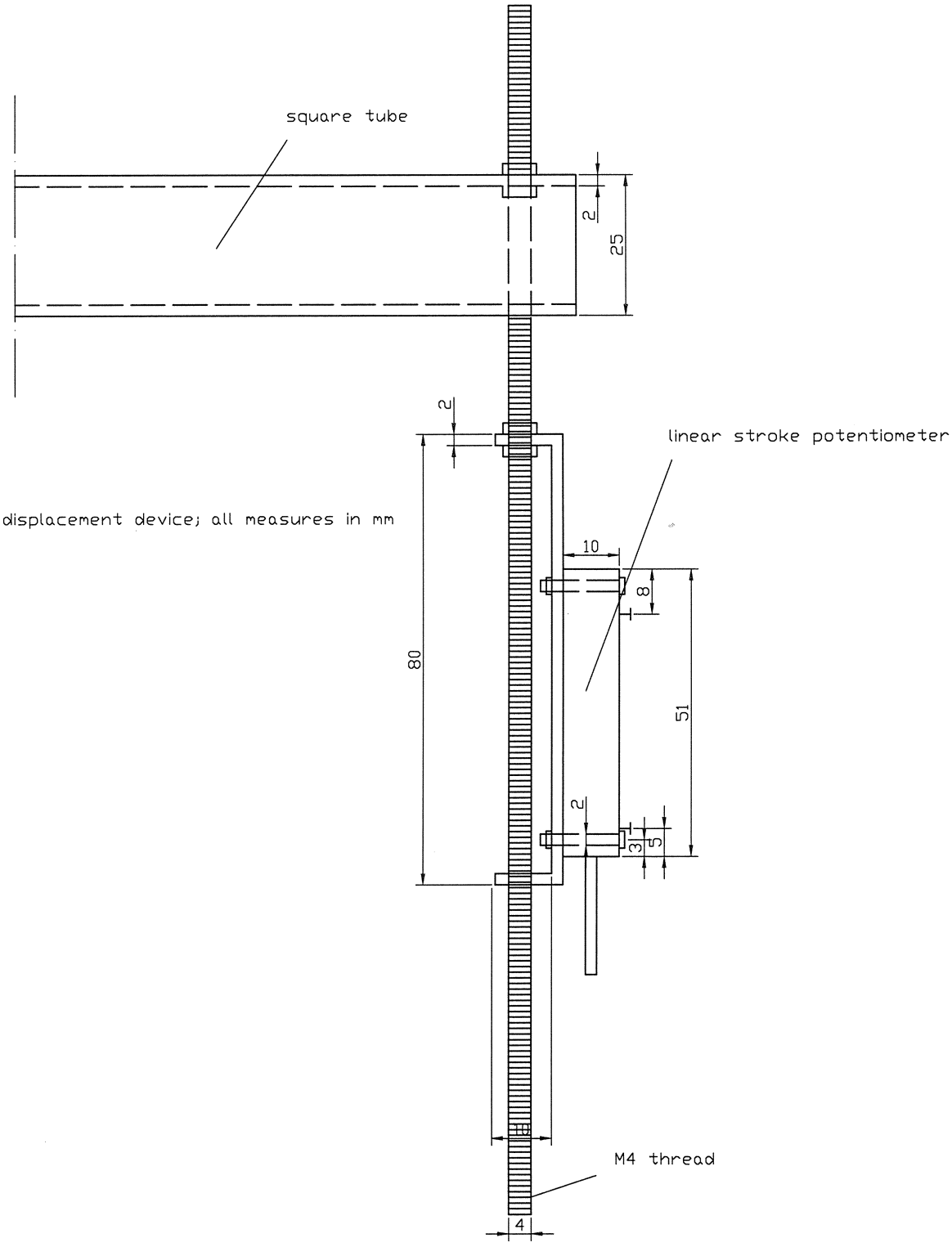

mounting of displacement device; all measures in mm

Appendix N Some statistical analysis: paired-t method

10V 1.5F 1 pseudostatische test

punt	static tests				
	pre	post	X_dak	Y_dak	(X_dak-Ydak)^2
	10,8	10,1	-1,964286	-2,142857	0,031887755
	10,5	10,7	-2,264286	-1,542857	0,520459184
	14,1	14,4	1,335714	2,157143	0,674744898
	13,4	12,2	0,635714	-0,042857	0,460459184
	14,2	10,5	1,435714	-1,742857	10,10331633
	14,1	13,7	1,335714	1,457143	0,014744898
	10,8	11,5	-1,964286	-0,742857	1,491887755
	16,4	16	3,635714	3,757143	0,014744898
	12	10,7	-0,764286	-1,542857	0,606173469
	12,6	12	-0,164286	-0,242857	0,006173469
	15,6	15,4	2,835714	3,157143	0,103316327
	10,3	10,3	-2,464286	-1,942857	0,271887755
	9,9	10,8	-2,864286	-1,442857	2,020459184
	14	13,1	1,235714	0,857143	0,143316327
mean	12,76428571	12,24286			
sigma(X_dak - Y_dak)^2	16,46357143				
t_exp	1,733678216				
t uit tabel 5%	2,16036824				

10V 1.5F 1 pseudostatische test

schacht	static tests				
	pre	post	X_dak	Y_dak	(X_dak-Ydak)^2
	0,029	0,065	-0,038214	-0,000857	0,001395556
	0,057	0,055	-0,010214	-0,010857	4,13265E-07
	0,115	0,08	0,047786	0,014143	0,001131842
	0,08	0,075	0,012786	0,009143	1,32704E-05
	0,09	0,096	0,022786	0,030143	5,41276E-05
	0,063	0,056	-0,004214	-0,009857	3,18418E-05
	0,05	0,055	-0,017214	-0,010857	4,04133E-05
	0,067	0,06	-0,000214	-0,005857	3,18418E-05
	0,04	0,055	-0,027214	-0,010857	0,000267556
	0,065	0,06	-0,002214	-0,005857	1,32704E-05
	0,09	0,08	0,022786	0,014143	7,4699E-05
	0,055	0,055	-0,012214	-0,010857	1,84184E-06
	0,06	0,06	-0,007214	-0,005857	1,84184E-06
	0,08	0,07	0,012786	0,004143	7,4699E-05
mean	0,067214286	0,065857			
sigma(X_dak - Y_dak)^2	0,003133214				
t_exp	0,327089204				
t uit tabel 5%	2,16036824				

10V 1.5F 1 pseudostatische test

F op paalkop	static tests				
	pre	post	X_dak	Y_dak	(X_dak-Ydak)^2
	23,9	21,3	-2,078571	-3,357143	1,634744898
	21,8	20,9	-4,178571	-3,757143	0,177602041
	33,7	35	7,721429	10,34286	6,871887755
	27,6	27,7	1,621429	3,042857	2,020459184
	27,4	19,8	1,421429	-4,857143	39,42045918
	28,8	26,5	2,821429	1,842857	0,957602041
	20,5	21,7	-5,478571	-2,957143	6,357602041
	30,9	29,8	4,921429	5,142857	0,049030612
	24,4	22,5	-1,578571	-2,157143	0,334744898
	25,4	23,9	-0,578571	-0,757143	0,031887755
	31,3	28,7	5,321429	4,042857	1,634744898
	21,6	21,4	-4,378571	-3,257143	1,257602041
	20,1	20,9	-5,878571	-3,757143	4,500459184
	26,3	25,1	0,321429	0,442857	0,014744898
mean	25,97857	24,65714			
sigma(X_dak - Y_dak)^2	65,26357				
t_exp	2,206703				
t uit tabel 5%	2,160368				

10V 1.5F meerdere pseudostatische tests

punt	static tests				
	pre	post	X_dak	Y_dak	(X_dak-Ydak)^2
	11	10,5	-2,475	-1,85	0,390625
	12,2	10,9	-1,275	-1,45	0,030625
	17,3	16	3,825	3,65	0,030625
	13,4	12	-0,075	-0,35	0,075625
mean	13,475	12,35			
sigma(X_dak - Y_dak)^2	0,5275				
t_exp	5,365768276				
t uit tabel 5%	3,182449291				

10V 1.5F meerdere pseudostatische tests

schacht	static tests				
	pre	post	X_dak	Y_dak	(X_dak-Ydak)^2
	0,061	0,06	-0,01675	-0,0145	5,0625E-06
	0,071	0,07	-0,00675	-0,0045	5,0625E-06
	0,115	0,095	0,03725	0,0205	0,000280563
	0,064	0,073	-0,01375	-0,0015	0,000150063
mean	0,07775	0,0745			
sigma(X_dak - Y_dak)^2	0,00044075				
t_exp	0,536262988				
t uit tabel 5%	3,182449291				

10V 1.5F meerdere pseudostatische tests

F op paalkop	static tests				
	pre	post	X_dak	Y_dak	(X_dak-Ydak)^2
	25,4	21,4	-1,025	-3,525	6,25
	24,1	20,2	-2,325	-4,725	5,76
	31,3	28,4	4,875	3,475	1,96
	24,9	29,7	-1,525	4,775	39,69
mean	26,425	24,925			
sigma(X_dak - Y_dak)^2	53,66				
t_exp	0,709343				
t uit tabel 5%	3,182449				

$$\hat{X}_i = \left(X_i - \overline{X}\right)$$
$$\hat{Y}_i = \left(Y_i - \overline{Y}\right)$$
$$t_{exp} = \left(\overline{X} - \overline{Y}\right) \Big/ \sqrt{\frac{n(n-1)}{\sum_{i=1}^{n}\left(\hat{X}_i - \hat{Y}_i\right)^2}}$$

$$H_0 : \overline{X} = \overline{Y}$$
$$H_a : \overline{X} \neq \overline{Y}$$

geeft two tailed t verdeling met voor 95% interval een alpha/2 = 0,025

References

Al-Mhaidib A. I. “Bearing Capacity of Model Pile in Sand Under Different Loading Rates”, Proc. 9th (1999) International Offshore and Polar Engineering Conference Brest, France. pp 724-730

Briaud, J.L., DiMillio, A. F., 1985. “Residual driving stresses and vertically loaded piles in cohesionless soils”, Public Roads 49 (1985) 1, June, pp. 13-17

Broere, W. (2001) “Tunnel Face Stability & New CPT applications”, Delft University Press, 2001

Brown, M.J., (2004) The rapid load testing of piles in fine grained soils

Brown,M.J., Hyde, A.F.L. & Anderson, W.F. (2002) “The influence of loading rate on pile behaviour in clay.” In R. Philips, P.J. Guo & R. Popescu (eds) Int Conf. On Physical Modelling in Geotechnics ICPMG’02, Newfoundland, Canada, 10-12th July, 2002. A.A Balkema, Rotterdam. pp. 667-672.

Casagrande & Shannon. “Strength of soils under dynamic loads”, Proceeding of the American Society of Civil Engineering, Vol. 74, No.4, pp. 591-608.

Dayal, U. & Allen, J. H. “The Effect of Penetration Rate on the Strength of Remolded Clay and Sand Samples”, Can. Geotech. J., 12, 336 (1975) pp. 336-348

Eiksund, G., Nordal, S., (1996) “Dynamic model pile testing with pore pressure measurements”, Proc. 5th Int. Conf. Appl. Stress-Wave Theory to Piles, Orlando, Sept. 1996, Gainesville, Univ. Florida, Dep. Civ. Eng., 1996, pp 1-11.

Farr, J.V. “One Dimensional Loading-Rate effects”, J. Geotech. Eng., 116 (1990) 1, Jan., pp. 119-135

Fellenius, B. H., 2001. “Determining the true distribution of load in piles.” American Society of Civil Engineers, ASCE, International Deep Foundation Congress, An International Perspective on Theory, Design, Construction, and Performance, Geotechnical Special Publication No. 116, Edited by M.W. O’Neill and F.C. Townsend, Orlando, Florida, February 14-16, 2002, Vol. 2, pp.1455 -1470.

Gennaro, V. De, Frank, R. Bosco, G. & Canou, J. (2001) “Effet de la vitesse de chargement sur le comportement mecanique de pieux modele en chambre d’etalonnage”, Proc. 15th Int. Conf. Soil Mech. Geotech. Eng., Istanbul, Aug. 2001", Lisse, Balkema, 2001, Vol.2, pp.885-888.

Gibson, G.C. & Coyle, H.M. 1968. “Soil damping constants re-lated to common soil properties in sands and clays (Bearing Capacity for Axially Loaded Piles)”. Texas Transportation Institute Research Report 125-1 (Study 2-5-67-125). Texas: Texas A&M University.

Heerema, E. P. “Relationships between wall friction displacement velocity and horizontal stress in clay and in sand for pile driveability analysis”

Hölscher P. (1995) “Dynamical response of saturated and dry soils”, Delft University Press, 1995

Horvath R. G., (1991) “The Statnamic Loading Method for Testing Model Piles in Sand”, Department of Civil Engineering McMaster University Hamilton Ontario

Kimura, M. & Boonyatee, T. (2002) “Statnamic load tests on model piles and their 3D-elastoplastic FEM analyses”, Soils and Foundations vol. 42 No. 1, pp. 71-87

Lee, Seed & Dunlop (1969) “Effect of transient loading on the strength of sand”, Proceedings of the 7 th Int. Conf. on soil mechanics and foundation Eng., Vol. 1, pp. 239-247.

Linn, S-S, Hong, J.L., Lee W. F., Chang, Y.H., (2004) “Capacity evaluation of statnamic tested long piles”,Soil Dynamics and Earthquake Engineering 24 (2004) pp829-838.

Litkouhi & Poskitt (1980) “Damping constants for pile driveability calculations”, Geotechnique, Vol. 30, No. 1, pp. 77-86.

Maiorano, R., Viggiani, C., Randolph, M. “Residual stress system arising from different methods of pile installation”, Proc. 5th Int. Conf. Appl. Stress-Wave Theory to Piles, Orlando, Sept. 1996, Gainesville, Univ. Florida, Dep. Civ. Eng., 1996, pp 518-528.

Middendorp, P., Bermingham, P. & Kuiper, B. (1992) “Statnamic load testing of foundation piles”, Proc. 4th Int. Conf. Appl. Stress-Wave Theory to Piles, The Hague, Sept. 1992, Rotterdam, Balkema, 1992, pp. 581-588

Poulos, H.G. (1987) “Analysis of residual stress effects in piles”, Journal Geotechnical Engineering Vol. 113 (1987) 3, March, pp. 216-229

Schellingerhout, A.J., Revoort, E., “Pseudo static pile load tester”, Proc. 5th Int. Conf. Appl. Stress-Wave Theory to Piles, Orlando, Sept. 1996", Gainesville, Univ. Florida, Dep. Civ. Eng., 1996, pp. 1031-1037
Schimming, Haas & Saxe (1966) “Study of Dynamic and Static Failure Envelopes”, Journal of the soil mechanics and foundations division, ASCE, Vol.92, No. SM2, pp. 105-124.
Seed & Lundgren (1954) “Investigation of the effect of transient loadings on the strength and deformation characteristics of saturated sands”, Proceedings of the American Society for Testing and Materials, Vol. 54, pp. 1288-1306.
Whitman & Healy (1962) “Shear strength of sands during rapid loading”, Journal of the soil mechanics and foundations division, ASCE, Vol.88, No. SM2, pp. 99-132.